

POLITECNICO DI TORINO

Collegio di Ingegneria Chimica e dei Materiali

**Corso di Laurea Magistrale
in Ingegneria Chimica e dei Processi Sostenibili**

Tesi di Laurea Magistrale

**Porous ZnO nanostructures for drug
delivery**



Relatori

Prof. Valentina Alice Cauda
Dr. Marco Laurenti

Candidato

Domenico Carubia

Marzo 2018

Ringraziamenti

Arrivato alla fine della carriera universitaria è doveroso fare un bilancio di ciò che è stato questo percorso di vita e di ringraziare le persone che mi sono state accanto. Sono stati sei anni molto intensi, pieni di sacrifici, studio matto e disperato, ansie pre-esame e delusioni per un esame non superato ma anche e soprattutto gioie e soddisfazioni personali. Sono stati gli anni dell'indipendenza e della crescita personale.

Grazie alla mia famiglia che mi è sempre stata vicina nei momenti di difficoltà, supportandomi emotivamente e andando incontro a sacrifici economici che per fortuna sono sempre stati ripagati.

Grazie di cuore ad Anita, per aver sempre creduto in me e per aver rispettato la scelta di allontanarmi temporaneamente da lei due anni fa, con la consapevolezza di stare meno tempo assieme rispetto a prima.

Ringrazio i miei relatori, Valentina e Marco, per avermi seguito costantemente in questi mesi di laboratorio, per i consigli e per avermi dato la possibilità di crescere dal punto di vista della praticità.

Grazie agli amici di una vita, Ignazio, Manfredi, Sarah, Rosario, Alessia, Vincenzo, Gaetano, Felice, Federica, Gaetano e Fabiola per esserci sempre stati e per aver condiviso le esperienze più belle di questi anni.

Grazie anche ai ragazzi della residenza Paoli per aver condiviso questi due anni a Torino tra risate, pranzi e serate. Sono sicuro che ci saranno altre occasioni per rivedersi in futuro

RIASSUNTO

Introduzione e obiettivi

Negli ultimi anni, l'interesse verso la progettazione di dispositivi biomedicali impiantabili con nuove funzionalità è notevolmente aumentato e ha riguardato diversi settori, come quello cardiovascolare, ortopedico e urologico. Nonostante gli evidenti benefici terapeutici, l'impianto di un dispositivo può causare reazioni avverse da parte dell'organismo ospitante, come infezioni, infiammazioni, mancanza di integrazione con i tessuti e nel caso peggiore, il completo rigetto del dispositivo stesso da parte dell'organismo. Una possibile soluzione per il superamento di suddetti limiti è l'utilizzo di materiali nanoporosi come rivestimenti (film) in grado di fornire al dispositivo funzionalità aggiuntive rispetto a quelle per cui originariamente progettato. Per esempio, grazie alla loro elevata area superficiale, questi rivestimenti sono capaci di agire come vettori per il rilascio controllato di un farmaco nella regione in cui il dispositivo viene impiantato. In genere, le caratteristiche di un sistema a rilascio controllato sono l'abilità nel mirare specifiche parti del corpo e la capacità di regolare il profilo di rilascio del farmaco nel tempo per massimizzarne i benefici terapeutici. Questo permette anche di ridurre le concentrazioni di farmaco assunte e quindi mitigare l'insorgenza di eventuali effetti collaterali. Tra le varie alternative esistenti, i film mesoporosi di ossido di zinco (ZnO) rappresentano una soluzione idonea in questo campo perché possono ospitare e rilasciare farmaci grazie alla presenza di pori di dimensioni adatte. Inoltre, lo ZnO possiede proprietà osteogeniche e bioattive, favorendo la proliferazione di cellule del tessuto osseo e la precipitazione di idrossiapatite (fase minerale dell'osso) se messo a contatto con i fluidi corporei. Dal punto di vista biomedicale, lo ZnO è estremamente interessante anche grazie alle sue proprietà antibatteriche e di biodegradazione. Quest'ultima lo rende unico rispetto ad altri materiali chimicamente più stabili poiché permette di ottenere una degradazione prevedibile nel tempo e alquanto desiderata nelle applicazioni di rigenerazione tissutale.

Questo lavoro di tesi si inserisce in questo contesto e si pone l'obiettivo di studiare le proprietà di caricamento e rilascio di un farmaco da parte di film sottili di ZnO con struttura mesoporosa. I film di ZnO sono ottenuti per deposizione tramite magnetron sputtering a radiofrequenza su wafer di silicio e successivo trattamento termico di ossidazione. Il farmaco utilizzato per tutti gli esperimenti è stato l'antibiotico gentamicina solfato (GS). Nella prima parte del lavoro è stata investigata l'interazione tra i film porosi di ossido di zinco e differenti soluzioni di adsorbimento di GS. In particolare, sono stati realizzati due set di esperimenti separati, partendo da GS in acqua deionizzata (GS/DIW) e GS in simulated body fluid (SBF), un fluido capace di simulare la composizione fisiologica inorganica del plasma nel corpo umano. In entrambi i casi sono stati studiati attraverso differenti tecniche sia qualitative che quantitative l'effetto delle soluzioni di adsorbimento di GS sul comportamento a degradazione dei film di ossido di zinco e l'abilità nel caricare il farmaco al variare del tempo di immersione del campione stesso nella soluzione sotto determinate condizioni di agitazione orbitale. Una volta identificate le condizioni ottimali di adsorbimento, sia in termini di concentrazione di GS nella soluzione sia in termini di tempo che garantisce la maggiore quantità di farmaco caricata, il rilascio del farmaco in SBF è stato investigato. Nella seconda parte del lavoro sono stati effettuati gli stessi esperimenti usando film porosi di ossido di zinco ricoperti di uno strato di ossido di grafene

sulla superficie. In particolare, l'obiettivo principale nell'utilizzo dell'ossido di grafene è l'ottenimento di un sistema a rilascio controllato in cui il GO, grazie alla sua struttura, è in grado di produrre un effetto barriera andando ad occludere parzialmente le porosità dello ZnO e rallentare la cinetica di rilascio, in modo da avere un miglior controllo del processo utile per massimizzare i benefici terapeutici in molte applicazioni. Sia prima che dopo gli esperimenti i campioni sono stati caratterizzati in termini di morfologia, struttura cristallina e composizione chimica ed elementare. In particolare le metodologie sperimentali utilizzate sono: microscopio elettronico a scansione (FESEM), diffrazione ai raggi X (XRD), spettroscopia di massa a plasma accoppiato induttivamente (ICP-MS), spettroscopia a dispersione di energia (EDS), spettroscopia a trasformata di Fourier (FT-IR), spettroscopia ultravioletta/visibile (Uv-Vis).

Caratterizzazione dei materiali

Prima degli esperimenti di adsorbimento e rilascio di gentamicina solfato, entrambi i materiali, film di ZnO poroso e film di ZnO poroso ricoperto di GO, sono stati caratterizzati in termini di morfologia, struttura cristallina, composizione chimica e elementare, in modo da poter confrontare le loro inerenti proprietà dopo entrambi gli esperimenti.

Film di ZnO poroso e film di ZnO-GO poroso

In primo luogo, i campioni sono stati caratterizzati in termini di morfologia attraverso l'analisi al microscopio elettronico a scansione. Nella figura 1 sono riportate le immagini ottenute per i due campioni a diversi ingrandimenti. Si può notare come, nel caso del solo ZnO, sono presenti più zone scure rispetto al campione col GO, le quali rappresentano la porosità intrinseca del materiale che non ha una struttura compatta. Nel campione col GO si possono invece notare i fiocchi di GO ricoprenti la superficie del materiale di partenza.

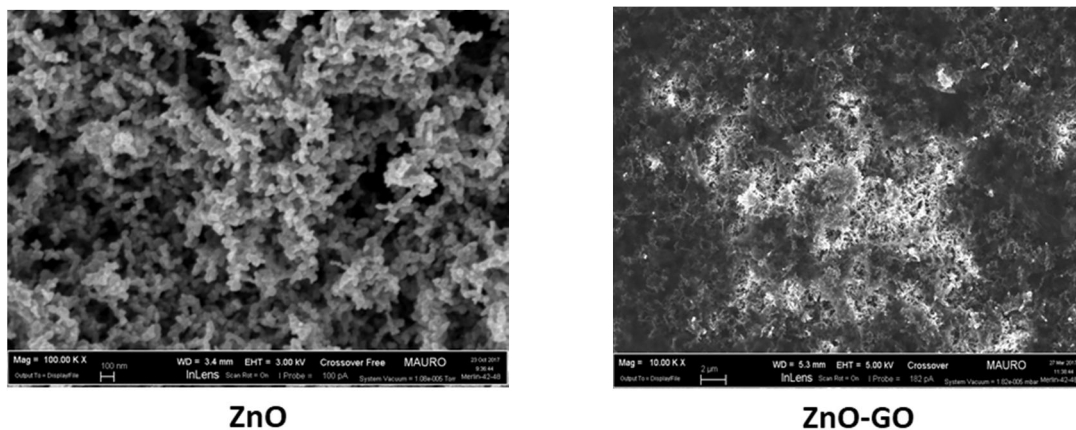
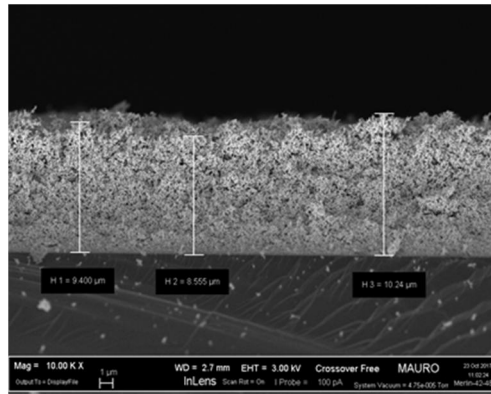


Figura 1: immagini al microscopio elettronico dei campioni ZnO e ZnO-GO

L'analisi al microscopio elettronico permette inoltre di valutare lo spessore medio dei film depositati che è all'incirca di 9,5 μm. La figura 2 mostra la sezione del film di ZnO poroso, dove sono riportati tre valori di spessori valutati in tre differenti posizioni del campione.



Cross-section

Figura 2: Sezione trasversale di film sottile di ZnO depositato su substrato di silicio

La caratterizzazione della struttura cristallina è stata effettuata attraverso diffrazione ai raggi X. In figura 3 sono riportati i pattern di diffrazione del solo ZnO e dello stesso confrontato con il sistema contenente il GO. Entrambi i film mostrano una struttura policristallina, in cui i picchi di diffrazione (1 0 0), (0 0 2), (1 0 1), (1 0 2) e (1 1 0) appartengono alla tipica struttura cristallina esagonale di tipo wurtzite.

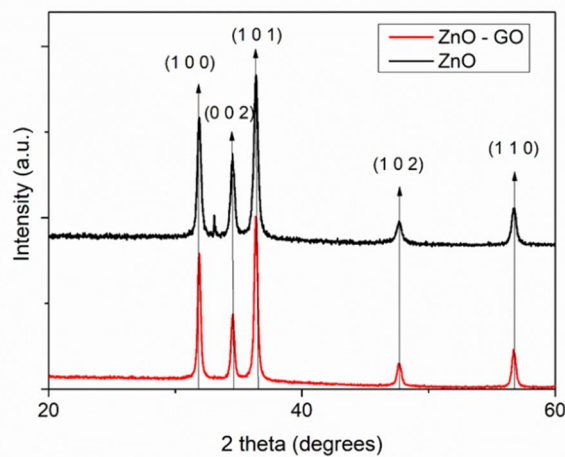


Figura 3: pattern di diffrazione di raggi X di ZnO e ZnO-GO

La struttura chimica di superficie e la composizione dei campioni sono stati analizzati attraverso spettroscopia infrarossa a trasformata di Fourier. Nella figura 4, sono messi a confronto gli spettri IR del campione di solo ZnO e del campione di ZnO-GO. Il picco corrispondente al legame Zn-O si trova nell'intervallo $500-400\text{ cm}^{-1}$ ed è comune ad entrambi i campioni. Essendo molto pronunciato, per poter apprezzare le differenze in termini di altri picchi tra i due campioni si è preferito omettere quella zona. Si può notare come lo spettro IR dello ZnO sia piuttosto piatto non essendoci altre bande significative, mentre nel caso dello ZnO-GO sono stati rilevati lo stretching tipico dei gruppi alchilici -CH_x tra $3000-2800\text{ cm}^{-1}$, la banda relativa ai gruppi aromatici a circa 1600 cm^{-1} e i gruppi C-O carbossile e alcossile a 1390 cm^{-1} e 1024 cm^{-1} rispettivamente.

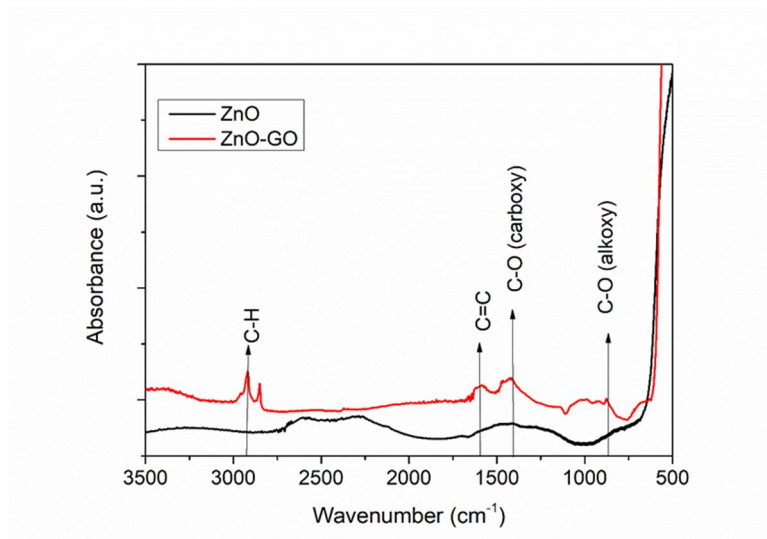


Figura 4: spettro IR di film di ZnO e ZnO-GO

La spettroscopia a dispersione di energia è stata effettuata su entrambi i campioni per valutare la composizione elementare e la loro presenza in superficie. Tale tecnica permette di ottenere delle mappe combinate di tutti gli elementi e allo stesso tempo dà un'analisi semi-quantitativa degli stessi. In Figura 5, sono riportate le mappe combinate dei campioni ZnO e ZnO-GO con la presenza di tutti gli elementi presenti in superficie.

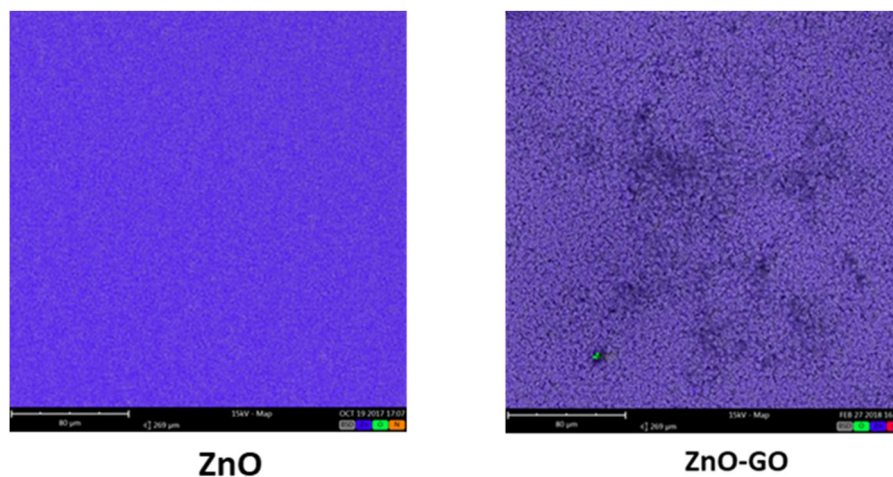


Figura 5: mappe combinate di ZnO con gli elementi azoto, ossigeno e zinco e di ZnO-GO con gli elementi carbonio, ossigeno e azoto

Nelle tabella 1 sono inoltre riportate in termini percentuali, le concentrazioni atomiche degli elementi sul campione di ZnO e su quello di ZnO-GO rispettivamente.

Tabella 1: percentuali atomiche sui campioni di ZnO e ZnO-GO



Adsorbimento GS su film porosi di ZnO a partire da soluzioni acquose

Gli esperimenti di adsorbimento sono stati dapprima effettuati in una soluzione di gentamicina solfato in acqua deionizzata. La soluzione è stata preparata miscelando il farmaco nel solvente a temperatura ambiente, sotto condizione di agitazione a 200 rpm per 30 minuti, ottenendo una concentrazione finale di $1 \text{ mg}\cdot\text{ml}^{-1}$. Successivamente, 5 ml della soluzione madre sono stati versati in 4 differenti contenitori di plastica. Ogni singolo campione di ZnO è stato immerso all'interno dei contenitori sotto agitazione orbitale a 160 rpm, a temperatura ambiente e per differenti tempi di adsorbimento pari a 1h, 2h, 5h, 24h. Questo ha permesso di investigare l'influenza del tempo di adsorbimento del farmaco sui film di ossido di zinco. Per ogni campione è stato misurato il valore di pH ai diversi tempi di adsorbimento per valutare l'effetto di degradazione della matrice di ZnO. La figure 6 mostra l'evoluzione del pH nel tempo. Si può notare come l'acidità della soluzione di partenza (pH iniziale di 4.4), porta ad una forte degradazione della struttura del materiale, che rilascia ioni Zn^{2+} causando un aumento graduale nel tempo del pH della soluzione che al tempo di 24h ha raggiunto la neutralità.

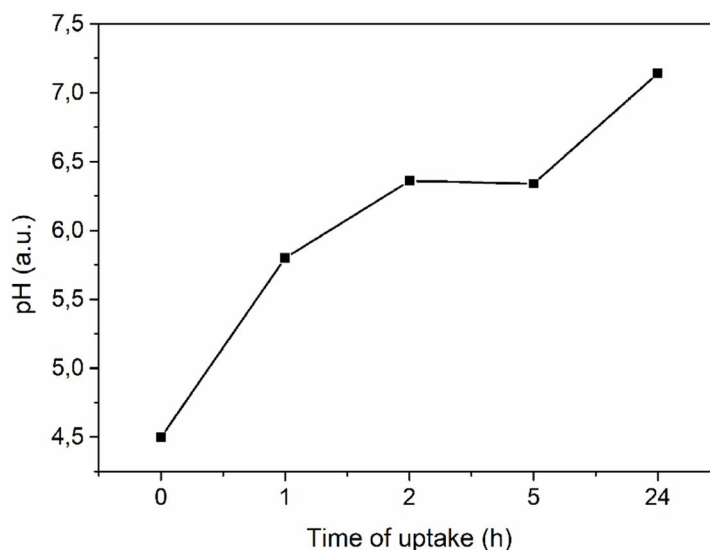


Figura 6: Evoluzione nel tempo del pH per soluzione di GS in acqua

Tale comportamento di dissoluzione dello ZnO in ambiente acido, è dovuto al suo essere un ossido anfotero. Nel momento in cui lo ZnO è immerso in soluzione acide, l'assorbimento di molecole d'acqua conduce all'idrolisi della superficie delle particelle di ZnO che formano idrossido di zinco $Zn(OH)_{2(s)}$. Tale idrossido è solubile in acqua, specie quando il pH è basso. Di conseguenza le reazioni predominanti che avvengono sono la dissoluzione dell'ossido di zinco e l'idrolisi della superficie dell'ossido di zinco che porta alla formazione dell'idrossido che a sua volta si decompone dando ioni Zn^{2+} in soluzione. Le reazioni sono mostrate rispettivamente nelle equazioni 1 e 2:



A confermare la degradazione in ambiente acido della matrice di ZnO sono state anche le altre caratterizzazioni effettuate tra cui la spettroscopia di massa ICP e l'analisi qualitativa al microscopio elettronico a scansione. Per quanto riguarda l'ICP, in figura 7 è riportato il profilo di rilascio degli ioni Zn^{2+} al variare del tempo di contatto. Si può notare come l'evoluzione nel tempo della concentrazione degli ioni Zn^{2+} , in ppm, ben riflette l'incremento di pH precedentemente osservato. In particolare, il massimo valore di concentrazione degli ioni Zn^{2+} è di circa 110 ppm ed è raggiunto dopo 24h.

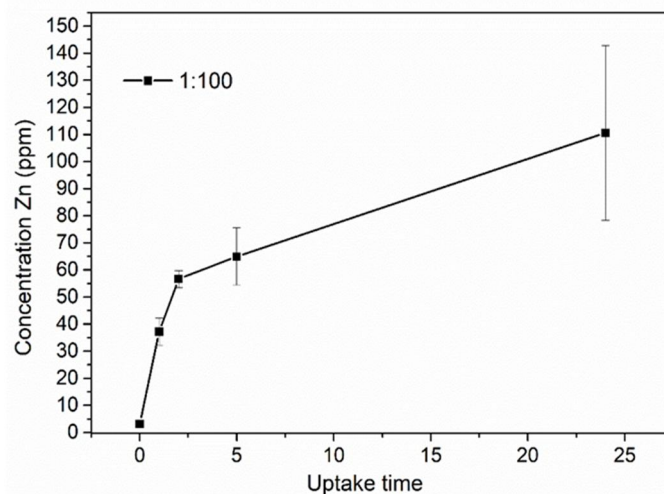
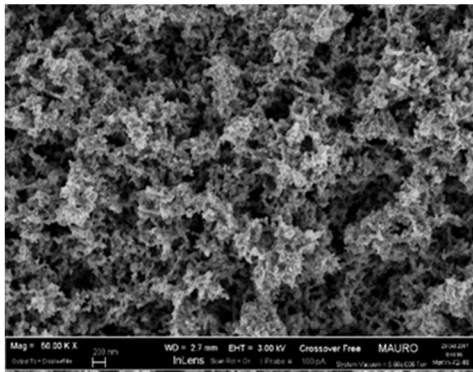
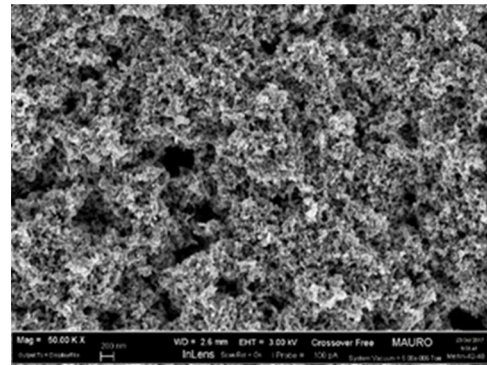


Figura 7: profilo di rilascio ioni Zn^{2+} in soluzione GS/DIW diluita 1:100, ottenuta tramite ICP-MS

L'analisi al microscopio elettronico ha permesso di rilevare delle differenze non trascurabili rispetto al campione di ZnO tal quale. In figura 8 è confrontata la morfologia del campione di ZnO tal quale e quella del campione di ZnO dopo un tempo di contatto di 24h. Nelle immagini si possono distinguere zone più scure, che rappresentano la porosità del materiale, e zone più chiare che danno informazioni riguardo il grado di compattezza dei campioni. In particolare il campione di ZnO, dopo essere stato 24h a contatto con la soluzione del farmaco, presenta una maggiore compattezza rispetto all'inizio, ovvero una minore porosità dovuta alla dissoluzione del materiale.



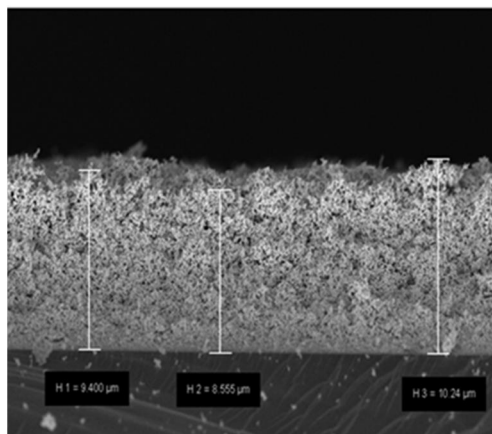
ZnO



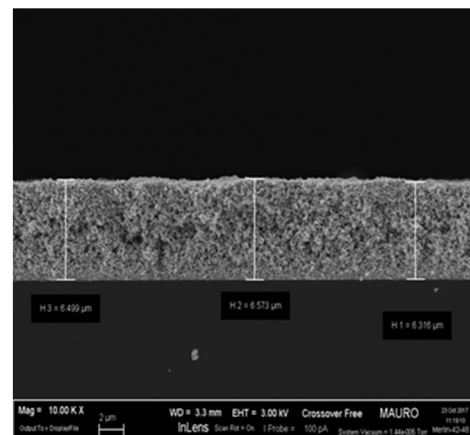
ZnO dopo uptake di 24h

Figura 8: immagini al SEM del film di ZnO tal quale e del film di ZnO dopo 24h dall'immersione nella soluzione del farmaco

Il microscopio elettronico ha inoltre permesso di valutare lo spessore medio dei campioni di ZnO mediante analisi in sezione. In figura 9 sono riportate le sezioni trasversali del campione di ZnO tal quale e dopo 24h di immersione nella soluzione del farmaco. E' evidente come lo spessore medio diminuisca in maniera marcata dopo 24h, passando da un valore di 9,5 μm ad un valore di circa 6,5 μm , a conferma della parziale dissoluzione del materiale all'aumentare del tempo.



(a)



(b)

Figura 9: (a) sezione trasversale del film di ZnO tal quale; (b) sezione trasversale del campione di ZnO immerso in soluzione dopo 24h

Adsorbimento GS su film porosi di ZnO a partire da soluzione in SBF

In modo da superare la limitazione della dissoluzione del film di ZnO causata dall'acidità della soluzione GS/DIW, gli esperimenti di adsorbimento del farmaco sono stati effettuati utilizzando come solvente SBF, un fluido capace di simulare la composizione fisiologica inorganica del plasma nel corpo umano. La concentrazione di partenza della soluzione è stata pari a $250 \mu\text{g}\cdot\text{ml}^{-1}$. Il pH della soluzione, monitorato per tutta la durata dell'esperimento si è mantenuto all'incirca costante. Questo aspetto previene parzialmente la dissoluzione del materiale, non influenzando l'adsorbimento del farmaco. L'analisi ICP-MS ha confermato una minore presenza di ioni Zn^{2+} in soluzione rispetto al precedente caso di adsorbimento in soluzione acquosa. La figura 10, confronta l'evoluzione nel tempo della concentrazione di ioni Zn^{2+} nei due casi. Si può evincere come in SBF la concentrazione di ioni Zn^{2+} a qualsiasi tempo, si mantiene sempre più bassa rispetto al caso in acqua deionizzata. In SBF, il più alto valore viene raggiunto dopo circa 1h ed è pari a circa 30 ppm. Comunque, il trend si può considerare all'incirca costante se confrontato con quello ottenuto in acqua.

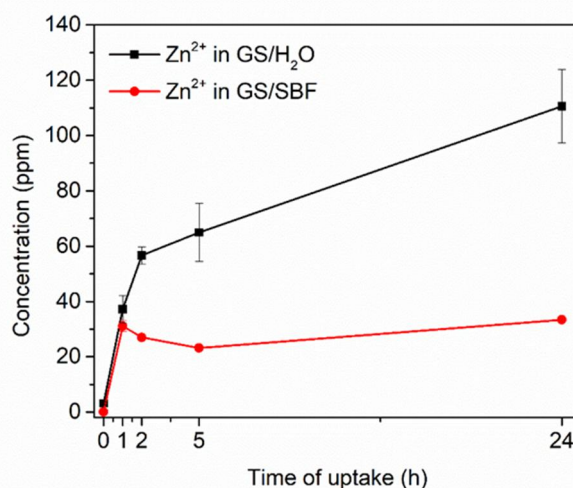


Figura 10: profilo di rilascio di ioni Zn^{2+} in soluzione acquosa (nero) e in SBF (rosso).

Mediante spettrofotometro UV-Vis è stato possibile valutare la quantità di gentamicina solfato caricata sul film di ossido zinco poroso. La retta di taratura è stata ottenuta analizzando la risposta UV-Vis di differenti soluzioni di gentamicina in SBF a concentrazione nota ($100 \mu\text{g}\cdot\text{ml}^{-1}$, $250 \mu\text{g}\cdot\text{ml}^{-1}$, $500 \mu\text{g}\cdot\text{ml}^{-1}$ and $1 \text{mg}\cdot\text{ml}^{-1}$) e monitorando il picco UV caratteristico del farmaco ad una lunghezza d'onda pari a 251 nm. Una volta misurata la risposta UV dello spettrofotometro alle diverse soluzioni di adsorbimento (1h, 2h, 5h, 24h) a concentrazione sconosciuta e monitorando il picco caratteristico a 251 nm è stato possibile risalire alla quantità di farmaco caricata sul campione dalla curva di calibrazione e considerando il volume caratteristico di 5 ml. Per gli esperimenti di adsorbimento ci si aspetta che, in accordo con la legge di Lambert-Beer, il picco di assorbimento caratteristico del farmaco sia meno intenso rispetto al picco di assorbimento della soluzione madre di partenza. Questo significa che la concentrazione di farmaco in soluzione dopo un certo tempo di adsorbimento sarebbe più bassa rispetto alla quantità iniziale e che

il processo di caricamento del farmaco è avvenuto efficacemente. La figura 11 mostra l'andamento della percentuale di GS caricata nel tempo, calcolata rispetto alla quantità di farmaco in soluzione all'inizio dell'esperimento (1250 ug). E' inoltre riportato in tabella il valore della massa di farmaco caricata in mg, rispetto al peso del campione di ZnO di circa 3 mg. Si può notare che la quantità di farmaco caricata aumenta progressivamente dal tempo zero al tempo di 2h. A questo punto è raggiunta la quantità massima di farmaco caricata, pari a circa 789 ug. Il valore a 5h è leggermente più basso, probabilmente dovuto sia al contributo dato dagli ioni Zn^{2+} alla soluzione sia al parziale desorbimento del farmaco precedentemente caricato. La quantità massima di farmaco caricata rispetto al peso dello ZnO tal quale è 263 mg/g. Inoltre, rispetto alla quantità di farmaco iniziale, solo il 60% di gentamicina solfato è stato correttamente caricato nel film poroso di ossido di zinco. Si può assumere che il sistema manifesta una discreta efficienza di adsorbimento.

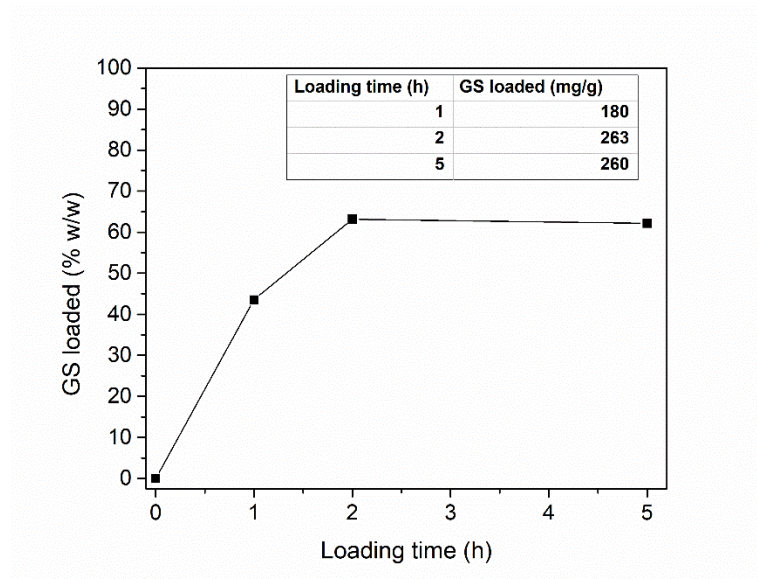


Figura 11: Percentuale di GS adsorbita rispetto alla quantità iniziale nella soluzione madre. La tabella riporta i mg di farmaco caricati rispetto al peso in g del campione di ZnO tal quale

Rilascio GS in SBF da film porosi di ossido di zinco

Dopo gli esperimenti di adsorbimento sulla matrice porosa di ZnO è stato valutato il rilascio del farmaco dal film poroso di ZnO in SBF. Gli esperimenti sono stati condotti in un agitatore orbitale, a 160 rpm e alla temperatura costante di 37 °C per simulare le condizioni del corpo umano. In base ai risultati ottenuti precedentemente, il tempo di adsorbimento ottimale scelto è di 2 ore poiché permette di caricare la quantità massima di farmaco rispetto agli altri tempi. A partire da un volume di SBF di 10 ml, sono state analizzate mediante spettrofotometro UV-Vis le aliquote di soluzione pari a 350 ul prelevate a diversi tempi (5 min, 15 min, 30 min, 1h, 2h, 4h, 6h, 24h, 48h, 72h, 7 giorni), in modo da valutare la cinetica di rilascio della GS. Una volta prelevate, le aliquote della soluzione sono state centrifugate a 20'000 rpm per 5 minuti prima di essere analizzate in modo da favorire la separazione di

eventuali impurità. Per gli esperimenti di rilascio ci si aspetta, in accordo con la legge di Lambert-Beer, che il picco di assorbanza caratteristico del farmaco a 251 nm aumenti nel tempo, fin quando non si raggiunge il 100% di rilascio. La figura 12 riporta la cinetica di rilascio del farmaco in termini di percentuale di farmaco rilasciato rispetto alla quantità iniziale adsorbita. Il profilo mostra che la percentuale di farmaco rilasciata aumenta gradualmente nel tempo fino a 6h dove viene rilasciato circa l'80%, mentre l'asintoto corrispondente al 100% di rilascio viene raggiunto a 24h, rimanendo costante fino ad una settimana.

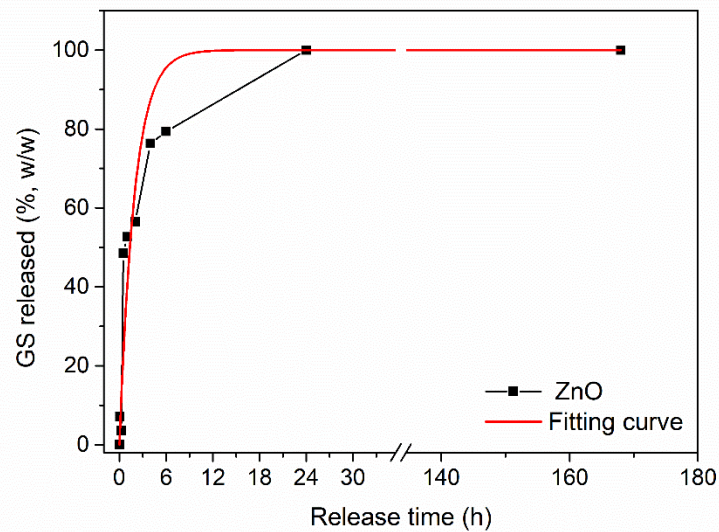


Figura 12: profilo di rilascio GS in SBF da film poroso di ZnO

Il profilo di rilascio segue un modello esponenziale del primo ordine (vedere fitting in rosso), con una costante cinetica di rilascio di 0.52 s^{-1} . In particolare, l'equazione 3 descrive matematicamente il modello del primo ordine:

$$\frac{\%Q_t}{\%Q_\infty} = 1 - e^{-bt} \quad (3)$$

Nell'equazione 3, $\%Q_t$ rappresenta la percentuale di farmaco rilasciata al generico tempo t , $\%Q_\infty$ è la percentuale totale di farmaco rilasciato e di conseguenza il loro rapporto è la frazione di farmaco rilasciato al generico tempo t , b è la costante cinetica di rilascio, mentre t è un tempo generico. Tale modello permette di affermare che il meccanismo di rilascio della gentamicina solfato è regolato dalla diffusione. Infatti il modello deriva dall'integrazione dell'equazione 4 che rappresenta l'equazione di Noyes – Whitney:

$$\frac{dC_t}{dt} = kS(C_s - C_t) \quad (4)$$

Nell'equazione 4, C_t è la concentrazione del farmaco al tempo t , S è la superficie specifica delle particelle di farmaco, C_s è la solubilità del farmaco alla temperatura di prova e k è una costante di proporzionalità. Tale costante dipende dal coefficiente di diffusione D e dalla geometria dei pori per mezzo della prima legge di Fick.

Rilascio GS in SBF da film porosi di ZnO ricoperti da uno strato di GO

La deposizione dell'ossido di grafene come strato ricoprente i film porosi di ossido di zinco è stata effettuata con l'obiettivo di ottenere un sistema capace di rilasciare il farmaco più lentamente rispetto al caso del film di ZnO tal quale. Infatti, una cinetica di rilascio controllato è un aspetto fondamentale in parecchie applicazioni di drug delivery. I fiocchi di ossido di grafene sono stati depositati dopo il processo di adsorbimento del farmaco nella matrice di ZnO, di conseguenza la loro presenza non influenza la quantità di farmaco adsorbita. Anche in questo caso il tempo di adsorbimento ottimale è di 2h e la quantità adsorbita è di circa 800 ug. Per poter avere un confronto idoneo col caso precedente, le condizioni applicate in termini di agitazione orbitale, temperatura e tempi di prelievo sono stati i medesimi. La figura 13 riporta il profilo di rilascio del sistema ZnO-GO.

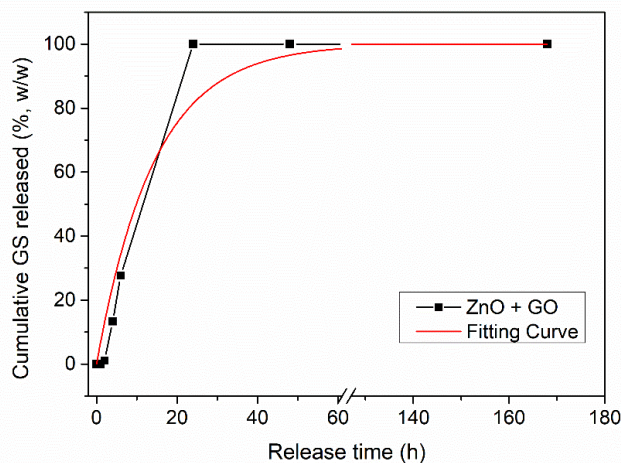


Figura 13: profilo di rilascio GS in SBF da ZnO-GO poroso

Anche in questo caso il profilo di rilascio segue un modello esponenziale del primo ordine descritto dall'equazione:

$$\frac{\%Q_t}{\%Q_\infty} = 1 - e^{-bt}$$

In questo caso, la costante di rilascio ottenuta è pari a 0.07 s^{-1} , un valore più basso rispetto al caso precedente (0.52 s^{-1}) e che ben rappresenta il rallentamento nel processo di rilascio. La Figura 14 riporta il confronto tra i profili di rilascio nei due casi a diverse scale temporali. Si può notare come nel sistema ZnO-GO la quantità di farmaco rilasciato sia circa zero durante la prima ora e raggiunge circa il 30% dopo 6h mentre nel sistema formato dal solo ZnO dopo 6h si raggiunge circa l'80%. Tuttavia anche nel caso ZnO-GO, dopo le 24h si raggiunge il 100% di rilascio, che rimane costante fino a 7 giorni. Di conseguenza, si può affermare che la presenza dell'ossido di grafene, grazie alla sua particolare struttura, offre un effetto barriera alla cinetica di rilascio del farmaco almeno durante le prime ore. Il raggiungimento del 100% di rilascio entro le 24h è probabilmente dovuto al parziale distacco dei fiocchi di GO causati dalla sua natura idrofila e dal legame debole formato con la struttura di ZnO.

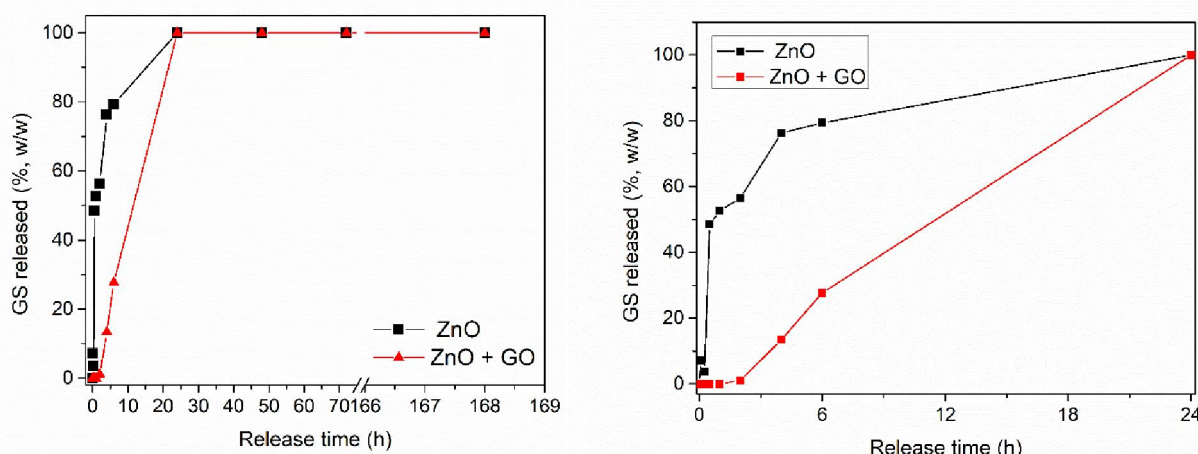


Figura 14: confronto tra i profili di rilascio di GS nei sistemi ZnO e ZnO-GO a diverse scale temporali

Conclusioni

Nel presente lavoro di tesi sperimentale sono state investigate le proprietà di adsorbimento e rilascio dell'antibiotico gentamicina solfato da parte di film porosi sottili di ossido di zinco tal quali e ricoperti da uno strato di ossido di grafene. È stato mostrato come il comportamento a degradazione della matrice di ossido di zinco è fortemente accentuato in presenza di soluzioni acide, quali la soluzione di farmaco in acqua. Questo influenza negativamente la struttura del materiale, soprattutto in termini di porosità, sfavorendo di conseguenza il processo di adsorbimento che è favorito invece in presenza di una soluzione bufferata (SBF). In particolare, è stata studiata l'influenza del tempo sulla quantità di farmaco adsorbita, trovando il valore di 2h come tempo ottimale. In queste condizioni, la quantità di gentamicina adsorbita è stata pari a circa 800 ug rispetto ai 1250 ug della soluzione di partenza. Il sistema dunque mostra una discreta efficienza di adsorbimento. A partire dalla quantità di farmaco adsorbita, il rilascio dello stesso fino a 7 giorni è stato valutato in SBF sia nel caso di film di ZnO puro, sia nel caso di film di ZnO ricoperto da GO. È stato mostrato come in entrambi i casi il rilascio totale del farmaco avvenga entro le 24h. Tuttavia la presenza del GO, che funge da barriera parziale nei confronti della matrice porosa di ZnO e quindi del farmaco, permette di ottenere una cinetica di rilascio piuttosto lenta nelle prime ore rispetto al rilascio ottenuto col solo ZnO.

In conclusione, i risultati hanno mostrato che film porosi di ossido di zinco, combinati con la presenza di fiocchi di ossido di grafene, potrebbero offrire un efficiente sistema per le applicazioni nel drug delivery. Per il futuro, la dimensione e la morfologia dei pori o la struttura superficiale della matrice dovrebbero essere ingegnerizzate, sfruttando ad esempio la chimica di superficie dello ZnO stesso o variando le condizioni di sputtering, in modo da raggiungere un controllo intelligente e remoto dell'intera cinetica di rilascio del farmaco. Inoltre, ulteriori test sulla biodegradazione completa dei rivestimenti di ZnO e sulle sue proprietà antibatteriche permetterebbero l'ottenimento di un rivestimento nanostrutturato programmabile e intelligente per le future generazioni di impianti biomedici.

Contents

| | | |
|-------|--|----|
| 1. | Introduction..... | 1 |
| 2. | Background theory..... | 3 |
| 2.1 | Zinc Oxide | 3 |
| 2.2 | Graphene Oxide..... | 8 |
| 2.3 | Gentamicin sulfate..... | 10 |
| 3. | Materials and methods | 13 |
| 3.1 | Preparation of porous ZnO thin films by radio frequency magnetron sputtering.... | 13 |
| 3.2 | Synthesis and deposition of graphene oxide flakes on porous ZnO structures..... | 15 |
| 3.3 | Simulated body fluid (SBF)..... | 15 |
| 3.4 | Characterization setups..... | 16 |
| 3.4.1 | Field Emission Scanning Electron Microscopy (FESEM)..... | 16 |
| 3.4.2 | X-Ray Diffraction (XRD) | 18 |
| 3.4.3 | Inductively Coupled Plasma (ICP) mass spectrometry..... | 19 |
| 3.4.4 | Energy-Dispersive X-Ray Spectroscopy (EDS) maps..... | 21 |
| 3.4.5 | Fourier Transform Infrared (FT-IR) spectroscopy | 22 |
| 3.4.6 | Uv-Vis spectroscopy | 22 |
| 4. | Characterization of materials..... | 23 |
| 4.1 | Porous ZnO thin films | 23 |
| 4.2 | Graphene oxide-coated porous ZnO thin films | 28 |
| 5. | Uptake of gentamicin sulfate | 33 |
| 5.1 | Uptake of gentamicin sulfate on porous ZnO thin films | 33 |
| 5.1.1 | Uptake of gentamicin sulfate in DI water | 33 |
| 5.1.2 | Uptake of gentamicin sulfate in SBF | 42 |
| 5.2 | Uptake of gentamicin sulfate on graphene oxide-coated porous ZnO thin films..... | 51 |
| 6. | Release of gentamicin sulfate | 53 |
| 6.1 | Release of GS from porous ZnO thin films | 53 |
| 6.2 | Release of GS from GO-coated porous ZnO thin films | 62 |
| 7. | Conclusion | 69 |
| | References..... | 70 |
| | Websites..... | 73 |

1. Introduction

In recent years, the interest in designing new implantable medical devices able to deliver drugs and biomolecules in a controllable way increased continuously. This is mainly due to the ever increasing need for rapidly and effectively treating those adverse reactions that occur in the human body after their implantation. Indeed, despite their therapeutic benefits, implantable devices generally induce the rise of different body reactions, including infections, inflammations and lack of tissue integration, finally leading to the complete implant rejection by the body in the worst case.

Generally, the purpose of a controlled drug delivery system is the ability to target specific locations in the body, regulate the temporal drug profile for maximum therapeutic benefits, and finally to limit the arise of potentially undesirable side effects by reducing drug concentrations at non-target sites. For such purposes, the use of nanostructured materials as carriers for the controlled delivery and release of drugs and biomolecules is representing an effective approach for the treatment of several diseases such as autoimmune and metabolic diseases, cancer, dominant genetic disorders and viral infections [1]. In particular, porous nanomaterials show outstanding characteristics such as high surface areas quantum confinement and surface effects, which can positively affect their chemical reactivity and other physical and chemical properties [2-3]. Indeed, most of the atoms positioned at the material's surface coupled with high surface area, effectively maximize their ability to be loaded with therapeutic drugs and to deliver these agents to target cells and tissues.

One of the most interesting applications of high-surface-area nanomaterials is their use as porous coatings in implantable devices for drug delivery. Thus, both the need to improve implants biocompatible properties and further raise their performances in terms for example of local drug delivery or antibacterial resistance have attracted the major attention of research on nanotechnologically-coated implants. These implants can be viewed as a combination product of drug/medical devices which is a new approach in therapeutics. Combination products allowing localized drug delivery have been used in a diversity of treatments from cardiovascular diseases to diabetes [4]. Device and drug combinations can be projected to rise the performance and life time of presently used implants, resulting in improved patient's life quality [4]. Drug-releasing implantable devices are characterized by some important features such as biocompatibility, biostability and ability to load and release drugs efficiently. The most common materials used in this field are polymers [5] and more recently carbon-based materials, such as graphene and graphene oxide [6], but also hard materials such as alumina [7], titania [8] and porous silicon [9] materials. An example of these devices are drug-eluting cardiovascular stents which have the ability of releasing single or multiple bioactive agents into the bloodstream and surrounding tissue. For specific applications, such as regenerative tissue or to avoid changing the implant, the ideal material

should be biodegradable in a predictable way. The materials above mentioned have not this feature, thus, the research of new materials satisfying all possible features is necessary to improve the quality of implants.

This experimental thesis is inserted into this context. The aim of this work is the study of drug uptake and release properties of porous and biodegradable zinc oxide (ZnO) thin films, deposited by radio-frequency (RF) magnetron sputtering technique, as coating for biomedical implantable devices ranging from the cardiovascular to orthopaedic or urological fields. Gentamicin sulfate (GS), a well-known antibiotic molecule, has been selected as drug for all the experiments.

In the first part of the work, the interaction between porous ZnO thin films and different GS uptake solutions has been investigated. In particular, two separate sets of experiments have been performed, starting from GS in deionized water (GS/DIW) and GS in simulated body fluid (GS/SBF). In both the cases, the effect of uptake solution on the degradation behaviour of the porous ZnO thin film structure has been studied. Then, by changing the soaking time, the loading ability of the porous ZnO nanostructures has been evaluated as well. Once identified the optimal uptake conditions, i.e. GS solution and time of uptake, the release of loaded drug has been investigated in Simulated Body Fluid (SBF), a fluid capable to simulate the inorganic physiological composition of plasma in the human body. Both during the uptake and the release processes, the transport mechanism of GS was a diffusion behavior and physisorption interaction with the ZnO surface.

In the second part of the work, similar experiments have been repeated using porous ZnO thin films covered on the surface by graphene oxide (GO) flakes. In particular, GS was loaded on the porous ZnO thin films and then GO flakes were deposited on the sample surface. Finally, the GS release profile was evaluated and the kinetic release compared with the one obtained in absence of the GO coating. It was found that GO is able to produce a “barrier effect”, slowing down the release rate and allowing for a better control of the drug delivery process. Before and after drug loading and release experiments, all the samples have been properly characterized in terms of morphology, chemical composition and crystal structure.

The results showed that porous ZnO thin films, combined with the presence of GO flakes, could serve as an efficient system for drug-delivery applications. For the future, the pore chemical structure or pore entrances should be further engineered in order to achieve a smart and even remote control over the drug delivery kinetics. Furthermore, tests on the final biodegradation of the ZnO coating and its antibacterial properties would corroborate to obtain a smart and programmable nanostructured coating for the next-generation of biomedical implants.

2. Background theory

2.1 Zinc Oxide

Physical and chemical properties

Zinc oxide (ZnO) is an inorganic chemical compound, that at room temperature appears as odourless white solid. It is a biocompatible semiconductor of the II-VI group [10] explored in multiple areas thanks to its interesting properties such as a wide band-gap energy of 3.37 eV, absorption of light in the UV range, a high electron mobility, a high thermal conductivity [11] and a strong luminescence at room temperature. ZnO is well-known also for its piezoelectric and pyroelectric properties [12]. These last features are due to its particular crystalline structure. Actually, ZnO presents different crystal structures depending thermodynamic conditions. At ambient conditions, the thermodynamic stable phase is the wurtzite structure, see Figure 2.1 and showing an hexagonal unit cell. Here, each single Zn atom (grey dots) is tetrahedrally coordinated with oxygen atoms (yellow dots). The cell parameters or reticular constants of an ideal wurtzite structure are $a = 3,81 \text{ \AA}$ and $c = 6,23 \text{ \AA}$. The cell parameter of the base plan (the length of the edge of the hexagonal base) is universally indicated with a while the cell parameter perpendicular to the hexagonal base (height of unit cell) with c .

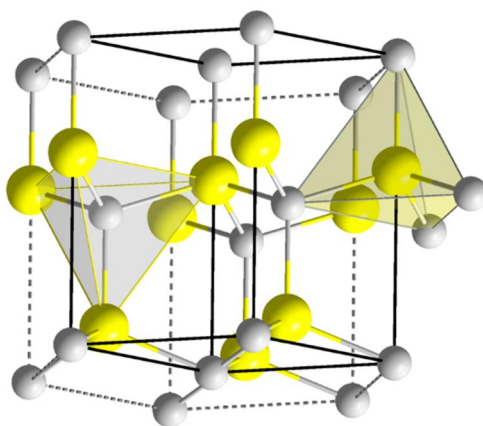


Figure 2.1: Wurtzite crystal structure for ZnO.

reacts with various chemical species. Particularly, an increase of surface area furnished an improvement of adsorbent, and catalytic properties. The positioning of majority atoms in the surface of materials lead to improve the surface reactivity in order to maximize their capability to be loaded with small molecules to deliver them to target cells, tissues and the specific organ in the body depending by kind of applications. Another important feature for use of ZnO nanomaterials in drug delivery applications is the electrostatic characteristics of the surface. In particular zinc oxide nanomaterials usually have neutral hydroxyl groups on their surface, which play a key role in surface charge behaviour. In fact in aqueous

environment and at high pH value, the chemisorbed protons (H^+) move out from the particle surface leaving a negatively charged surface with partially bonded oxygen atoms (ZnO^-). At lower pH, protons from the environment are presumably transferred to the particle surface, leading to a positive charge from surface $ZnOH_2^+$ groups. The isoelectric point of 9–10 [13] indicates that ZnO nanoparticles will have a strong positive surface charge under physiological conditions. The concentration of different chemical group ($ZnOH_2^+$, $ZnOH$, ZnO^-) on the surface of ZnO nanoparticles is pH dependent [14]. These chemical reactive groups allow anchoring of therapeutic agents, typically driven by electrostatic or H-bond interactions, which can lead to drug-delivery application and finally to the efficacy of treatment.

Synthesis methods of ZnO nanostructures and general applications

One of the most important features of ZnO nanostructures is the easiness of synthesis in a multiplicity of morphologies and with different sizes. Figure 2.2 [12] shows some of possible shapes of ZnO nanostructures, including nanoparticles which have approximately spherical shape (NPs), two-dimensional mesoporous thin films, one-dimensional nanowires, which present a cylindrical cross section of less than 100 nm but can be long hundreds of micron. At the same class of one-dimensional ZnO nanostructures belong nanotubes which have a hollow interior. Also exist nanorings, tetrapods and flower-like ZnO morphologies.

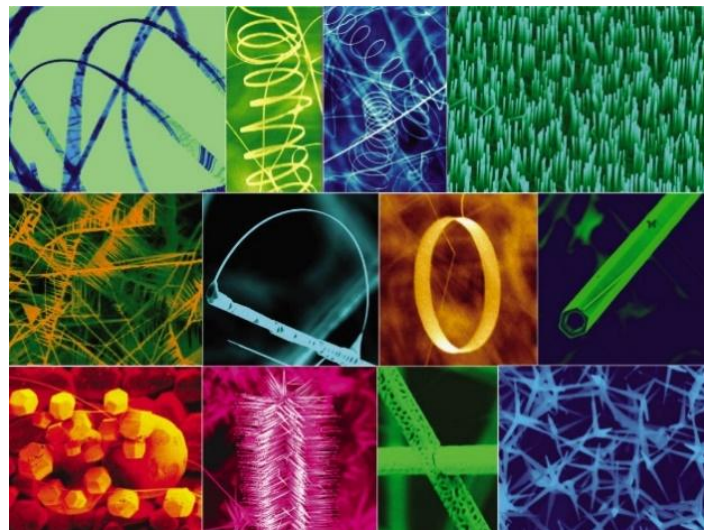


Figure 2.2 Some of possible morphologies of ZnO nanostructures [16].

Concerning the preparation methods, wet chemical approaches including electrodeposition, sol-gel and hydrothermal growth have been widely used for their low costs, low temperature processes and high versatility. On the other hand, vapor-phase methods like chemical vapour deposition and physical vapour deposition [15] are used because allow for an optimal control of process, reproducibility, high crystalline quality and minimum contamination, leading to a good purity of the final product. Some studies demonstrated that ZnO porous membranes, ZnO tubes and ZnO nanowires have been obtained by electrochemical deposition [16], hydrothermal solution synthesis [17] and high temperature vacuum-deposition technique [18].

It is widely recognized that potential applications of ZnO nanostructures depends, not only on the combination of physical-chemical properties with their high surface area, but also on other crucial parameters such as crystal orientation, morphology, size, density of crystals and consequently by synthesis methods. ZnO nanostructures show chemical sensitivity to volatile and other radical gases, possibility to doping, non-toxicity and low cost. These features permit their use as gas sensor [19]. ZnO nanowires with a typical length that can vary from 100 μm to 1 mm and diameter in the range of 50-500 nm show high-porosity, single-crystal wire-like structures and have potential applications as filters, catalyst supports, and gas sensors [20]. On the other hand, ZnO nanoparticles can be used in biomedical applications because of relatively small size, ease of transport within tissues/organs, ability to cross plasma membranes, and potential targeting of biologically active molecules. The application of ZnO nanoparticles in the biological fields requires a certain stability of ZnO nanoparticles in biological aqueous environment at neutral pH and physiological temperature. Also, ZnO thin films produced by deposition technique can have a certain porosity with a pores diameter of about 50 nm which allow to adsorb molecules, for example of pharmaceutical or biological interest. This aspect coupled with the biocompatibility and biodegradation features make them potential materials to be used as drug-eluting coating for biomedical implants.

For these interesting features, porous ZnO thin films have been used in this thesis as samples to study the drug uptake/release properties. The films are made by a huge amount of ZnO nanoparticles interconnected to each others, which is the reason why they are considered nano objects as well. The technique used for its preparation was Radio Frequency (RF) sputtering which has drawn considerable attention for ZnO film fabrication since the resulting film properties can be controlled by changing the sputtering conditions such as substrate temperature, deposition time, pressure, and RF power.

Biocompatibility and drug-delivery properties of ZnO

Different kinds of nanostructured materials with the role of drug carriers have been synthesized in the last decades. Several nanostructures are used in biomedical applications such as bioimaging and drug delivery [21-22] due to their unique properties based on their size similarly with biomolecules, their functionality on large surface areas and their quantum size effects. In the form of nanoparticles with sizes below 200 nm, they are able to enter cells through intracellular endocytic pathway and release drugs at target sites effectively [23-24], especially if the drug itself cannot be taken up by cells. The control of releasing process is affected by different parameters such as pH [25], temperature [26] and light [27]. The pH of tumors and inflammatory tissues are lower than the value of pH in blood and healthy tissues. Therefore, pH-responsive systems are suitable for this application. However, most of these semiconductor nanomaterials are toxic in animals and their biocompatibility is poor in-vivo [28]. Recently, ZnO nanostructures have been also considered because these present typical properties of nanomaterials which allow to load small molecules and reacts with various chemical species on their surface. Moreover, ZnO nanostructures also show an optimal degree of biocompatibility. Hence, these can be considered as a new type of low toxicity and low cost material, fully employable in biomedical applications as drug delivery.

Drug-delivery applications of ZnO nanostructures mostly deal with the use of nanoparticles for releasing anticancer agents. Recently, ZnO quantum dots loaded with doxorubicin (DOX) as a drug were demonstrated to be an effective drug carrier characterized by an initial rapid drug release followed by a controlled release in-vitro [29]. In this study, ZnO nanoparticles were encapsulated within chitosan, a polymer with drug release properties, to improve the stability of ZnO nanomaterial due to hydrophilicity and cationic charge characteristics of chitosan. Also, ZnO tetrapod-like nanostructures have been projected as new carriers for gene delivery. These functionalized tetrapods, consisting of silica-coated amino-modified tetrapod-like ZnO nanostructures, showed the capacity to effectively link plasmid DNA with electrostatic interactions and allows the transfection of A375 cells [30], a human melanoma cell line used in cytokine research. Another study is the synthesis of polycation-capped ZnO quantum dots which allowed to mediate efficient DNA transfer into COS-7 cells, a fibroblast-like cell lines derived from monkey kidney tissue, and allow for real-time imaging of gene transfer at the same time [31]. Alternatively, ZnO can be used in combination to other nanomaterials in order to obtain a composite nanostructured system showing improved performances for drug delivery applications. In this regard, a composite nanomaterial formed by mesoporous silica nanoparticles (MSNs) with doxorubicin (DOX) into the pores, and ZnO quantum dots as nanolids covering the pores [32]. This represent a pH-responsive system used to release DOX to HeLa cells in vitro. In particular, to assemble the system, the MSNs and ZnO quantum dots were functionalized with specific group. Whereas ZnO quantum dots had cationic surface groups and DOX molecules were cationic they were adsorbed by the anionic surface of MSNs. The system was stable in neutral environment at pH value of 7.4 and the release of DOX did not occurs. However, in acidic

solution ($\text{pH} \approx 4.5\text{--}5.0$) ZnO nanolids were decomposed and the drug was released to kill Hela cells.

However, the capacity of MSNs to load and release drug was found to be not very satisfactory. In particular, residual DOX in the MSNs was observed at the end of the release process. This aspect, coupled with the limited degradation of the carrier, could potentially give toxicity problems in in-vivo systems. In fact, in an efficient drug delivery system it is necessary to have biodegradable nanostructures having a good drug loading ability and complete delivery. To this purpose, a ZnO-polymer-DOX composite system have been developed [33]. In this case, biocompatibility properties and a high drug loading capacity were observed. In this case, DOX was released correctly to destroy DNA, while Zn^{2+} ions were released from lysosomes and enriched by zinosomes in the cytoplasm [33]. This aspect is very important avoiding possible cytotoxic effects because Zn^{2+} ions are used by body for different activities. It is essential in metabolism and immune processes; also it is a member of biologically active substances like hormones and enzymes, nucleotides, lipids and esters.

In this regard, biocompatibility is one of the most important features for biomedical applications. ZnO nanomaterials with an average size at least larger than 100 nm, are considered to be relatively biocompatible, with bulk ZnO being recognized as a GRAS (generally recognized as safe) substance by the FDA, making ZnO an optimal choice for drug delivery applications. Biocompatibility of ZnO nanostructures is tightly related to their dissolution behaviour in biological fluids and consequently with concentration of Zn^{2+} ions [34]. Specific concentrations of Zn^{2+} ions are expected to be well tolerated from human cells because about 10 mg/day of Zn^{2+} is necessary in adults for functions above mentioned. This aspect was confirmed in many studies, which demonstrated a high degree of biocompatibility for various ZnO nanostructures. For example, ZnO nanowires showed biodegradation into products (Zn^{2+} ions) that could be safely absorbed from the body, becoming part of the nutritional cycle. In some cases, the specific surface charge properties of ZnO nanostructures could be effective to modify the outer ZnO surface with suitable polymers. This finally allowed to increase the stability of ZnO nanocarrier in “danger” environments like biological fluids, and consequently optimize their biocompatibility [35].

2.2 Graphene Oxide

Graphene oxide (GO) is a unique material that can be viewed as a single layer of graphite terminated by various functional groups such as epoxide, carbonyl, carboxyl and hydroxyl ones. Graphene oxide thanks to unique geometry and structure, see Figure 2.3 (b), has outstanding physical and chemical properties such as large surface area, optimal thermal and electrical conductivity, a high Young's modulus, a high fracture strength. These features make it an interesting material in many applications, including quantum physics, nano-electronics, energy storage, catalysis and as biomaterial for biomedical applications. [36]

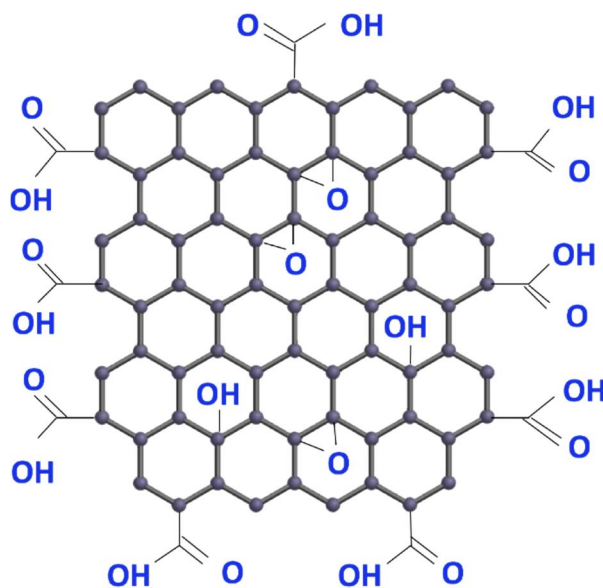


Figure 2.3: Chemical structure of graphene oxide

Recently, various nanomaterials with different sizes, shapes and chemical composition have been used as nanocarriers for delivery of therapeutic molecules. These include metal and metal oxide nanoparticles, polymeric micelles, liposomes, dendrimers and carbon nanotubes [37]. Among them, graphene and GO, have been successfully investigated as well as new and competitive drug delivery systems, due to their favorable properties. Particularly, their planar structure offers a great capacity to immobilize several substance like drugs, biomolecules, metals and fluorescent probes [36]. Others important features are low cost, easiness to synthesis and modification, a high surface area in the lateral dimension, layer number and surface chemistry. Regarding the surface area ($2600 \text{ m}^2 \cdot \text{g}^{-1}$), it is four times higher than the surface of any materials used for drug delivery applications. A monolayer of graphene is an extreme case where the number of atoms on surface is the highest, showing an outstanding capacity to load drugs and molecules. A large number of layers reduces the surface area, but improves the rigidity to penetrate cells and tissues. Concerning the surface chemistry, GO is hydrophilic and can be dissolves in water forming stable colloids. However, it aggregates in physiological buffers in the presence of salts due to the charge screening effect. For good biocompatibility in a biological environment it is necessary to modify the surface of GO. Essentially, two possible methods for surface modifications are covalent and non-covalent methods. The first is carry out through some

technique such as reaction with oxygen groups formed by destruction of unsaturated structure of graphene or atom doping. The second method uses Van Der Waals forces and electrostatic bond.

For these features, GO has generated great interest in biomedical applications as excellent drug delivery platform for anti-cancer/gene delivery and chemical-controlled drug delivery. Figure 2.4 provides an overview of the general scheme for drug delivery systems based on GO and graphene. These have been successfully used to deliver different therapeutic agents, from small drug molecules to antibodies, DNA, proteins and genes.

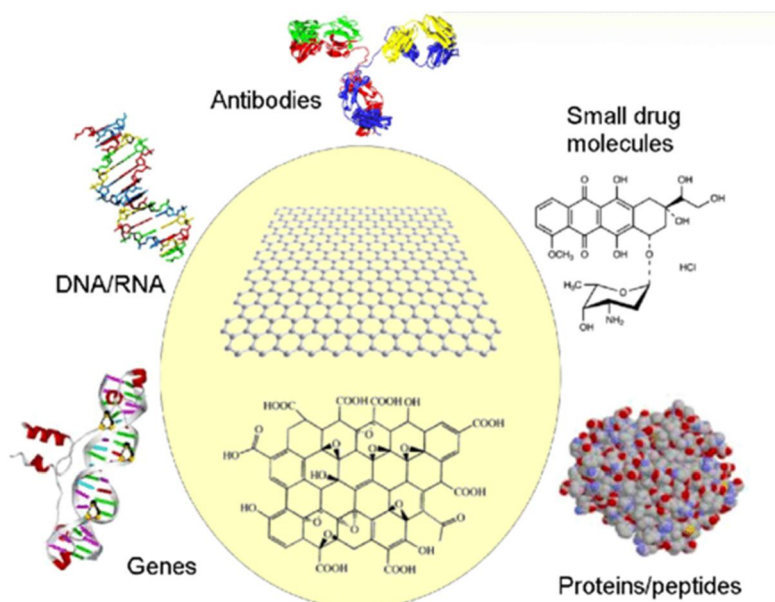


Figure 2.4 Scheme of application of graphene and GO for drug delivery of various therapeutic agents and biomolecules.

GO has been used as targeting drug delivery system [38]. In this case GO has been functionalized with sulfonic acid groups in order to improve the GO stability in biological environment. Then, it was linked with a covalent binding to folic acid (FA) molecules in order to target specifically human breast cancer cells with folic acid receptors. The drugs used to be loaded on GO-FA composite system were doxorubicin (DOX) and camptothecin (CPT). They were loaded with p-p stacking and hydrophobic interactions and their results demonstrated that the loaded FA-GO shows specific targeting to MCF-7 cells and remarkably high cytotoxicity compared to GO loaded with either DOX or CPT only. In another experimental work, a GO drug delivery system for anti-cancer therapy was designed. In particular, this system consists in the combination of GO with gold nanoparticles (AuNP) [36]. It was established that DOX loaded on combined system

inhibits HepG2 cell growth more efficiently than DOX or AuNP–GO alone. This means a more efficient transport into the cell by AuNP-GO compared to free DOX.

In this thesis work, the graphene oxide has been deposited from a solution on the porous ZnO samples. Such system was then further evaluated for the gentamicin sulfate uptake/release and compared with the drug uptake/release at the same operating conditions using only ZnO thin films. We expected a slight decrease of drug release due to a partial occupation of samples pores by graphene oxide which would exploit a “barrier effect” delaying the delivery kinetics of the drug.

2.3 Gentamicin sulfate

Gentamicin is an antibiotic from the class aminoglycoside having a wide activity spectrum. It is a bactericidal agent which is used to treat and prevent mycobacterial, enterococcal and severe Gram-negative bacterial infections [39]. Another typical use in clinical applications is against infections arising from orthopaedic surgeries. It is readily soluble in water due to the presence of hydroxyl groups on its chemical structure, while it is insoluble in organic solvents [40].

Gentamicin sulfate has been used as drug in many drug delivery applications. For example, it was studied in smart bioimplants able to release drug under an external stimuli. The stimuli was based on local decrease of pH occurring in case of infection [41]. The antibiotic is engaged onto biomaterial, a titanium alloy, with a pH-sensitive bond. When the infection occurs, the pH decreases locally, the bond is broken allowing the release of gentamicin. In this way the local release of antibiotic limits systemic toxicity and antibiotic resistance. A great challenge in the future will be the production of biomaterials functionalized with multifunctional nanostructures using various drugs in order to avoid antibiotic resistance. In another work, ZnO nanoparticles, prepared through hydrolysis of zinc acetate, were coated with gentamicin sulfate in order to test the biological activity against *Escherichia coli*, *Pseudomonas aeruginosa*, *Staphylococcus aureus*, *Bacillus cereus* and *Listeria monocytogenes*. The ZnO-gentamicin hybrid was carried out by classic method for biocompatible materials. The freshly prepared ZnO was suspended in an aqueous solution of gentamicin and ultrasonicated for 30 min and kept for 24 h under stirring at 80°C. Then, a centrifugation step occurred and the hybrid system dried in air at 80°C.

In our experiments, gentamicin sulfate is the drug used to evaluate the capacity of porous ZnO thin films to first uptake and then release it. Both processes occurred through a diffusion mechanism. The choice of gentamicin sulfate is mainly due to its solubility in aqueous environments, which allows to avoid the use of toxic organic solvents. Figure 2.5 shows the chemical structure of gentamicin sulfate.

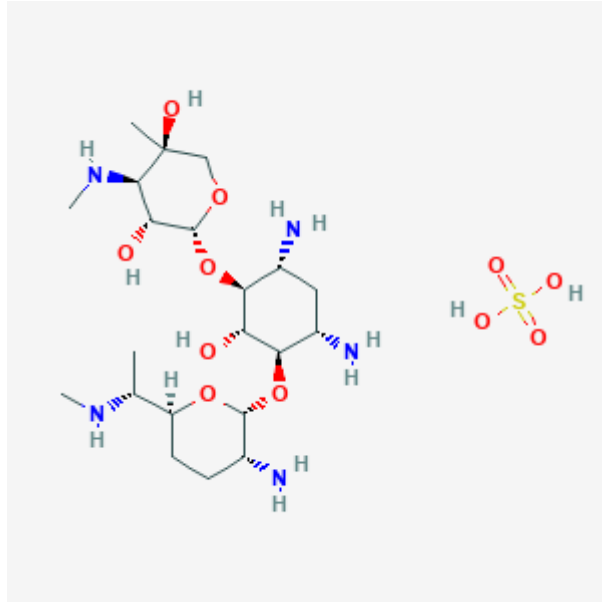


Figure 2.5: Chemical structure of gentamicin sulfate

3. Materials and methods

The aim of this chapter is to illustrate the synthesis methods followed for preparing porous ZnO thin films and porous ZnO thin films covered by a layer of graphene oxide (GO). Also, the various characterization techniques used for the analyses of the prepared materials will be described.

3.1 Preparation of porous ZnO thin films by radio frequency magnetron sputtering

The process followed to prepare porous ZnO thin films consists in the combination of two distinct steps. Briefly, the first one deals with the preparation of metallic Zn layers by a physical vapour deposition approach named sputtering. The second one is a final oxidation treatment in order to convert the starting Zn layers in their corresponding oxide counterparts.

The sputtering technique is a process where atoms are physically extracted from the surface of a solid source, called target, due to the bombardment of the target surface by high-energy particles. These are positive ions coming from the ionization of an inert gas (Ar) present into the deposition chamber. Consequently, it is necessary to provide an electric discharge in order to obtain a plasma made of charged particles. This is obtained by providing an electric signal voltage between a couple of electrodes: the anode, coinciding with the substrate holder, and the cathode, where the target is clamped. The atoms extracted from the target by ionic bombardment are mainly neutral atoms. Therefore, the applied electric field do not affect them. In this way, it is possible to deposit homogenous and uniform coatings on the whole substrate surface.

In this work, the deposition of Zn layers is carried out through a radio-frequency (RF) magnetron sputtering monotarget system. The setup is characterized by a cylindrical stainless steel deposition chamber, a single cathode where the target is clamped facedown and a substrate holder where the samples are placed, facing upwards in direction of the target. These main components are visible in Figure 3.1.



Figure 3.1: View of the inner part of the deposition system.

In order to ensure a high cleaning of the deposition atmosphere and avoid the contamination of thin films due to gases usually present in the air as nitrogen, oxygen and moisture, it is necessary working in high vacuum conditions before starting the deposition process. This requirement is obtained by the presence of a two-stage pumping system connected to the deposition chamber, which allows to reach vacuum base pressures as low as $2 \cdot 10^{-7}$ Torr. The two pumps are connected in series and consist of a rotary pump, to reach low-vacuum conditions (10^{-3} Torr), and a turbomolecular pump, which allow to obtain the desired high-vacuum conditions in the range of 10^{-7} Torr. Once the optimal vacuum conditions have been reached, the process gas (Ar) can be injected in the deposition chamber. A RF signal generator working at frequency of 13.56 MHz is used to generate the plasma while a matching network, necessary to make the reflected power equal to zero, allows to maximize the RF signal power provided to the cathode.

In this experimental work, Si (1 0 0) wafers were used as substrates for supporting porous ZnO thin films. Firstly, the Si substrates were cut into 1 cm x 1 cm pieces. Secondly, the Si substrates were cleaned to improve the adhesion of the ZnO thin films to the substrate surface and avoid the presence of contaminants as well. Acetone and ethanol were used as solvents. The Si substrates were washed in 50 ml of each solvent in ultrasound bath for 10 minutes, then washed with clean solvent and finally dried with nitrogen flow. The parameters used for the sputtering deposition are listed in Table 3.1. The RF power, Ar pressure and flow were set in order to obtain a mesoporous structure within the Zn thin films. A 4"-diameter metallic Zn target is clamped on the cathode and used as the solid source material to deposit metallic Zn layers. After the deposition, the Si/Zn samples were thermally oxidized to convert the Zn films into mesoporous ZnO films. This calcination process also promoted the mechanical and chemical stability of the resulting mesoporous ZnO structures. The oxidation process was carried out at 380 °C for 120 minutes in a muffle furnace. Figure 3.2 shows a picture representative for Zn thin films on Si substrates, obtained after the deposition process.

Table 3.1: Set of deposition parameters for preparing mesoporous Zn thin films

| Target | Vacuum pressure [Torr] | T [°C] | Pressure [mTorr] | RF power [W] | Argon flow [sccm] | Deposition time [min] |
|--------|---------------------------|-----------|---------------------|-----------------|----------------------|--------------------------|
| Zn | $1,7 \times 10^{-7}$ | 21 | 5 | 30 | 10 | 240 |



Figure 3.2: Overview of Zn thin films on Si substrates.

3.2 Synthesis and deposition of graphene oxide flakes on porous ZnO structures

The coating of GO flakes was obtained by drop-casting method. In particular, GO dispersion in water with concentration of 0.5 mg/mL was prepared using a modification of the Hummers method [36]. In particular, a droplet of the GO solution with a fixed volume of 50 μ L was drop-casted on the surface of each ZnO sample. Then, each sample was dried with air overnight, with the aim of favouring water evaporation and adsorption of the GO flakes on the ZnO surface and finally forming a continuous GO layer.

3.3 Simulated body fluid (SBF)

Simulated body fluid (SBF) is a solution able to mimic the inorganic composition of human body plasma thanks to the presence of the same ions with a similar concentration. It is buffered at pH 7.4 and at 36.5 $^{\circ}$ C. Table 3.2 gives a comparison between the ions concentration in the SBF and in the plasma.

Table 3.2: Comparison between ions concentration in SBF and in human body plasma

| Ion | Simulate Body Fluid | Blood plasma |
|--------------------------------|---------------------|--------------|
| Na ⁺ | 142.0 | 142.0 |
| K ⁺ | 5.0 | 5.0 |
| Mg ²⁺ | 1.5 | 1.5 |
| Ca ²⁺ | 2.5 | 2.5 |
| Cl ⁻ | 148.8 | 103.0 |
| HCO ³⁻ | 4.2 | 27.0 |
| HPO ₄ ²⁻ | 1.0 | 1.0 |
| SO ₄ ²⁻ | 0.5 | 0.5 |

For obtaining this solution, one litre polyethylene bottle was filled with 500 ml of ion exchanged and distilled water and a magnetic stirrer into it for dissolving the reagents. The reagents are added as shown in the Table 3.3:

Table 3.3: Reagents for preparing SBF solution

| Order | Reagent | Amount |
|---|--|---------------|
| 1 | NaCl | 7.996 g |
| 2 | NaHCO ₃ | 0.350 g |
| 3 | KCl | 0.224 g |
| 4 | K ₂ HPO ₄ ·3H ₂ O | 0.228 g |
| 5 | MgCl ₂ ·6H ₂ O | 0.305 g |
| 6 | 1M-HCl | 40 mL |
| (About 90 % of total amount of HCl to be added) | | |
| 7 | CaCl ₂ | 0.278 g |
| 8 | Na ₂ SO ₄ | 0.071 g |
| 9 | (CH ₂ OH) ₃ CNH ₂ | 6.057 g |

Once all the reagents were dissolved, the temperature was adjusted at 36.5 °C with a water bath and the pH adjusted at 7.40 by stirring the solution and titrating 1N · HCl solution. After that, a transfer of the solution to a volumetric glass flask and an adjustment of the total volume of the solution to one litre by adding ion exchanged and distilled water and shaking the flask at 20 °C were done. [37] Finally, the bottle was stored in the refrigerator at 5°C and used within one month from the production.

3.4 Characterization setups

3.4.1 Field Emission Scanning Electron Microscopy (FESEM)

The surface morphology of mesoporous ZnO and ZnO-GO thin films was evaluated by using a MERLIN FESEM from Carl Zeiss. After cleavage of the samples, cross-section imaging was also performed to evaluate the average thickness of the materials.

The field emission scanning electron microscopy (FESEM) is a particular kind of electron microscopy. Concerning its working principle, it based on a field emission cathode in the electron cannon of microscope which supply more narrow beams at high or low electron energy in order to play down both sample damage and charging and at the same time improve spatial resolution.

It is a very powerful tool able to detect meticulous information regarding the morphology and the composition of analyzed materials at enlargement of 12x to 900,000x, with a depth of field unlimited.

In this thesis, scanning electron microscopy analyses have been used in order to evaluate the possible changing in the morphology of the ZnO samples after the soaking in the various solutions. The instrument used was SUPRA™ 40 (ZEISS), an extremely versatile FESEM able to deliver high quality imaging resolutions, as request in the present field of nanotechnology. Table 3.4 shows the parameters of instrument.

Table 3.4: SUPRA™ 40 (ZEISS) parameters

| Nominal resolution at 10kV and WD= 2mm | Probe current | Accelerat ion ion voltage | Enlargment | Working Distance |
|--|---------------|---------------------------|---------------|------------------|
| 1.5nm | 4pA– 10nA | 0.1 – 30 kV | 12 – 900,000X | 1 – 50mm |

The sample holder can host nine stubs. Each stub can contain samples of about 1 cm².

Figure 3.3 shows the equipment with the course of electrons.

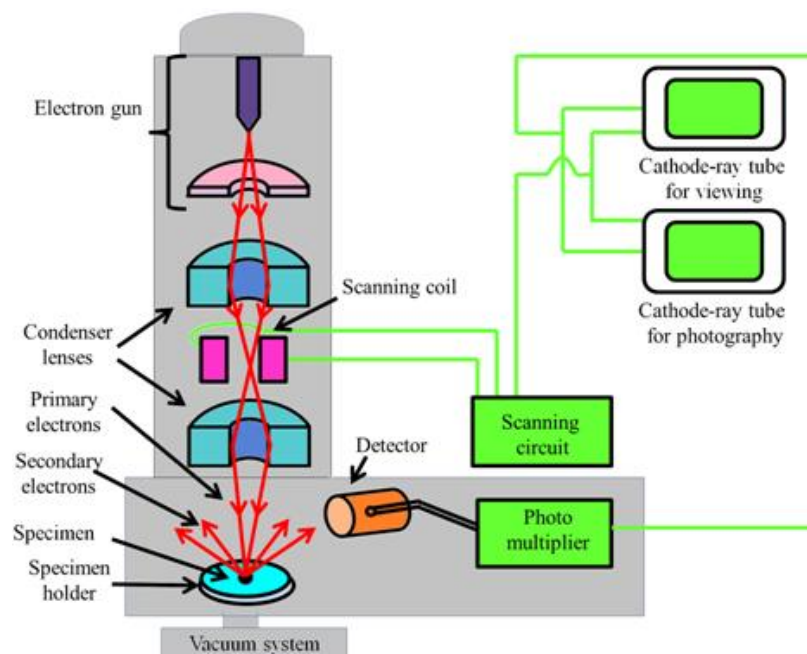


Figure 3.3: FESEM equipment with course of electrons

3.4.2 X-Ray Diffraction (XRD)

X-Ray Diffraction measurements were performed to analyze the crystal structure and orientation of the raw materials and after the drug uptake/release experiments. XRD was carried out by means of a Panalytical X'Pert PRO diffractometer in Bragg-Brentano configuration, equipped with a Cu K α monochromatic radiation ($\lambda = 1.54059 \text{ \AA}$) as X-ray source. The XRD patterns were collected in the range of 10° - 60° 2θ angle, with an acquisition time of 10 min and a step size of 0.026° .

X-ray diffraction (XRD) is an analysis suitable to determine the crystallinity of a material. It is mainly used for different scopes:

- Identification of different polymorphic forms
- Identification of crystal structure materials
- Quantify the crystallinity degree of samples
- Differentiate among crystalline and amorphous materials

This method is characterized on the interaction between monochromatic X-rays and a crystal structure of the sample capable to create a constructive interference. The equipment consisting in a cathode ray tube able to generate the X-rays, which are filtered in order to produce a monochromatic radiation, collimated to result spatially localized and finally directed in direction of the sample.

Only when working conditions verify the Bragg's Law ($n\lambda=2d \sin \theta$), the interaction among sample and incident rays generate the constructive interference and a diffracted ray. Particularly, the Bragg's law takes into account the dependence of wavelength λ of electromagnetic radiation with the angle of diffraction θ and reticular distance in a crystalline sample.

A typical XRD analysis produced a characteristic x-ray diffraction pattern, which represent a unique "fingerprint" of the crystal structure of the sample. Consequently, the fingerprints enable the identification of crystalline structure as a result of the comparison between the standard reference patterns and the measurement.

XRD analysis give as result a diffractogram where it reports the intensity of diffracted beam in function of the diffraction angles (2θ). With this analysis it was expected to obtain the diffraction peaks corresponding to ZnO crystalline structure.

Figure 3.4 shows the application of Bragg Law, where n is an integer, λ is the wavelength of the X-Ray incident and d is interplanar spacing.

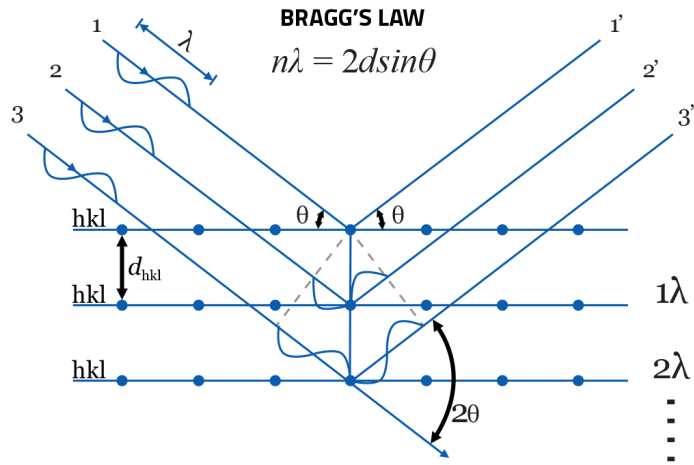


Figure 3.4: Application of Bragg's law

3.4.3 Inductively Coupled Plasma (ICP) mass spectrometry

Inductively Coupled Plasma Mass Spectrometry (ICP-MS) is a versatile and sensible technique able to determine the majority of periodic table elements present in concentration lower to a part of billion. It uses the combination of plasma torch ICP to produce the ionization of atoms belonging to sample and a mass spectrometry in order to separate and detect the produced ions. In this thesis ICP-MS analyses were carried out to evaluate the release of Zn ions from the mesoporous ZnO samples during drug uptake experiments, and due to ZnO degradation. ICP-MS analyses were performed by using an ICP-MS instrument (mod. 7500cc, AGILENT TECHNOLOGIES, Milan, Italy). The use of plasma has several advantages in fact the ionization take place in an inert chemical environment, also the ionization process is complete and the torch has a temperature profile uniform. Figure 3.5 shows a scheme of ICP torch with the sample.

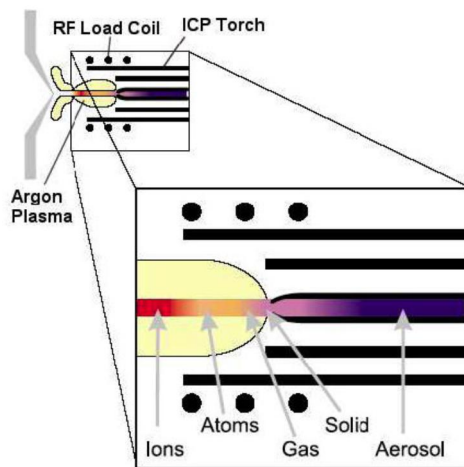


Figure 3.5: ICP Torch with the fate of the sample

Firstly, the sample is introduced in the equipment. There are several insertion methods which depends by physical features of the sample. Typically, the samples are introduced into the ICP plasma torch in a liquid form or as an aerosol by liquid aspiration or dissolution of the sample into a nebulizer. In the case of solid samples, the introduction can be carried out using a laser in order to convert solid sample into an aerosol.

ICP torch is equipped with a copper induction coil wrapped around a concentric quartz structure. The gas used to produce the plasma is Argon. Argon gas is continuously flowing in the quartz torch and a radio-frequency (RF) generator provides power to the RF coil at oscillating frequencies. Once produced the plasma, it reaches an equilibrium at temperature of about 6000 °C. The aerosol enters in contact with high temperature plasma, where it undergoes to the atomization process. These atoms travel continuously through the plasma, absorb energy and consequently they are ionized.

Secondly, these formed ions travel out of the torch and come to mass spectrometry through the interface cones. Consequently, the interface portion of instrument allows the coupling between MS and ICP. At the interface, there are two interface cones within which the pressure is reduced, which allow to enter in the mass spectrometry at desired pressure and temperature conditions. In details, the plasma gas at high temperature enter in a first cone, called sampler, a small orifice where there is a quick cooling and so a quick expansion of the gas. Then, a part of this gas pass in a second cone, called skimmer, in order to reach the optimal thermodynamic conditions. Figure 3.6 shows a scheme of interface cones.

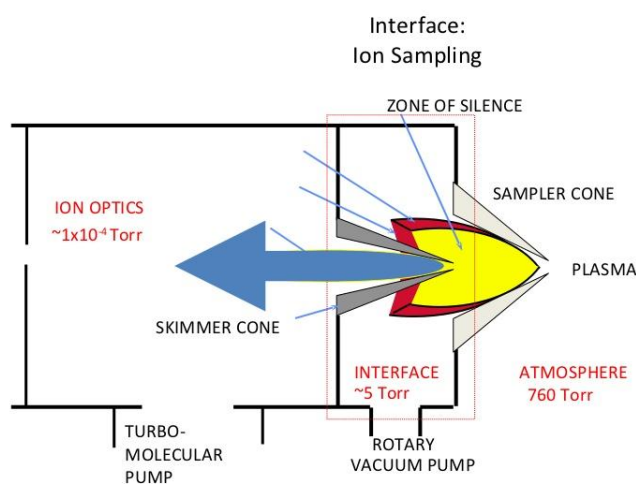


Figure 3.6: Interface region of ICP-MS

Once passing through interface cones, the ions are focused into the mass spectrometry by electrostatic lenses present in the system. Here, they are separated by their mass/charge ratio. The mass spectrometry more common is the quadrupole mass filter, formed by four parallel cylindrical rods, which function as electrodes. Figure 3.7 shows a typical quadrupole mass filter.

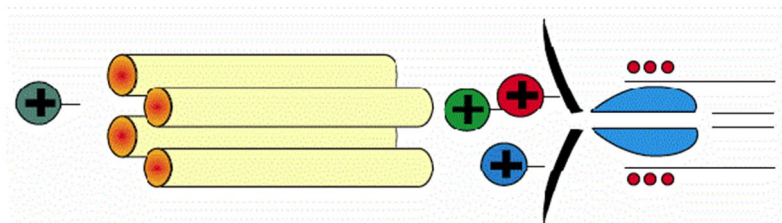


Figure 3.7: Scheme of quadrupole mass filter

3.4.4 Energy-Dispersive X-Ray Spectroscopy (EDS) maps

The chemical composition of the samples was investigated by Energy Dispersive Spectroscopy (EDS), using a desktop SEM Phenom XL (Phenom-World B.V. Eindhoven, The Netherlands) equipped with an EDS analyzer. For each detected chemical element, the corresponding EDS map was acquired on a 1000X SEM image, with a resolution of 128 pixels and an acquisition time of 20 ms for pixel.

Energy dispersive X-ray spectroscopy is an analytical technique allowing the chemical characterization of the sample. It is generally integrated within an electron microscope, both TEM and SEM, so offering the great advantage to determine the elemental composition of the samples, in terms of quantity and distribution. It is based on the interaction between the incident primary electron beam and the sample, which consequently emits X-Ray. These X-rays are characteristic of the atom from which they spring and consequently from elements constituting the material. Therefore, the intensity of these characteristic radiations is proportional to the concentration of the element in the sample from which it is also possible to obtain a semi-quantitative analysis. The spectrum is represented by a series of peaks, which the position and the related height is characteristic of a specific element. With a dedicated software it is possible to obtain the mappings for each single element of the sample. The single pixel of the image corresponds to one point on the surface of the sample from which the signal was collected. The graduation of colour is an index of the number of photons coming from characteristic point of the selected element.

Four primary components of the EDS setup are:

- the excitation source (electron beam or x-ray beam)
- the X-ray detector
- the pulse processor
- the analyser

In this thesis, EDS maps were carried out with the twofold aim of estimating the chemical composition of the samples and the distribution of the elements on the samples surface. The setup used in this thesis work consisted of a desktop SEM Phenom XL equipped with EDS analyser.

3.4.5 Fourier Transform Infrared (FT-IR) spectroscopy

IR spectroscopy was carried out in transmission mode with a Nicolet 5700 FTIR Spectrometer (ThermoFisher, Waltham, MA, USA), equipped with a room temperature working DLaTGS detector. All the spectra were background subtracted and acquired with 2 cm^{-1} resolution and 64 scans accumulation.

The infrared spectroscopy or IR spectroscopy is a spectroscopy absorption technique generally used in the field of materials characterization to investigate about chemical bonds. When a molecule absorbs an infrared photon passes from its fundamental vibrational state to a vibrational excited state. The IR spectroscopy is obtained using an interferometer, which allows the scanning of all frequencies present in the IR radiation generated by the source. Applying the Fourier transform, the IR spectra is produced with the intensity representation in the frequency domain.

In this thesis work, FT-IR analysis has been used to investigate the chemical characteristic groups of gentamicin sulfate present on surface of ZnO thin films in order to establish the efficacy of uptake process.

3.4.6 Uv-Vis spectroscopy

UV-Vis absorbance spectra were collected in the range 200–285 nm, by means of a double-beam Varian Cary 5000 UV-vis-NIR spectrophotometer (Milan, Italy). UV analysis of drug solutions were carried out in a quartz cuvette, with an optical path length of 1 mm, analyzing a volume of 350 uL. All the UV spectra were background subtracted. It represent a quantitative analysis based on Lambert-Beer law, see equation 3.1:

$$A = \varepsilon \cdot c \cdot d \quad (3.1)$$

Where A is the absorbance of the sample, ε is wavelength-dependent molar absorptivity coefficient, c is the analyte concentration and d is path length. The law express the proportionality between absorbance and concentration of absorbent substance.

4. Characterization of materials

In this part of the work, both porous ZnO thin films and graphene oxide (GO)-coated ZnO thin films have been characterized in terms of morphology, crystal structure, chemical and element compositions before the uptake and release experiments of Gentamicin Sulfate (GS) in order to compare their inherent properties with those after both experiments. The techniques used to evaluate these features were FESEM, X-ray diffraction, IR spectrometry, ICP-Mass Spectroscopy, and EDS maps.

4.1 Porous ZnO thin films

Porous ZnO thin films deposited through RF-magnetron sputtering technique on silicon wafers were characterized with the techniques above mentioned.

Field emission scanning electron microscopy (FESEM)

Figure 4.1 shows the morphology of pure ZnO thin films for different magnifications of field emission scanning electron microscope (FESEM). This analysis allows to evaluate the dimension, shape and dispersion of particles. Qualitatively, the dark areas visible in the figures represent the intrinsic porosity of the materials, which have not a strongly compact structure.

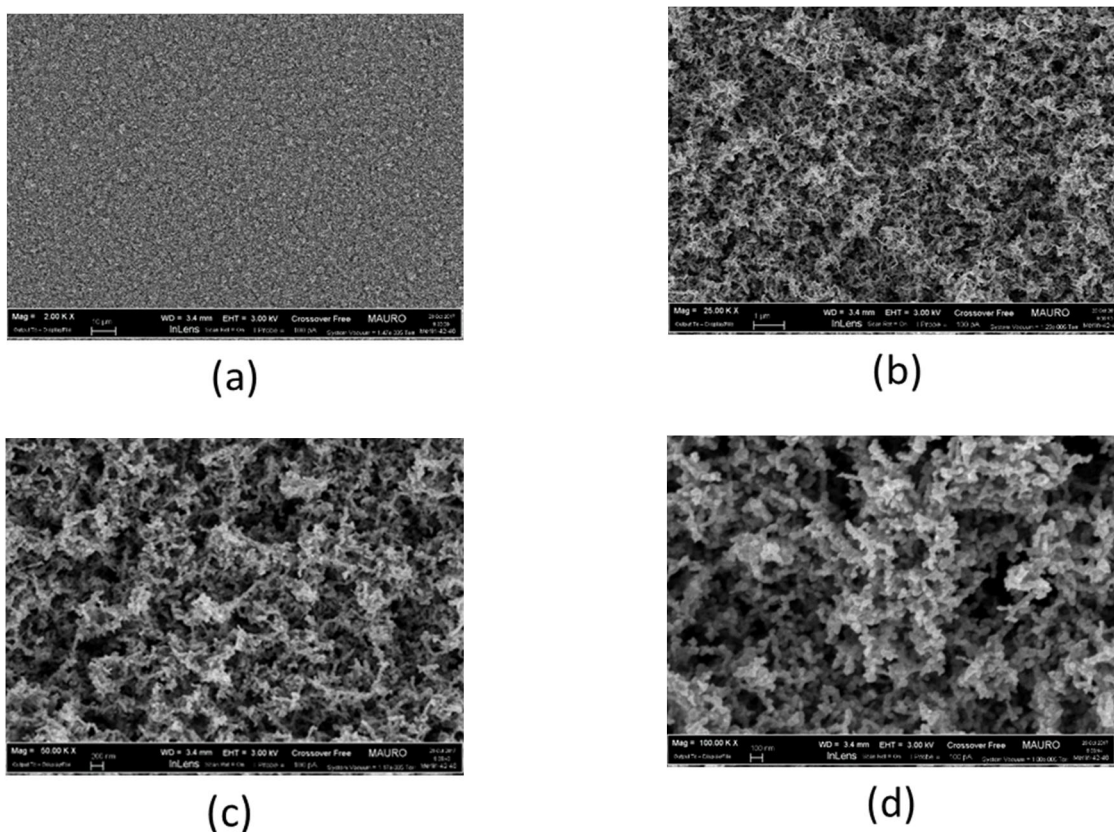


Figure 4.1: FESEM images of porous ZnO thin films : (a) 2.00 K X; (b) 25.00 K X; (c) 50.00 K X; (d) 100.00 K X.

In particular, the average thickness of deposited films detected by cross section is about 9,5 μm . Figure 4.2 reports the cross-section view of ZnO thin films, where the three thickness values were measured in three different positions of the sample.

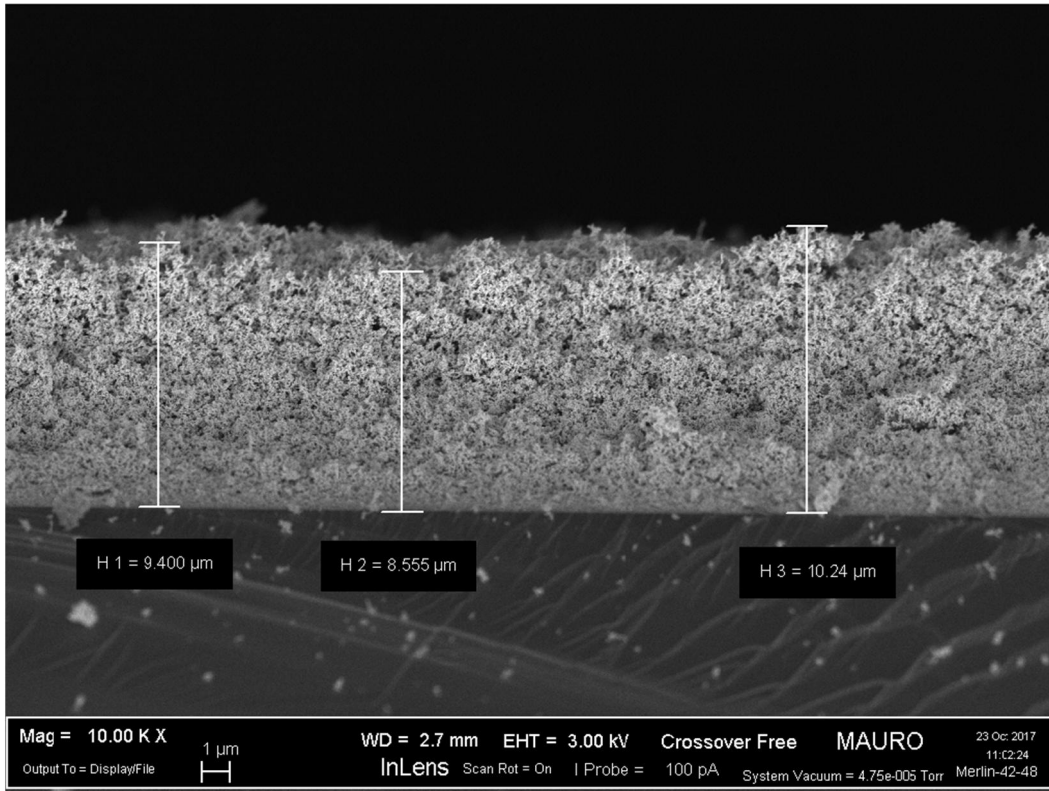


Figure 4.2: Cross-section view of mesoporous ZnO thin film deposited on Si substrate.

X-ray Diffraction

X-ray Diffraction was performed to investigate the crystalline structure and orientation of mesoporous ZnO thin films. The corresponding XRD pattern is shown in Figure 4.3. The film shows a polycrystalline nature, with (1 0 0), (0 0 2), (1 0 1), (1 0 2) and (1 1 0) diffraction peaks belonging to the hexagonal ZnO wurtzite-like structure. Each peak has been indexed according to [42] and the corresponding 2θ positions are summarized in Table 4.1.

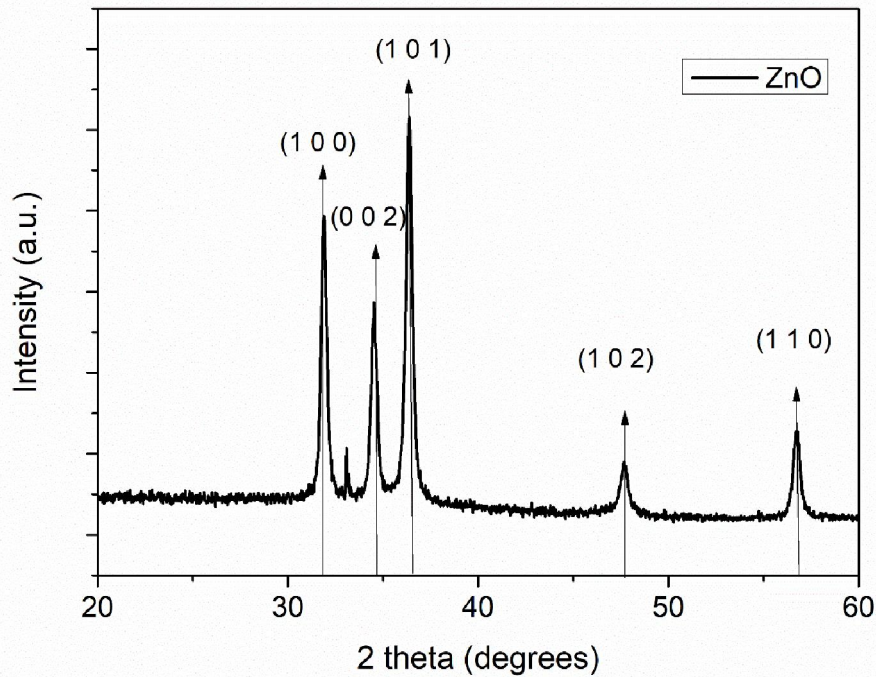


Figure 4.3: XRD pattern of mesoporous ZnO thin film.

Table 4.1: XRD peaks position detected for mesoporous ZnO thin films, and the corresponding Miller indexes.

| Miller Index | ZnO (1 0 0) | ZnO (0 0 2) | ZnO (1 0 1) | ZnO (1 0 2) | ZnO (1 1 0) |
|--------------------|-------------|-------------|-------------|-------------|-------------|
| <i>2θ position</i> | 31.80° | 34.18° | 36.29° | 47.61° | 56.67° |

FTIR spectroscopy

The chemical surface structure and composition of the ZnO samples was investigated by means of Fourier Transform InfraRed (FTIR) spectroscopy. Figure 4.4 shows the FTIR spectra of the mesoporous ZnO thin film on Si substrate, prior to any contact with solutions or the GS drug. The analysis has detected the characteristic strong Zn-O bond vibration at about 408 cm^{-1} . No other significant vibration peak was detected.

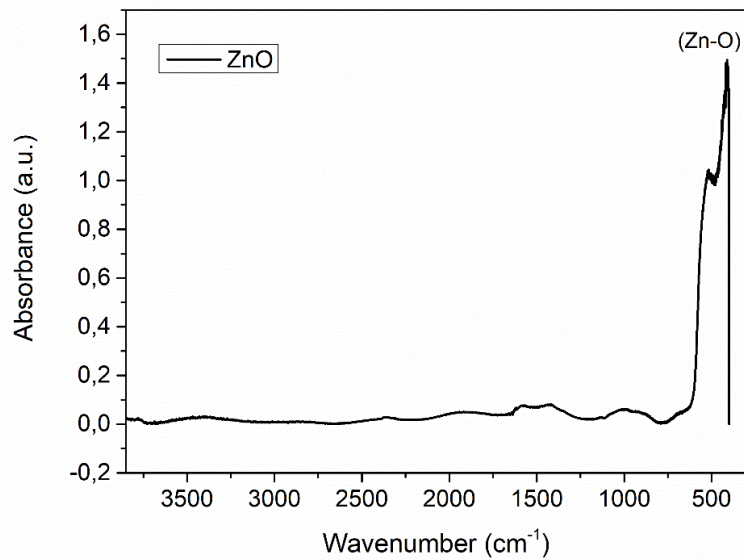


Figure 4.4: FTIR spectrum obtained for mesoporous ZnO thin film.

Energy-Dispersive X-Ray Spectroscopy (EDS) maps

EDS maps were carried out to evaluate the element composition and presence at the surface of the ZnO samples.

Figure 4.5 shows the EDS map of ZnO thin film, highlighting the presence of nitrogen (N, in orange), zinc (Zn, in blue) and oxygen (O, in green) overlapped to the corresponding Scanning Electron Microscopy (SEM) image. The EDS spectrum of Figure 4.6 also reports the characteristic peaks associated to each detected element. In particular, on the x-axis are reported the emission energies (in eV) specific for each chemical element while y-axis shows the corresponding number of photons emitted in the X-Ray wavelength range and with a specific energy, arriving at the detector in a certain period of time. Figure 4.7 gives the atomic concentration percentage of each detected element.

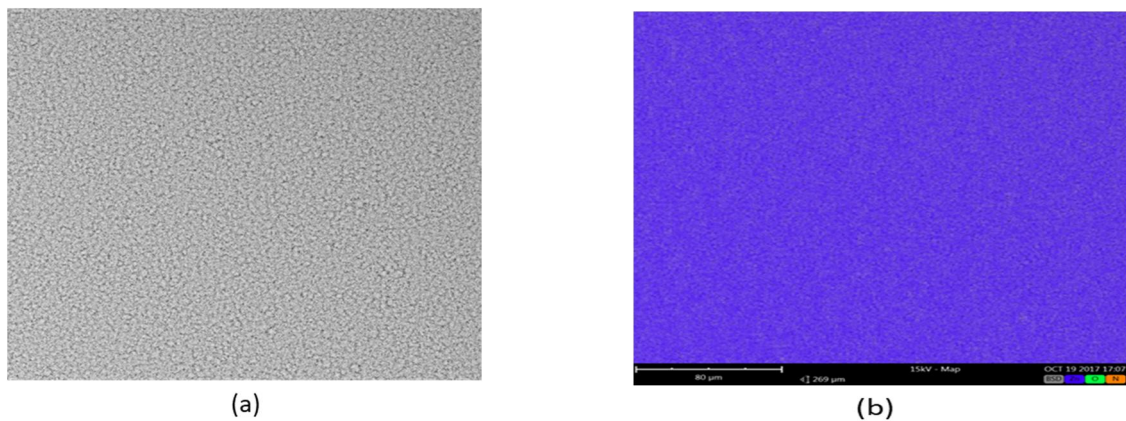


Figure 4.5: (a) SEM image of porous ZnO thin film; (b) EDS combined map of porous ZnO film with nitrogen, zinc and oxygen elements

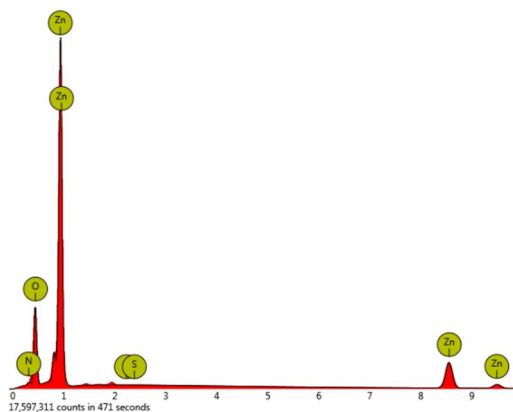


Figure 4.6: spectra of characteristic elements on porous ZnO film

| Element | Atomic percentage |
|---------|-------------------|
| Zn | 48.82 % |
| O | 47.56 % |
| N | 3.61 % |
| S | 0.00 % |

Figure 4.7: Semi-quantitative estimation of elements present in the sample

4.2 Graphene oxide-coated porous ZnO thin films

In the second part of thesis, porous ZnO thin films were covered with a layer of GO. Similarly to pristine ZnO thin films, the samples were characterized in terms of morphology, crystal structure and chemical composition, as reported in the following.

Field-Emission Scanning Electron Microscopy (FESEM)

Figure 4.8 shows the FESEM images about the morphology of graphene oxide-coated porous ZnO thin films. Different magnifications and views of the surface are reported.

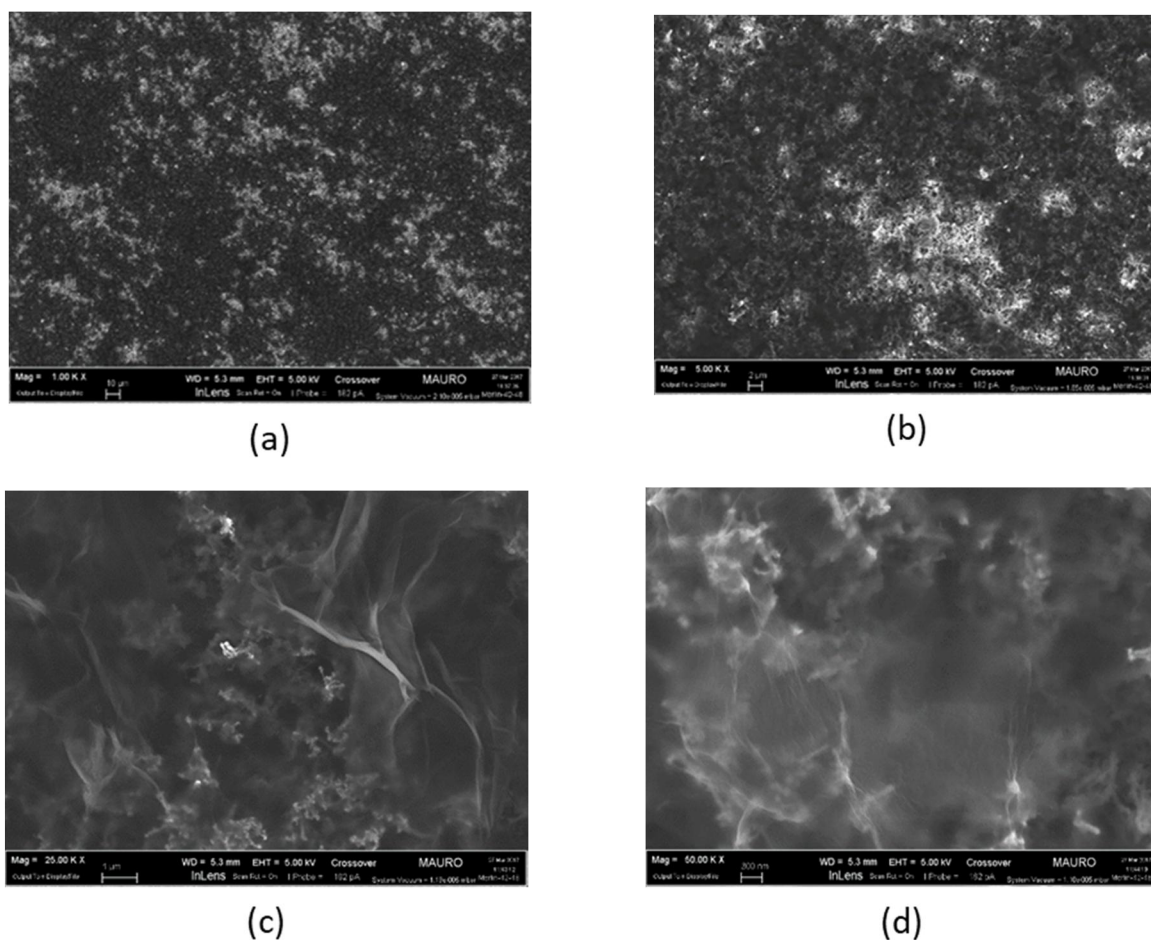


Figure 4.8: FESEM images of porous ZnO thin films covered by GO: (a) 1.00 K X; (b) 5.00 K X; (c) 25.00 K X; (d) 50.00 K X

It is possible to observe a major quantity of dark, smooth areas with respect to bright, particle-like areas. This is due to the layer of GO deposited on the top of the ZnO surface film. The characteristic flake-like structure of the GO partially occludes the pores

X-ray Diffraction

Figure 4.9 shows the XRD spectra of graphene oxide-coated porous ZnO film compared with the XRD spectra of pristine ZnO. The presence of GO does not affect the crystalline structure of ZnO film. It is clear that the XRD spectra and position of peaks are the same respect to only ZnO.

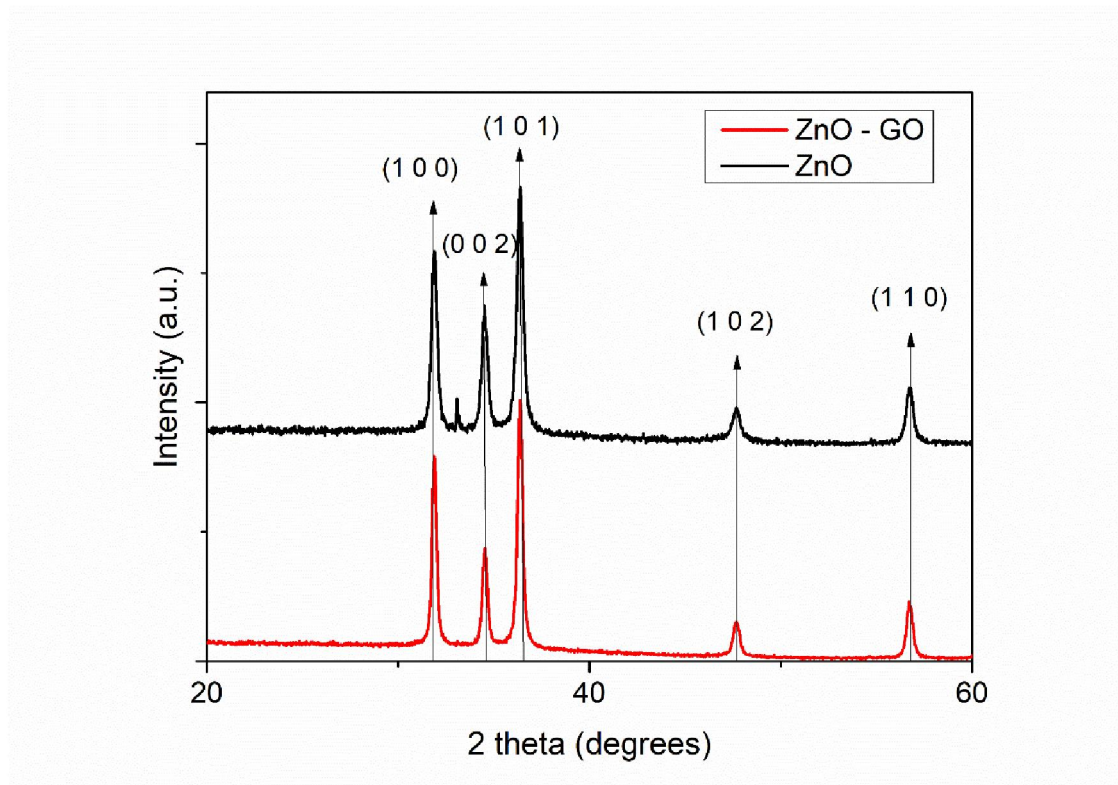


Figure 4.9: XRD spectra of pristine ZnO and GO-coated ZnO film

FTIR spectroscopy

Figure 4.10 shows the IR spectra of ZnO thin film covered with GO. With respect to the IR spectrum of the pristine ZnO, see Figure 4.10 here the region between 3000 and 2800 cm^{-1} shows the stretching typical of alkyl groups, i.e. $-\text{CH}_x$ stretching. These groups are present on the GO flakes deposited on the ZnO thin films. Also, it can be seen the aromatic group $\text{C}=\text{C}$ at about 1600 cm^{-1} and $\text{C}-\text{O}$ carboxyl and alkoxy groups at about 1390 cm^{-1} and 1024 cm^{-1} respectively.

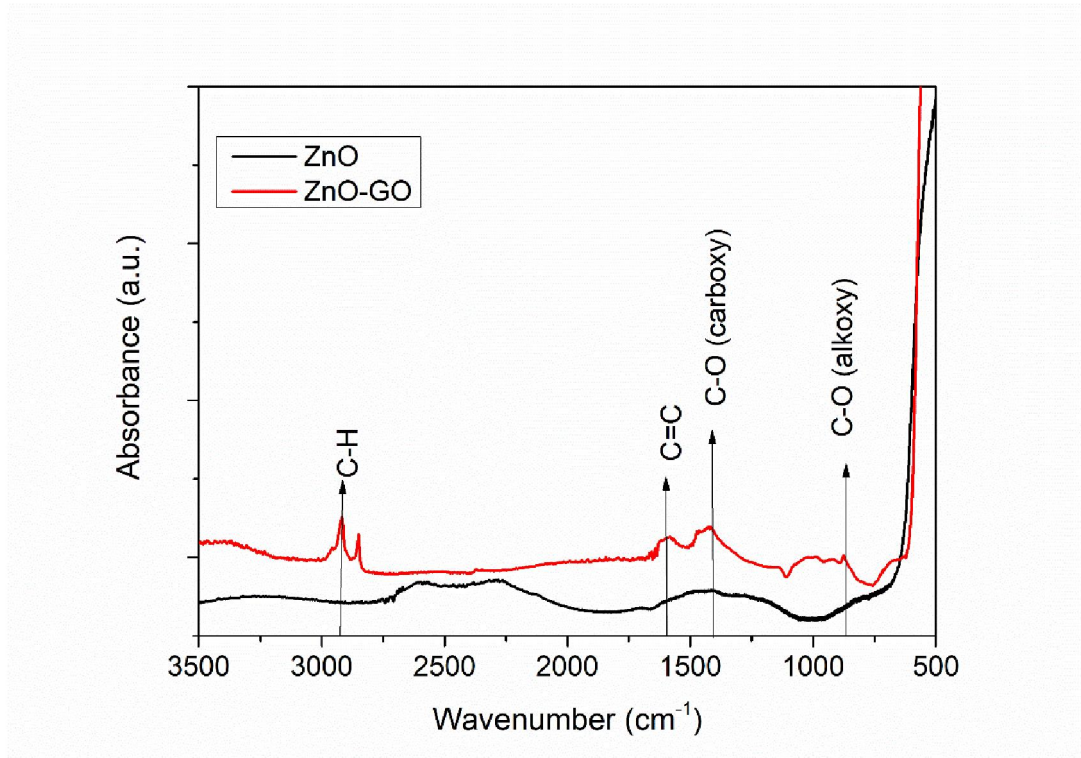


Figure 4.10: IR spectra of pristine ZnO and GO-coated ZnO film

Energy-Dispersive X-Ray Spectroscopy (EDS) maps

Figure 4.11 shows the EDS map of ZnO thin film covered by a layer of GO highlighting the presence of carbon (C, in red), zinc (Zn, in blue) and oxygen (O, in green) overlapped to the Scanning Electron Microscopy (SEM) image. The corresponding EDS spectrum is shown in Figure 4.12 while Figure 4.13 gives the atomic concentration percentage of each detected element.

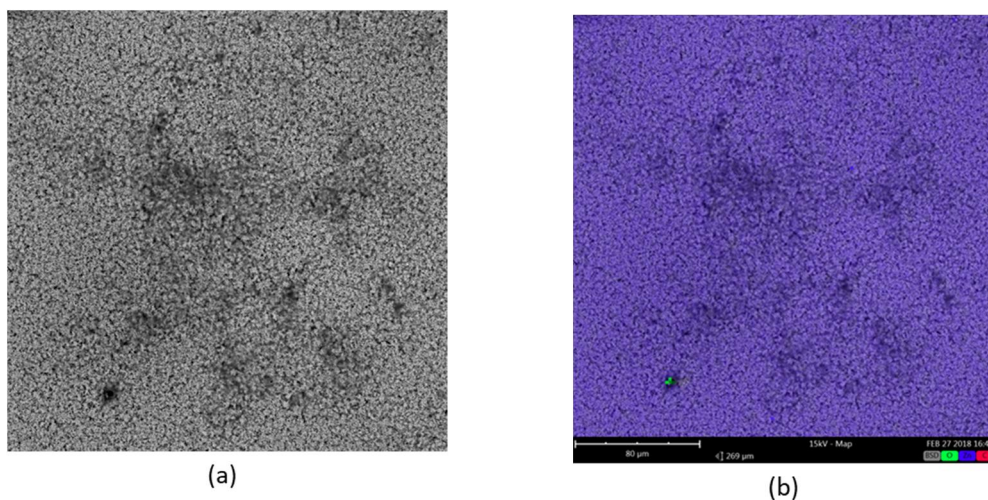


Figure 4.11: (a) SEM image of porous ZnO thin film covered by GO; (b) EDS combined map of porous ZnO-GO sample with carbon, zinc and oxygen elements

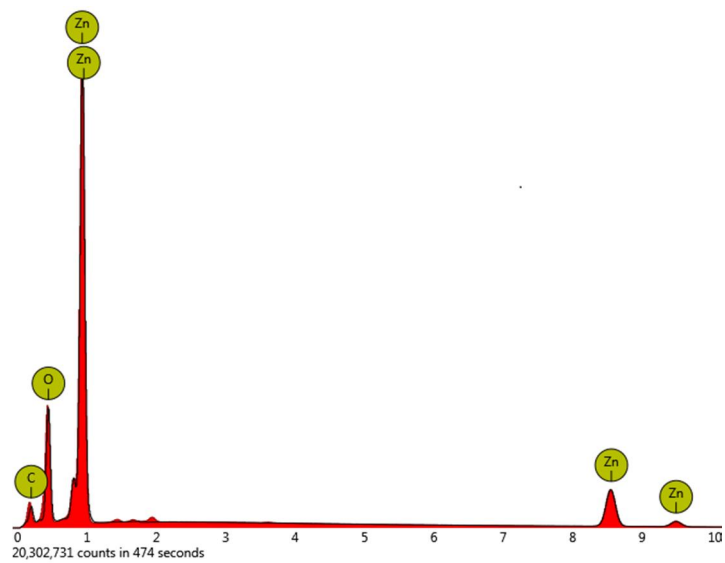


Figure 4.12: spectra of characteristic elements on ZnO-GO sample

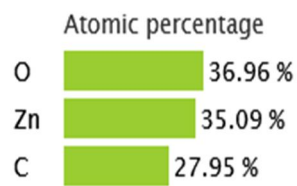


Figure 4.13: Semi-quantitative estimation of elements present in the sample

5. Uptake of gentamicin sulfate

Different uptake experiments were performed both using pristine porous ZnO thin films and ZnO porous films covered by layers of graphene oxide. In this way, it was possible to evaluate the efficiency of the loading process in both cases and choosing the optimal process conditions as starting point for the following release experiments.

5.1 Uptake of gentamicin sulfate on porous ZnO thin films

In this part of the work, two uptake experiments of gentamicin sulfate (GS) on porous ZnO thin films were performed using different solutions: deionized water (DIW) and simulated body fluid (SBF). The interaction between porous ZnO thin films and GS solutions (GS/DIW and GS/SBF) was investigated by means of several characterisation techniques, including: X-Ray Diffraction (XRD), Field-Emission Scanning Electron Microscopy (FESEM), Inductively Coupled Plasma Mass Spectrometry (ICP-MS), Energy Dispersive X-ray Spectroscopy (EDS), Ultraviolet-visible spectrophotometry (UV-Vis) and InfraRed (IR) spectroscopy. Afterwards, similar uptake experiments of the drug were carried out on porous ZnO thin film coated by a layer of graphene oxide in order to evaluate the influence of GO on the drug loading ability.

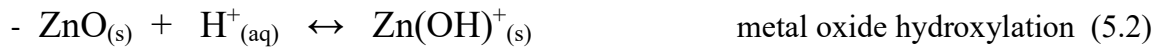
5.1.1 Uptake of gentamicin sulfate in DI water

Uptake experiments were first performed using a solution of gentamicin sulfate in deionized water (GS/DIW). The solution was prepared by mixing gentamicin sulfate salts in water at room temperature, under continuous stirring at 200 rpm for 30 min, to get a final concentration of $1 \text{ mg}\cdot\text{ml}^{-1}$ (here defined as mother solution). Then, four different plastic tubes were filled with 5 ml of the mother solution. A single ZnO sample has been soaked within each tube under orbital shaking conditions (160 rpm), at room temperature and for different uptake times of 1 h, 2 h, 5 h and 24 h. This allowed to investigate the influence of different uptake times of the GS on the porous ZnO thin films. Each sample was weighted before and after the uptake experiments (see Table 5.1). After the uptake, each sample was washed with DIW and dried with nitrogen flow. In the following, each sample is labelled according to the uptake time and solution, as shown in Table 5.1.

Table 5.1: Starting and, final weights of porous ZnO thin films soaked in GS/DIW for up to 24h. pH values of the corresponding uptake solutions measured at the end of the uptake.

| Sample name | Soaking time | Starting weight | Final weight | pH at the end of the uptake |
|-------------|--------------|-----------------|--------------|-----------------------------|
| ZnO_1h_DIW | 1 h | 0.1131 g | 0.1132 g | 5.8 |
| ZnO_2h_DIW | 2 h | 0.1178 g | 0.1179 g | 6.36 |
| ZnO_5h_DIW | 5 h | 0.1107 g | 0.1108 g | 6.34 |
| ZnO_24h_DIW | 24 h | 0.1049 g | 0.1044 g | 7.14 |

Figure 5.1a shows the weight percentage variation for each sample. It may be seen that there is a slight increase of the sample's weight by increasing the soaking time from 1h to 5h, while the sample weight strongly decreased after 24h. This aspect suggests that ZnO dissolution could take place for prolonged soaking times (24h). To evaluate any significant change in the pH of the uptake solution, the corresponding value was measured before starting the experiments and after each soaking time. The measured values are listed in Table 5.1 while the corresponding time evolution is represented in Figure 5.1b. The pH value increased with uptake time, changing from 4.45 (corresponding to the pH of mother solution) up to 7.14 after 24h uptake. This change can be correlated to the dissolution behaviour of ZnO-based materials when interacting with acidic media. In fact, zinc oxide is an amphoteric oxide and can easily dissolve both acids and bases. The reactions take place once after immersion of ZnO in deionized water with the hydrolysis of the ZnO particle surface into $Zn(OH)_{2(s)}$, due to adsorption of water molecules. This zinc hydroxide is soluble in water, especially when the pH value is low. The predominant reactions are the dissolution of $ZnO_{(s)}$ into $Zn^{2+}_{(aq)}$ and $O^{2-}_{(aq)}$ and the surface hydroxylation of $ZnO_{(s)}$ to $Zn(OH)^+_{(s)}$. The reactions can be shown schematically with the following, equations (5.1) and (5.2) [43]:



At very low pH values, other important reactions can occur. Among these, the most important are shown in Equations (5.3) and (5.4) [43]:



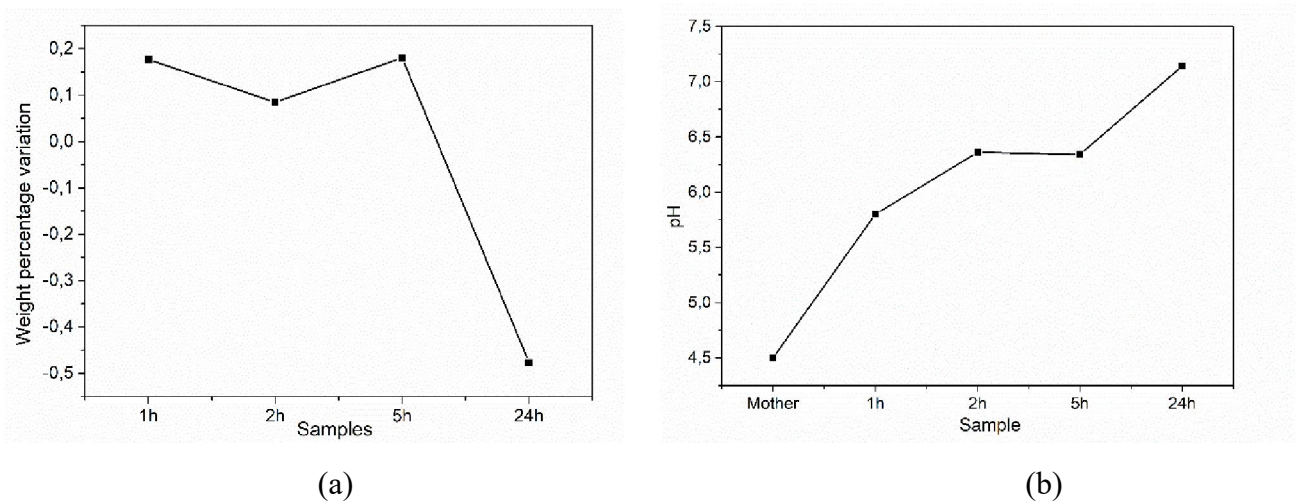


Figure 5.1: (a) Weight percentage variation of ZnO samples vs. soaking time; (b) Time evolution of pH for GS/DIW solution.

Inductively Coupled Plasma mass spectrometry (ICP-MS)

In order to evaluate the ZnO degradation, ICP-MS analyses were performed on each uptake solution. Actually, this analysis provides information on the concentration of specific elements present in the analysed solution. Figure 5.2 shows the release profile for Zn^{2+} ions against the soaking time. The mother and the different uptake solutions were diluted 1:100 in order to find the best condition allowing for Zn^{2+} concentration to be properly detected.

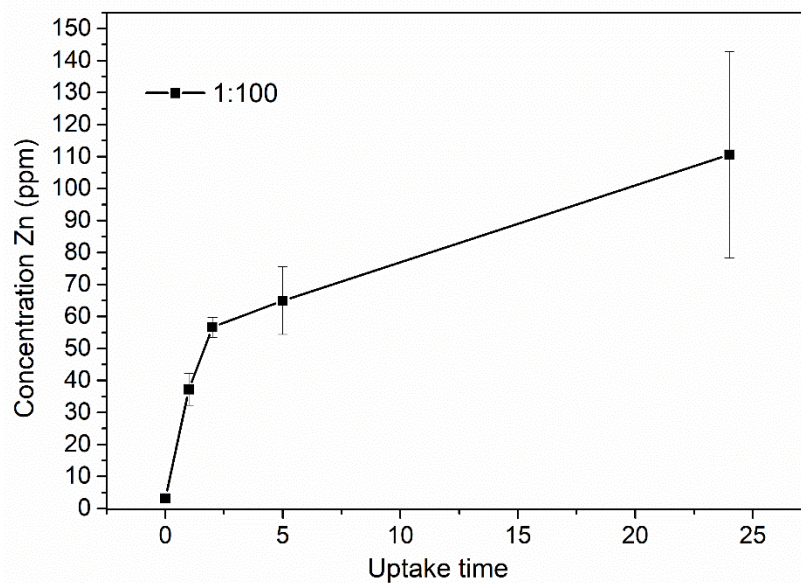


Figure 5.2: ICP-MS release profile for Zn^{2+} ions from diluted 1:100 solution.

The time evolution for Zn^{2+} ions well reflects the increase in pH previously observed as well as the variation of weight for the ZnO samples. By increasing the uptake time up to 2h, the amount of dissolved Zn^{2+} ions in the solution increased. Then, the Zn^{2+} dissolution rate partially slowed down from 2h up to 5h, increasing again up to 24h. This data finally confirms that ZnO dissolution occurred when soaking the samples in acidic media like GS/DIW solution.

Field-Emission Scanning Electron Microscopy (FESEM)

ZnO thin films were analyzed by FESEM to evaluate any change in the corresponding surface morphology by increasing the uptake time. Figure 5.3a and 5.3b show the top-view FESEM images acquired on ZnO samples soaked in GS/DIW for 5h and 24h, in comparison with a FESEM image of a ZnO sample before any interaction with the uptake solution (Figure 5.3c).

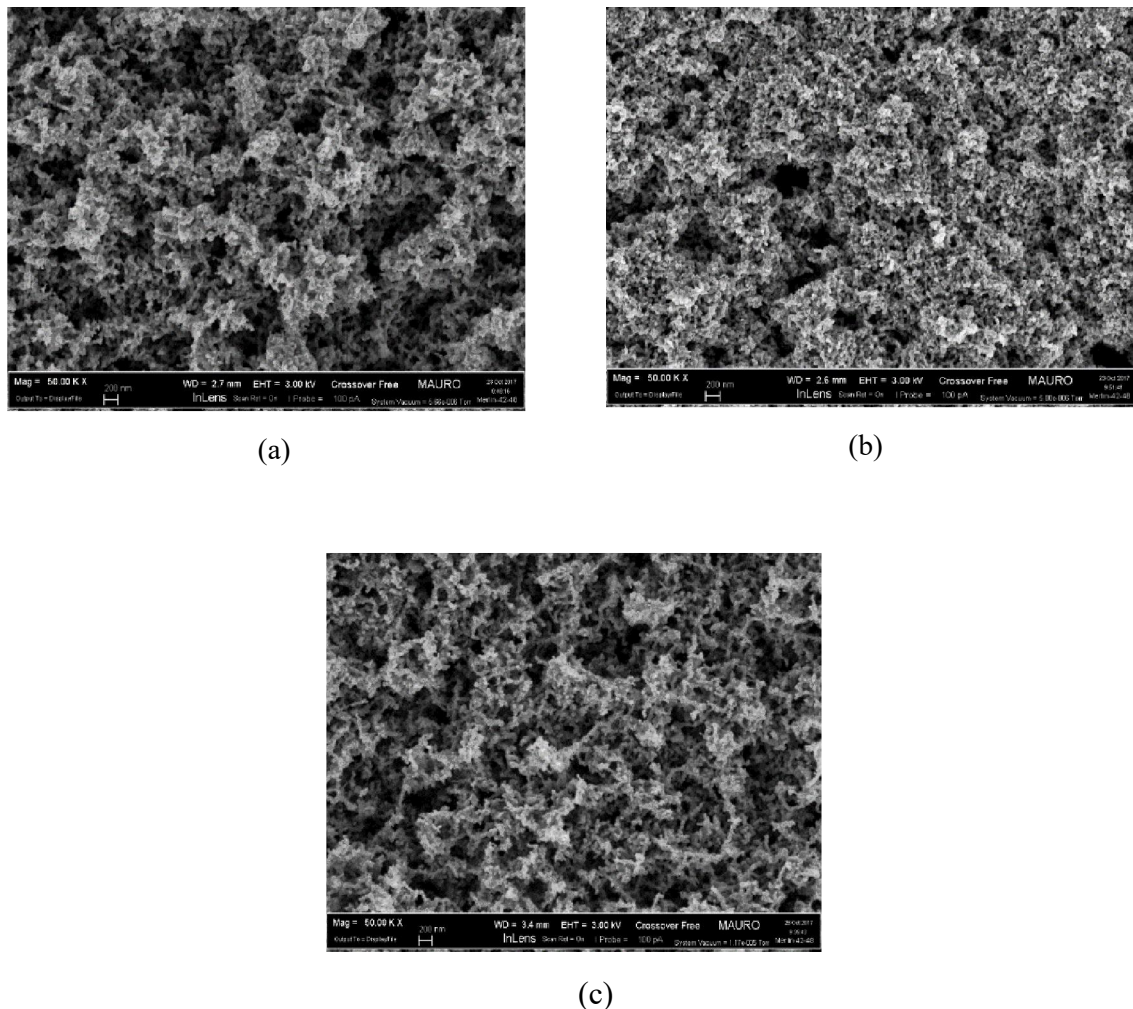


Figure 5.3: FESEM images of porous ZnO thin films: (a) after uptake in GS/DIW for 5 h ; (b) after uptake in GS/DIW for 24 h; (c) before the uptake experiments.

In the images it is possible distinguish dark areas, which represent the porosity, and bright areas which give information about the degree of compactness of the samples. In particular, there are not great difference in morphology between the pristine ZnO before any uptake (Figure c) and the 5h-uptake sample (figure a). In contrast, from 5h to 24h-samples there is an increase of bright and compact areas. This is due to the dissolution of the ZnO material, as described above, owing to the lower porosity and higher compactness of the ZnO sample afeter the uptake for 24h wth respect to the other ones.

The average thickness of the different ZnO samples was also evaluated by cross-section FESEM analyses. Figure 5.4a and 5.4b show the cross section images of pristine ZnO sample and soaked ZnO sample after 24h. It can be see that the average thickness of sample decrease strongly to 24h at average value of about 6,5 um respect the initial average value of about 9,5.

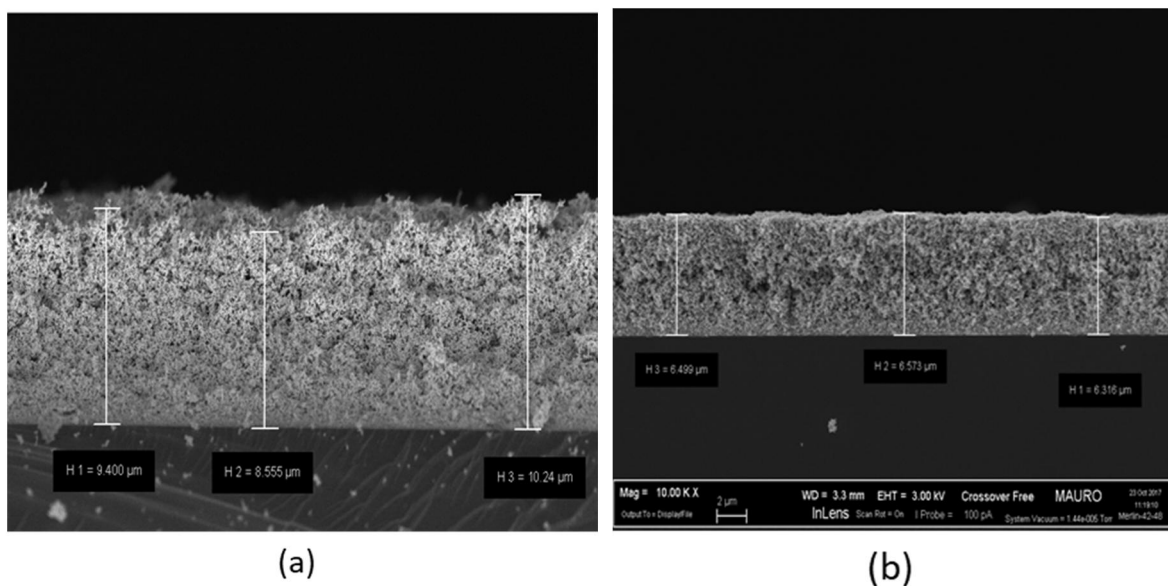


Figure 5.4: (a) cross section of pristine ZnO; (b) cross section of soaked ZnO sample after 24h

Therefore, Figure 5.5 shows a decrease of the ZnO film thickness with increasing the uptake time, due to the loss of material, as previously discussed.

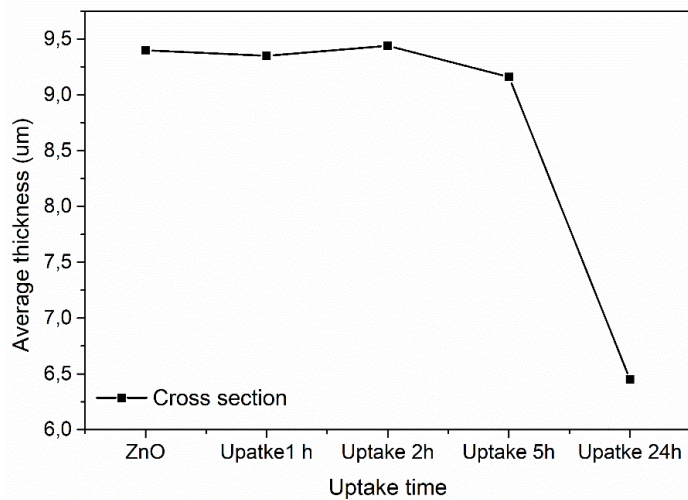


Figure 5.5: Average thickness estimated from cross-view FESEM images, for each ZnO sample soaked for different times.

X-Ray Diffraction (XRD)

XRD analyses were performed before and after soaking the porous ZnO thin films in GS/DIW uptake solution to evaluate any change in the corresponding crystal structure. Figure 5.6 shows the XRD patterns of all the investigated ZnO samples. No relevant changes were observed; independently of the soaking time, all the samples were characterized by the presence of the same diffraction peaks characteristics of the hexagonal ZnO wurtzite structure.

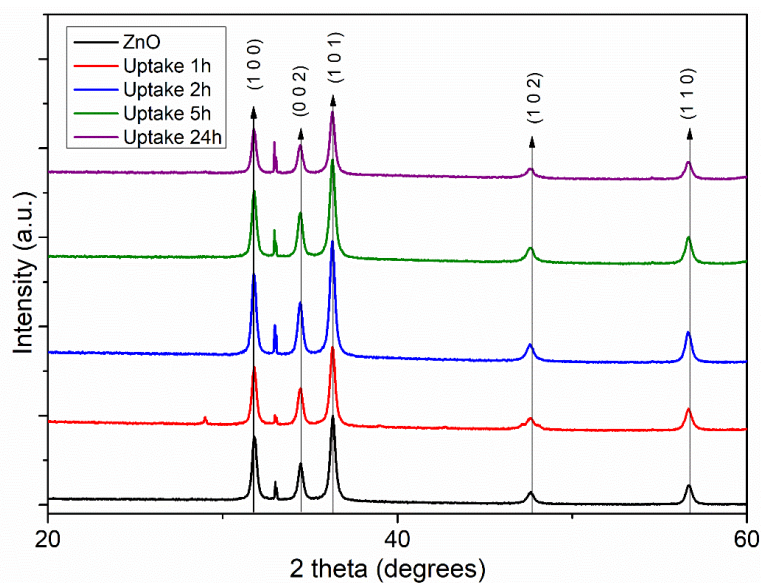


Figure 5.6: XRD patterns of porous ZnO thin films before and after soaking in GS/DIW for up to 24 h

IR spectroscopy

IR spectroscopy is an effective way to investigate the chemical composition of a particular compound. Therefore, it was performed on porous ZnO thin films to evaluate the presence of GS after the uptake experiments. Figure 5.7 shows the IR spectra obtained for porous ZnO samples soaked in GS/DIW for the different uptake times. As reference, the IR spectra of GS/DIW solution and of a porous ZnO thin film before the uptake are reported as well. Table 5.2 summarizes the IR vibrational modes along with the corresponding position. The band of SO_2 group at about of 618 cm^{-1} , the band of HSO_4^- at 1118 cm^{-1} , the bands of amine between 1500 cm^{-1} and 1600 cm^{-1} and the C-O-C band at about 1100 cm^{-1} were detected especially for the ZnO samples soaked for a higher uptake time. These peaks are characteristic of chemical structure of gentamicin sulfate and represent a qualitative proof of the drug loaded into the porous films.

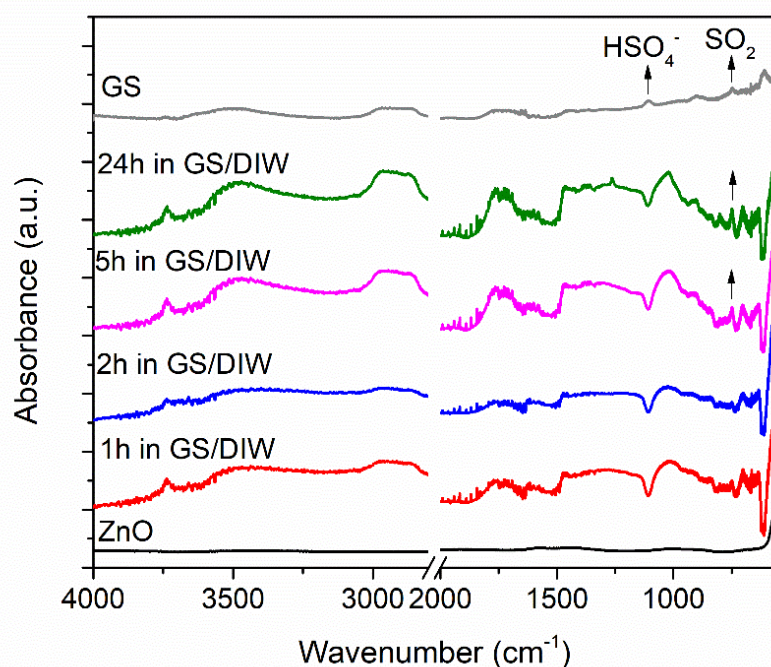


Figure 5.7: IR spectra of GS/DIW solution, porous ZnO thin film, and porous ZnO samples after soaking in GS/DIW.

Table 5.2: Different IR detected chemical groups with corresponding wavelenght

| | | | | | | | |
|------------------------------|------|----------------|--------------|---------------|-----|-------------------------------|-------|
| Wavenumber, cm^{-1} | 3700 | 1620-1650 | 1530 | 618 | 163 | 111 | 900- |
| | - | | - | | 7 | 8 | 1110 |
| | 3600 | | 1560 | | | | |
| Chemical group | O-H | $-\text{NH}_2$ | $-\text{NH}$ | SO_2 | C=O | HSO ₄ ⁻ | C-O-C |

Energy Dispersive X-ray Spectroscopy (EDS)

EDS analyses were performed on the different porous ZnO thin films after soaking in GS/DIW for different times. This analysis allowed to obtain a semi-quantitative estimation of the elements present in the samples, along with the corresponding distribution. The elements opportunely identified were nitrogen (N) and sulfur (S), because they occur in the chemical structure of the drug and their detection is a proof of the efficient drug loading. Figure 5.8 shows the EDS maps for the different elements (S in red, N in light blue) detected for the starting ZnO sample (panel (a) of Figure 5.8) and for the ZnO samples after interacting with GS/DIW solution for different times. The figures show that sulfur (red) is absent on the starting porous ZnO sample as expected, while it is present on the other samples after the uptake experiments. This finding qualitatively confirms the successful GS uptake on the porous ZnO thin films. Table 5.3 reports the atomic concentration percentage (at.%) of each detected element.

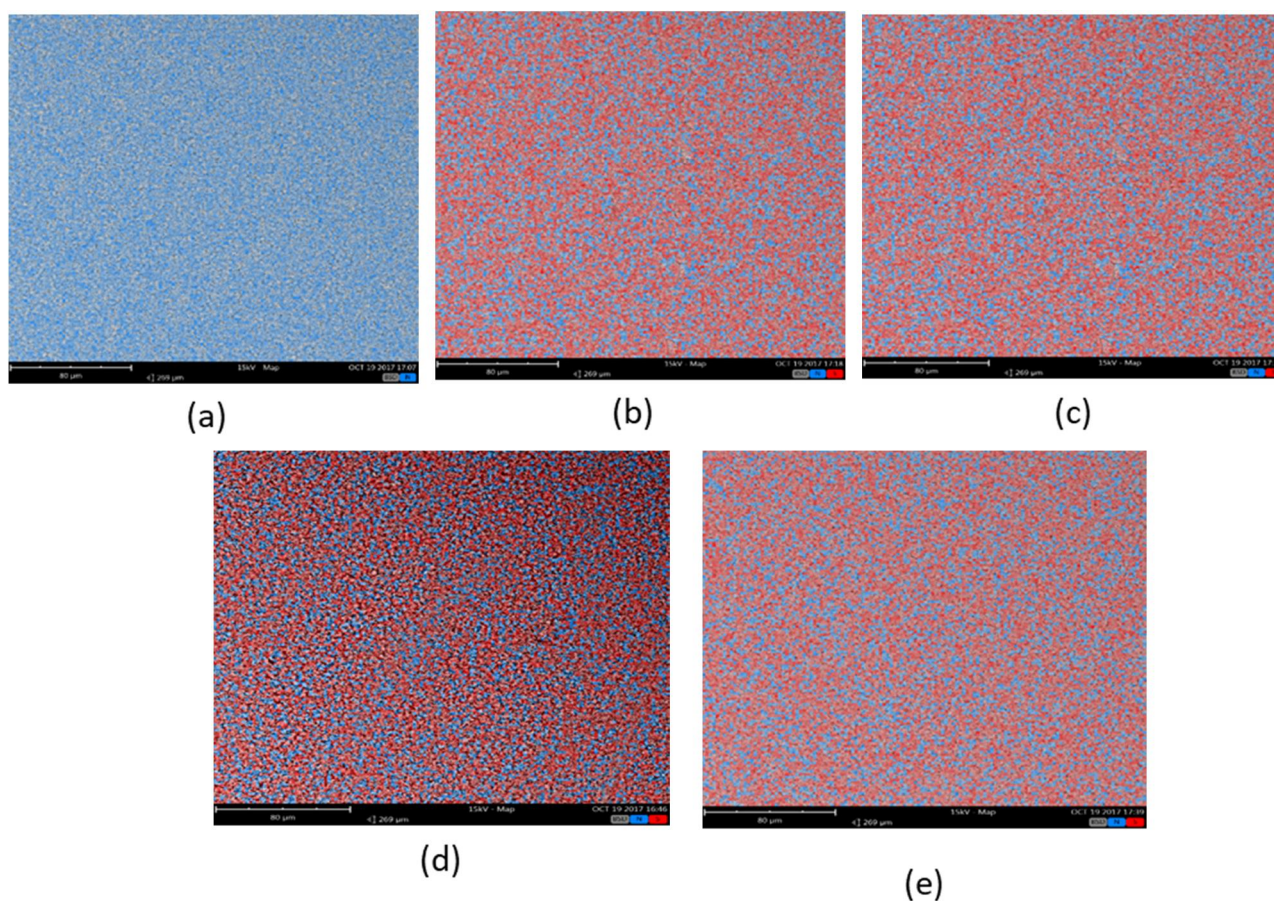


Figure 5.8: Combined EDS maps for S and N elements: (a) starting ZnO sample; (b) ZnO soaked in GS/DIW for 1 h; (c) for 2 h; (d) for 5 h; (e) for 24 h.

Table 5.3: Semi-quantitative estimation for S, N, Zn and O elements, obtained from EDS maps.

| Sample name | S at.% | N at.% | Zn at.% | O at.% |
|-------------|--------|--------|---------|--------|
| ZnO | 0 | 3,6 | 48,8 | 47,6 |
| ZnO_1h_DIW | 0,06 | 3,75 | 48,9 | 47,3 |
| ZnO_2h_DIW | 0,04 | 3,74 | 48,6 | 47,6 |
| ZnO_5h_DIW | 0,04 | 3,82 | 48,5 | 47,7 |
| ZnO_24h_DIW | 0,05 | 3,76 | 47,9 | 48,3 |

Ultraviolet-visible spectrophotometry (UV-Vis)

UV-Vis spectrophotometry was exploited to evaluate the amount of GS loaded on the porous ZnO thin films, by monitoring the UV absorption peak characteristic of GS and positioned at 251 nm. Concerning the uptake experiments, the UV absorbance at 251 nm of the uptake solution should be lower if compared to the mother solution, as far as GS is loaded on the porous ZnO sample. Therefore, UV-Vis analyses were performed on all the different uptake solutions, in order to monitor how the uptake time affected the amount of GS loaded on the porous ZnO. To this purpose, a calibration curve was obtained by analyzing the UV-Vis response of GS/DIW solutions prepared at prefixed concentrations ($100 \mu\text{g}\cdot\text{ml}^{-1}$, $250 \mu\text{g}\cdot\text{ml}^{-1}$, $500 \mu\text{g}\cdot\text{ml}^{-1}$ and $1 \text{ mg}\cdot\text{ml}^{-1}$), which are reported in Figure 5.9a. For each curve, the corresponding UV absorbance value at 251 nm was considered and the experimental points were linearly fitted, as shown in Figure 5.9b. The unknown amount of GS loaded on the porous ZnO thin films was then estimated according to the calibration curve.

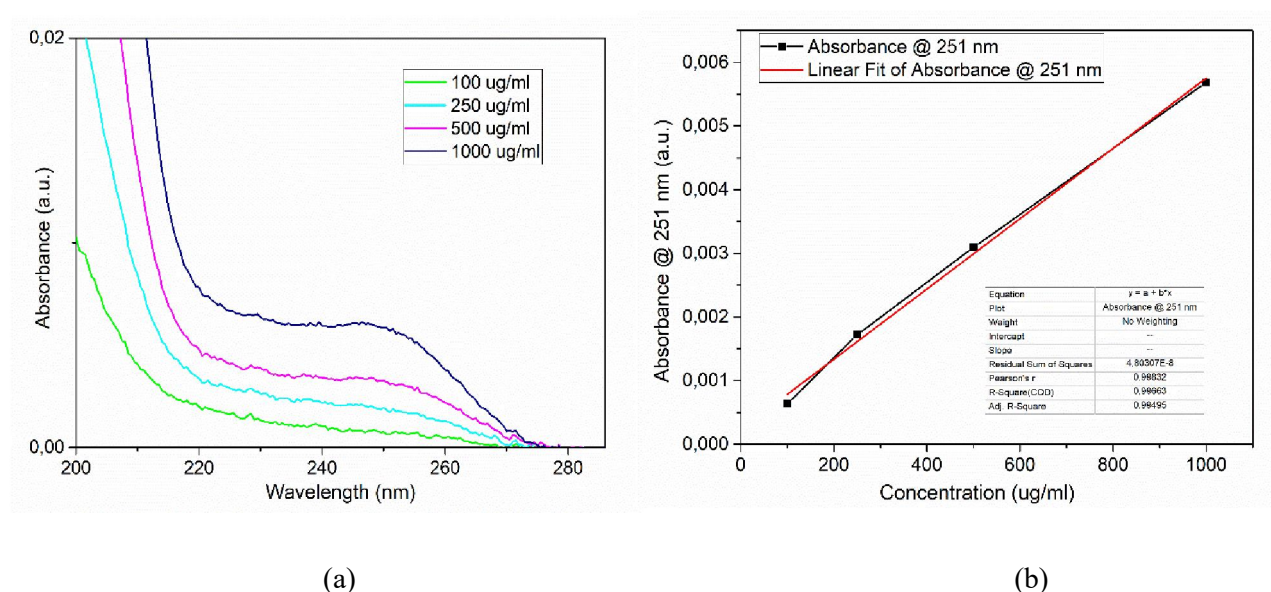


Figure 5.9: (a) UV-Vis spectra of GS/DIW solutions, prepared at pre-fixed concentrations; (b) calibration curve for GS/DIW solution.

Figure 5.10 shows the UV spectra collected from the GS/DIW solutions after the different uptake times. With respect to the UV spectrum of the mother solution, UV spectrum of solutions to different uptake times unfortunately present a value of absorbance greater in correspondence of the peak at about 251 nm. This aspect is mainly due to the contribution of Zn^{2+} ions in solution, derived from the dissolution process of ZnO samples and confirming the results of other characterizations above mentioned.

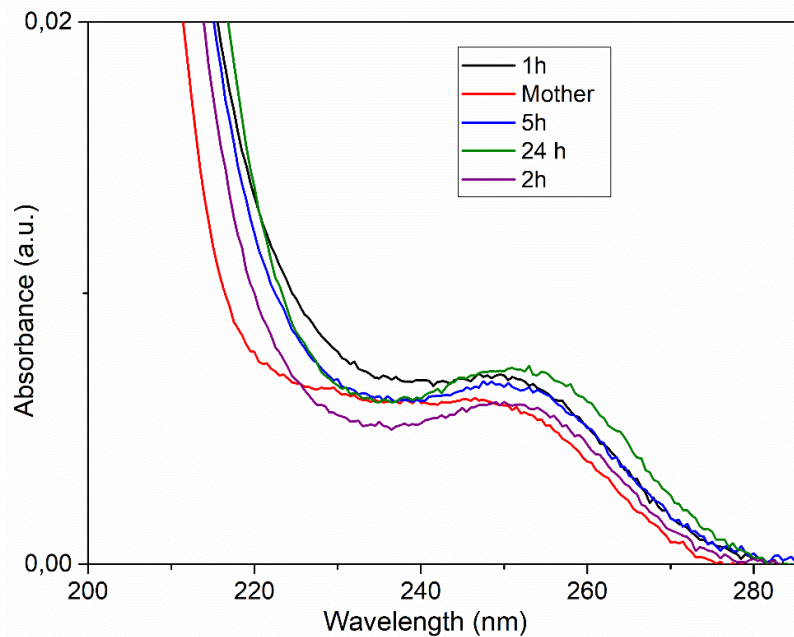


Figure 5.10: UV-Vis spectra of GS/DIW solutions for different uptake times of 1 h, 2 h, 5 h and 24 h.

5.1.2 Uptake of gentamicin sulfate in SBF

In order to overcome the limitation of ZnO dissolution due to the acidity of GS/DIW solution, the same experiments discussed in the previous paragraph were carried out by using simulated body fluid (SBF) as the aqueous medium to host GS. In this case, the starting concentration was $250 \mu\text{g}\cdot\text{ml}^{-1}$. The pH of the starting solution (7.66) was kept slightly constant during the overall uptake experiment, as shown in Table 5.4. This ensured the partial prevention in ZnO dissolution, hence not affecting GS uptake. The limited ZnO dissolution was first confirmed by the little variations of the sample's weight, as summarized in Table 5.4.

Table 5.4: Start weight, final weight and pH of the solution at the end of the uptake for each sample.

| Sample name | Soaking time | Start weight | Final weight | pH at the end of the uptake |
|-------------|--------------|--------------|--------------|-----------------------------|
| ZnO_1h_SBF | 1 h | 0,1370 | 0,1369 | 7,68 |
| ZnO_2h_SBF | 2 h | 0,1257 | 0,1258 | 7,69 |
| ZnO_5h_SBF | 5 h | 0,1277 | 0,1278 | 7,69 |
| ZnO_24h_SBF | 24 h | 0,1337 | 0,1333 | 7,71 |

Inductively Coupled Plasma mass spectrometry (ICP-MS)

As for the water solutions, the ICP-MS analyse was performed in order to investigate the presence of Zn^{2+} ions in the SBF solution due to the dissolution of material. On the base of the recorded values of weights and pH, we expect a minimal presence of Zn^{2+} ions in solution with respect to the previous uptake in water solutions. This aspect is confirmed by figure 5.11, where the concentration of Zn^{2+} ions in function of the uptake time reported for both solutions. It is clear that the concentration of zinc ions in GS/SBF (in red) is always lower for every time than GS/water solution. In particular, the concentration of Zn^{2+} ions reach the maximum value of about 30 ppm after the uptake time of 1h. Then, the concentration decreases slightly until 5h and finally it increases slightly until uptake time of 24h. Anyway, the trend keeps almost constant values if compared with the trend in water solution (in black).

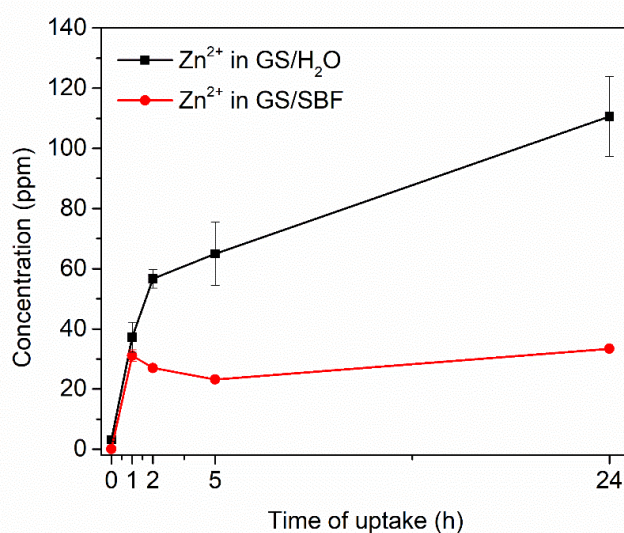


Figure 5.11: Figure X: ICP-MS release profile for Zn^{2+} ions from diluted 1:100 water solution (black) and SBF solution (red)

Field Emission Scanning Electron Microscopy (FESEM)

In order to evaluate the possible changes on the surface morphology after the soaking of ZnO samples in SBF solution, FESEM analyses was performed. Figure 5.12 from a to d represent the FESEM images of ZnO samples soaked in GS/SBF solution for 1h, 2h, 5h, 24h respectively. In particular, the images show that after soaking in GS/SBF solution the samples keep the starting porous morphology. It also possible to note the presence of discontinuity due to the precipitation of calcium phosphate (CaP) compounds.

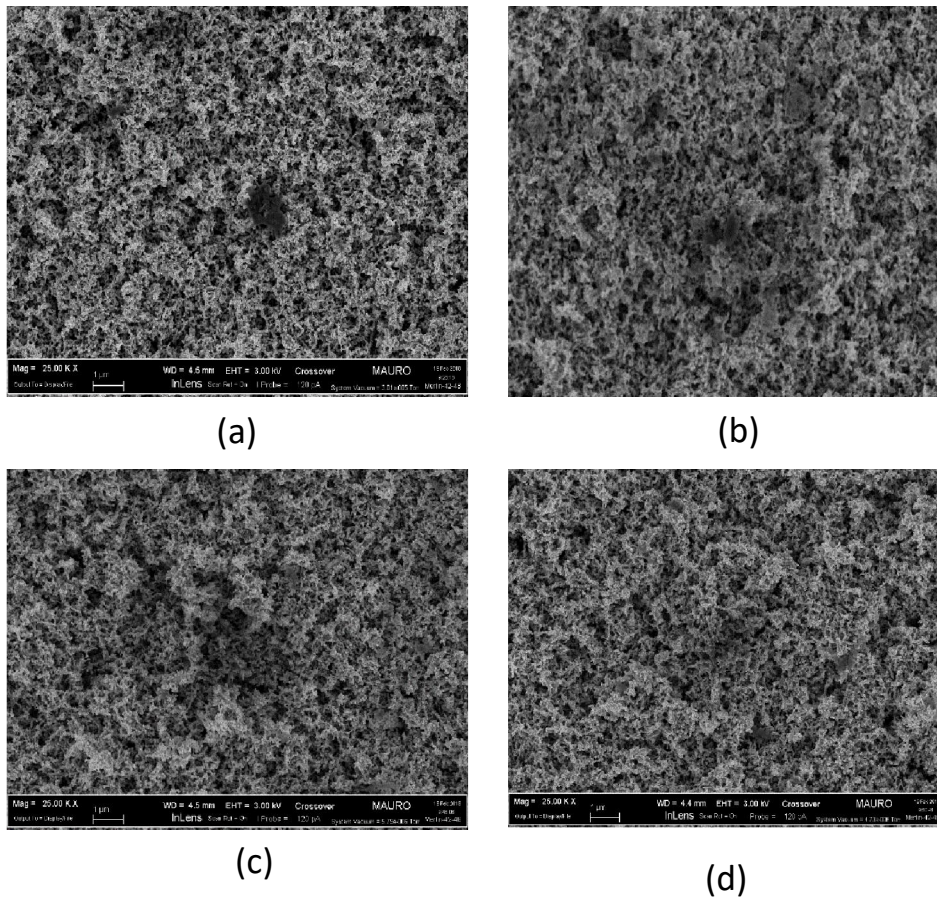


Figure 5.12: FESEM images of porous ZnO thin films soaked GS/SBF solution: (a) after 1h, (b) after 2h, (c) after 5h, (d) after 24h.

X-Ray Diffraction (XRD)

XRD was performed to investigate the crystal structure and orientation of porous ZnO thin films, before and after the uptake experiments in GS/SBF. Figure 5.13 shows the XRD patterns of all the investigated samples, showing that all samples are characterized by the same diffraction peaks, i.e. (1 0 0), (0 0 2), (1 0 1), (1 0 2) and (1 1 0), typical of hexagonal ZnO wurtzite structure. As before, there are no appreciable changes between the different samples.

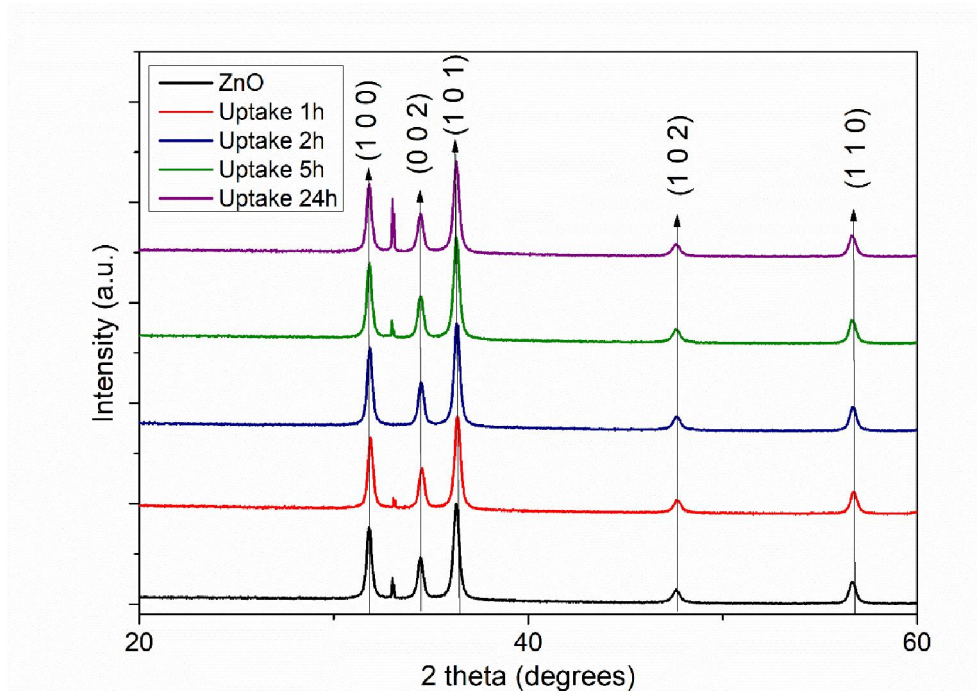


Figure 5.13: XRD patterns of porous ZnO thin films before and after soaking in GS/SBF for up to 24 h.

IR spectroscopy

Figure 5.14 shows the IR spectra related to the starting porous ZnO thin film and to the different ZnO samples after the uptake experiments in GS/SBF for 1h, 2h, 5h, respectively. The IR absorbance bands for each characteristic chemical group for gentamicin sulfate are also reported in Table 5.5. In particular, the identified peaks are the band of SO_2 group at 618 cm^{-1} , the band of HSO_4^- at 1118 cm^{-1} , the bands of amine groups between 1500 cm^{-1} and 1600 cm^{-1} and the C-O-C band at about 1100 cm^{-1} . HSO_4^- , NH_3^+ , NH_2^+ groups are characteristic of gentamicin structure. The ZnO sample before uptake does not show any of the above-mentioned peaks, whereas the ZnO samples soaked in SBF solution shows the vibration peaks belonging to GS. In particular, the peaks are more intense as the uptake time increases. This aspect demonstrates qualitatively the higher GS loading in the ZnO samples upon time.

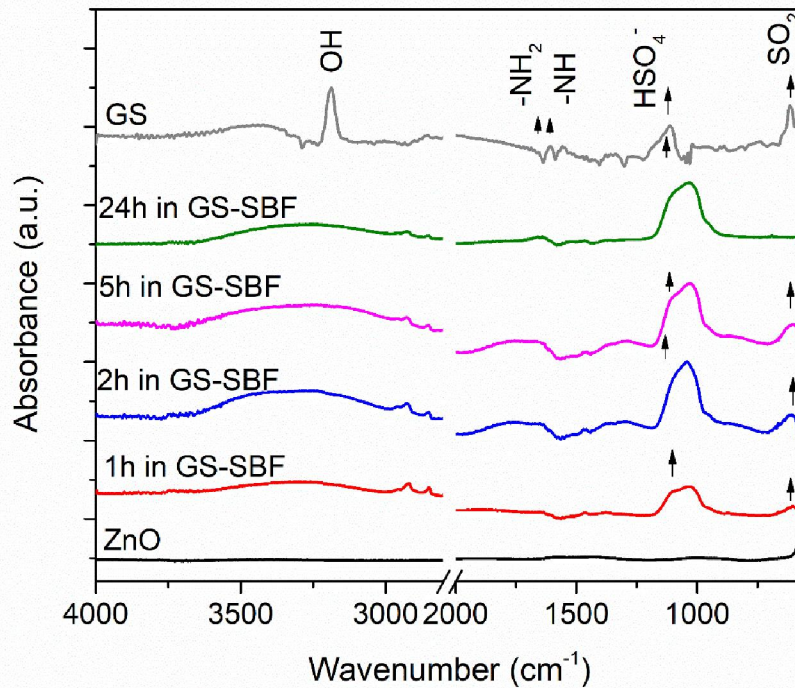


Figure 5.14: IR spectra of gentamicin, ZnO film and ZnO samples soaked in SBF solutions for 1h, 2h, 5h, 24h.

Figure 5.5: IR spectra of GS/SBF solution, porous ZnO thin film, and porous ZnO samples after soaking in GS/SBF.

| | | | | | | | |
|------------------------------|-----------|------------------|-----------|-----------------|------|-------------------------------|----------|
| Wavenumber, cm^{-1} | 3700-3600 | 1620-1650 | 1530-1560 | 618 | 1637 | 1118 | 900-1110 |
| Chemical group | O-H | -NH ₂ | -NH | SO ₂ | C=O | HSO ₄ ⁻ | C-O-C |

Energy Dispersive X-ray Spectroscopy (EDS)

EDS analyse was carried out in order to obtain the element composition map. In particular, N, S, Ca and P have been detected. The following Figure 5.15 shows the EDS maps for the different elements (S in red, N in light blue, Ca in purple and P in yellow) detected for the starting ZnO sample (panel (a) of Figure 5.15) and for the ZnO samples after interacting with GS/SBF solution for the different uptake times.

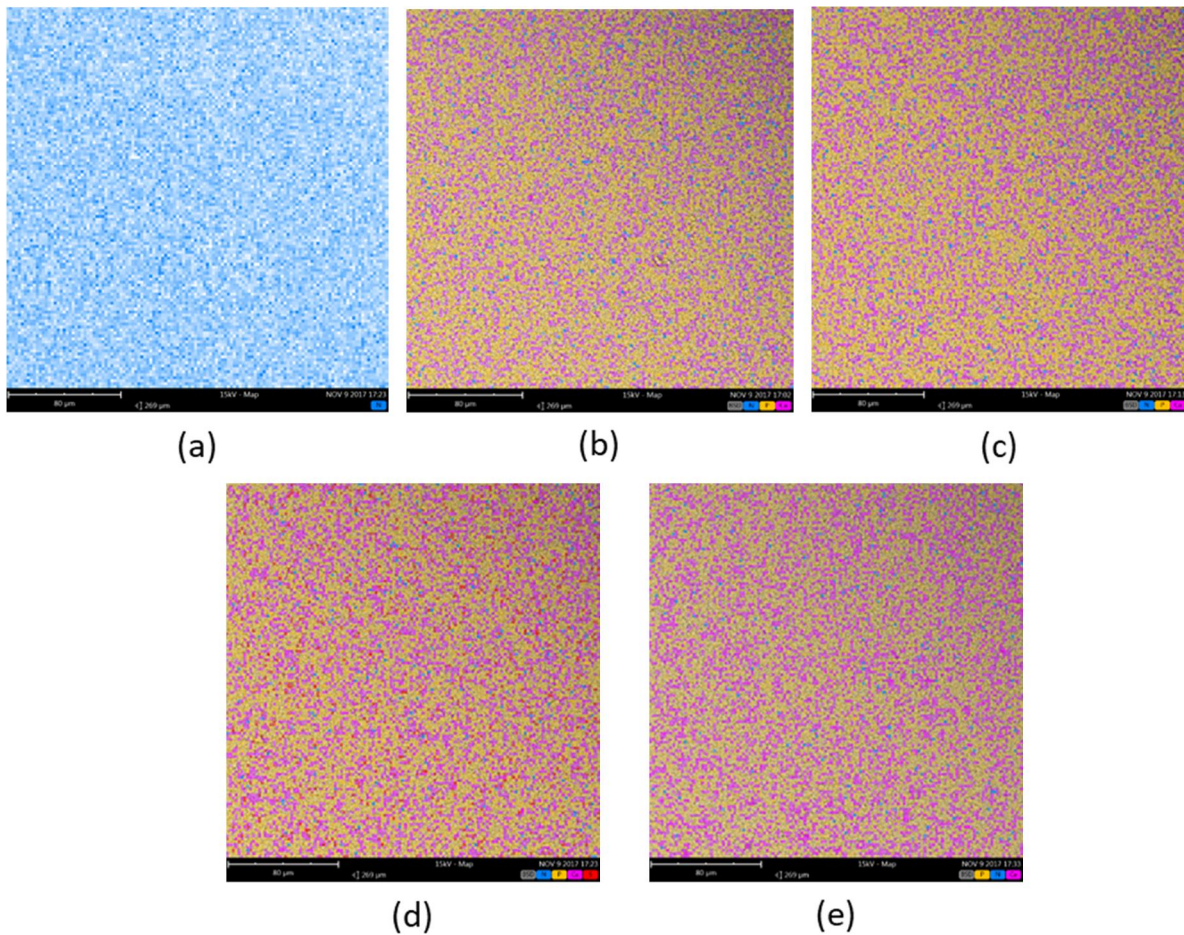


Figure 5.15: Combined EDS maps for N, S, P and Ca elements: (a) starting ZnO sample; (b) ZnO soaked in GS/SBF for 1 h; (c) for 2 h; (d) for 5 h; (e) for 24 h.

In this case, after the uptake experiments, the presence of calcium and phosphorus was detected. The corresponding amount increased with the uptake time. This is due to the precipitation of CaP that occurred because of the interaction between the ZnO and SBF solution, as previously reported in another Master Thesis [44]. Besides, the presence of sulphur was difficult to be detected because of the low concentration of the starting mother solution. Indeed, this was less concentrated than the gentamicin/H₂O solution (1 mg/ml), consequently the sensibility of instrument is not able to detect it. Table 5.6 shows the atomic concentration percentage (at.%) for each detected element. It is worth to note that, except sulphur, the content of the other elements increases consistently against uptake time increase, whereas Zinc and Oxygen remains almost constant.

Table 5.6: Semi-quantitative estimation for S, N, Zn, O, P and Ca elements, obtained from EDS maps.

| Sample name | S (at.%) | N at. % | Ca at. % | P at. % | Zn at. % | O at. % |
|-------------|----------|---------|----------|---------|----------|---------|
| ZnO | 0 | 3,6 | 0 | 0 | 48,8 | 47,6 |
| ZnO_1h_SBF | 0 | 3.97 | 0,24 | 1,55 | 46,4 | 47,8 |
| ZnO_2h_SBF | 0 | 4,08 | 0,33 | 1,57 | 46,3 | 47,8 |
| ZnO_5h_SBF | 0,02 | 4,12 | 0,37 | 1,73 | 45,8 | 48 |
| ZnO_24h_SBF | 0 | 4,17 | 0,51 | 1,92 | 45 | 48,4 |

Ultraviolet-visible spectrophotometry (UV-Vis)

UV-Vis spectrophotometry has been used as quantitative measure to evaluate the amount of gentamicin sulfate loaded on porous ZnO thin films. The calibration curve was obtained by analyzing the UV-Vis response of gentamicin solutions prepared in SBF at prefixed concentrations of ($100 \mu\text{g}\cdot\text{ml}^{-1}$, $250 \mu\text{g}\cdot\text{ml}^{-1}$, $500 \mu\text{g}\cdot\text{ml}^{-1}$ and $1 \text{mg}\cdot\text{ml}^{-1}$), which are reported in Figure 5.16.

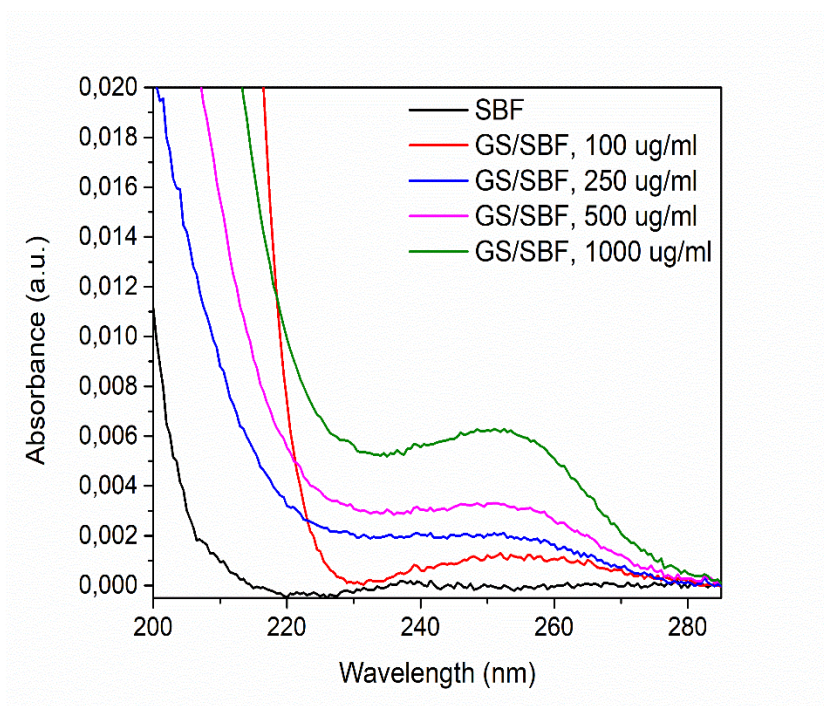


Figure 5.16: UV-Vis spectra of the calibration GS/SBF solutions, prepared at pre-fixed concentrations.

As for the calibration curve in DI solution, for each curve, the corresponding UV absorbance value at 251 nm was considered and the experimental points were linearly fitted, as shown

in Figure 5.17. From these curves, the unknown amount of gentamicin loaded on porous ZnO thin films after different times of uptake was estimated.

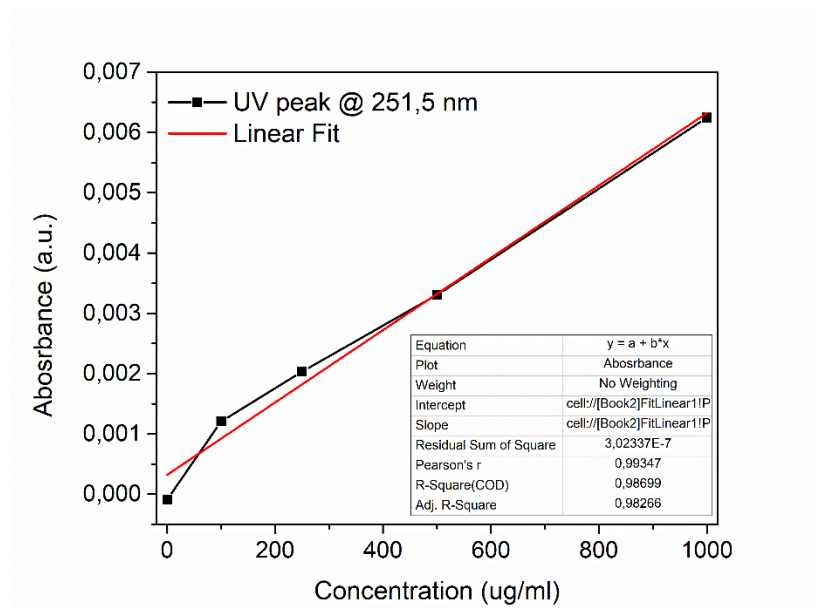


Figure 5.17: calibration curve for GS/SBF solution.

The uptake curves refer to solutions of GS with unknown concentrations and the characteristic peak of gentamicin, positioned at 251 nm, with corresponding value of absorbance were monitored for an accurate measurement, as reported in Figure 5.18. In particular, for the uptake experiments we expect that the corresponding peak of drug is less intense than the peak of the starting mother solution. This would mean that the concentration of GS in solution after a certain uptake time is lower than the starting quantity (250 ug/ml) and that the loading process has efficiently progressed.

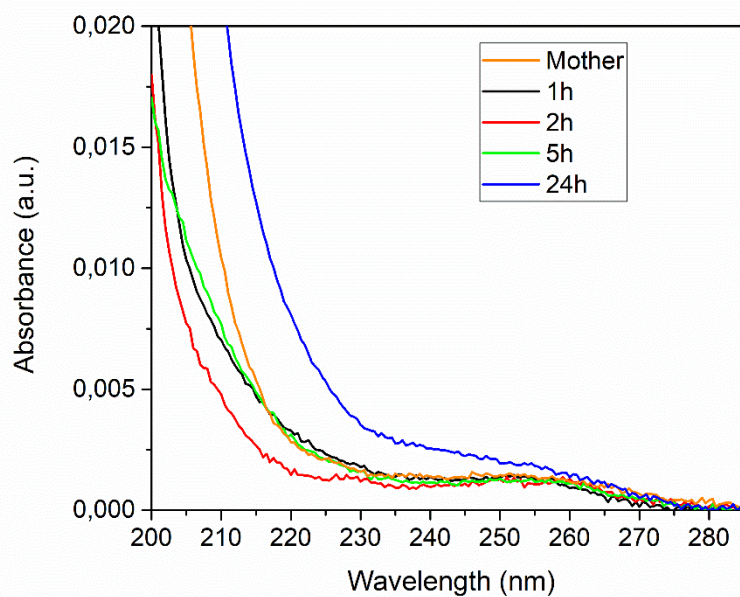


Figure 5.18: Uptake curves of GS/SBF soaking ZnO samples

Table 5.7 illustrates the obtained data about the different uptake solutions. Particularly, the value of absorbance at 251 nm, the concentration of each solution, the amount of drug in solution obtained considering a volume of 5 ml for each sample, the drug loaded on ZnO samples and the percentage of loading are reported. The amount of drug loaded on the ZnO samples increases at increasing uptake time from 1h to 5h. The sample at 24h presents at negative value. This means that the amount of drug in solution is greater than the initial amount of 1250 ug. This incongruence is due to the dissolution of both the gentamicin and the ZnO in solution and it causes a value of absorbance detected that gives a meaningless value of concentration.

Table 5.7: Amount of drug loaded on the porous ZnO thin films.

| Uptake time [h] | Abs @ 251 nm [a.u.] | Concentration [ug/ml] | Amount of drug in solution [ug] | Loaded drug [ug] | Percentage of loading [%] |
|-----------------|---------------------|-----------------------|---------------------------------|------------------|---------------------------|
| 0 | 0 | 250 | 1250 | 0 | 0 |
| 1 | 0,00143 | 141,14 | 705,7 | 544,3 | 43,544 |
| 2 | 0,00115 | 92,09 | 460,45 | 789,55 | 63,164 |
| 5 | 0,00116 | 94,09 | 470,45 | 779,55 | 62,364 |
| 24 | 0,00259 | 336,03 | 1680,15 | -430,15 | -34,412 |

Figure 5.19 shows the trend about the percentage of GS loading versus time, calculated with respect to the amount of drug in solution at the beginning (1250 ug). The mass of loaded drug in mg reported to the weight of ZnO sample (about 3 mg) is also shown. In particular, the mass of ZnO has been obtained by subtracting the weight of ZnO sample (including the weight of the silicon substrate) to the weight of the bare silicon substrate measured before the sputtering deposition of zinc.

It can be seen that the amount of drug loaded increases progressively from time zero to the uptake time of 2h. At this point it reaches the maximum amount of drug loaded (about 789 ug) and consequently it represents the optimal uptake condition. Then, it decreases lightly until the uptake time of 5h and finally it drops from 5 h to 24 h. As already described, this behaviour is due to the dissolution of ZnO: even if the pH is kept almost constant in the buffered SBF solution, a certain quantity of Zn^{2+} ions is released upon time. Therefore, with respect to the initial GS amount in the mother solution, only 60% of the drug is correctly loaded into the porous ZnO thin film. It can be assumed that the system displays a discrete loading efficiency.

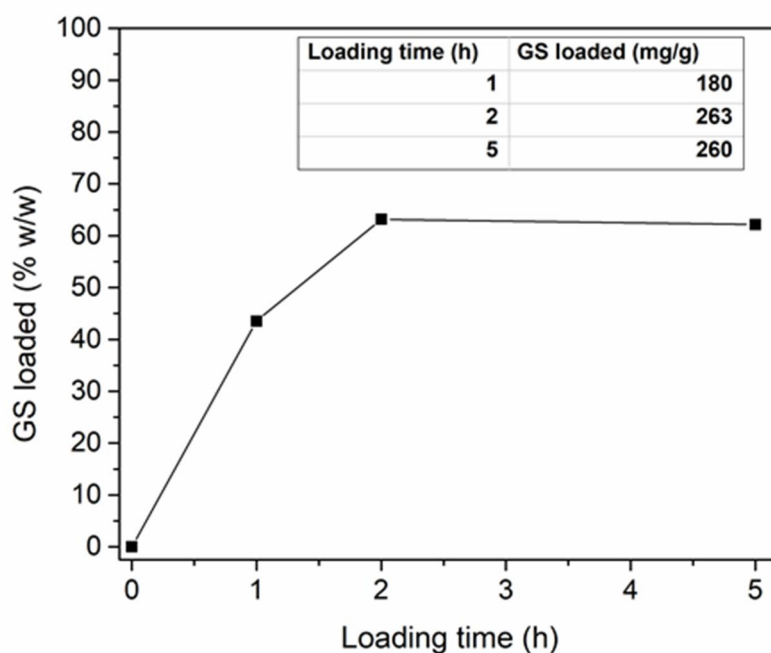


Figure 5.19: Percentage of GS loading (with respect to the initial GS amount in the mother solution) with uptake time. The table in the inset reports the loaded drug with respect to the pristine ZnO film weight.

5.2 Uptake of gentamicin sulfate on graphene oxide-coated porous ZnO thin films

After the uptake experiments on the pristine porous ZnO thin films, the same experiments were carried out on the porous ZnO thin films covered by a layer of GO. The starting solution was GS/SBF with a concentration of 250 ug/ml. Both modalities of solution preparation and uptake experiments are the same described in the previous paragraphs about uptake of GS in SBF solution. Owing to the results obtained by the pristine ZnO films in bi-distilled water, the uptake experiments were not performed in GS/DIW solutions, but only in GS/SBF. The aim of these experiments were to investigate the influence of GO, both on dissolution behaviour of ZnO and on uptake process of gentamicin sulfate. In this way it was possible to compare the two uptake experiments and choose the better one in terms of higher drug loaded and minor ZnO dissolution.

Ultraviolet-visible spectrophotometry (UV-Vis)

The only analysis performed was the UV-Vis one, which gives a quantitative information on the loaded drug. Because the starting solution of the drug is the same of the previous experiments, it is possible to use the same calibration curve obtained previously. Figure 5.20 reports the uptake curves of GS/SBF solution in contact with ZnO-GO samples.

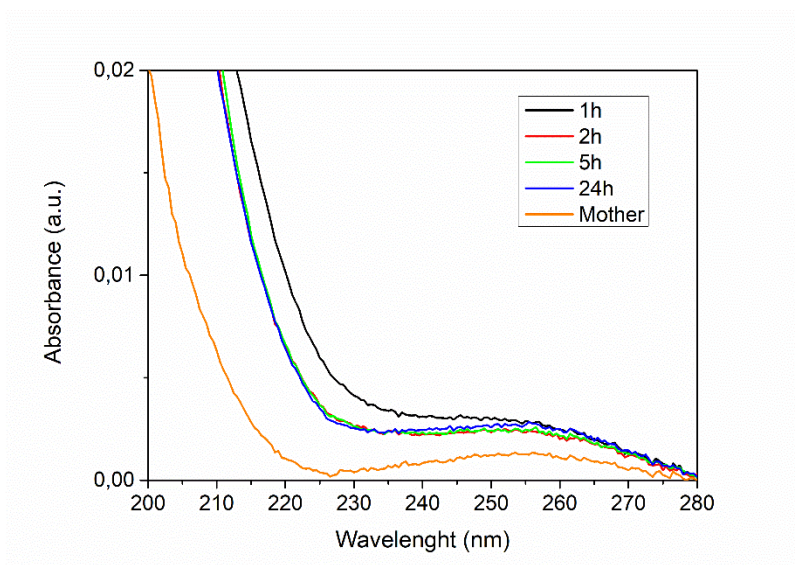


Figure 5.20: Uptake curves of GS/SBF soaking ZnO-GO samples

The uptake curves show a meaningless trend with respect to time. In fact, it can be observed that the curve referred to the mother solution has a lower absorbance than those measured for the uptake curves at different times. This is probably due again to the effect of ZnO dissolution and a co-precipitation of CaP due to the interaction between ZnO and SBF. Unfortunately, the contribution of Zn^{2+} ions was not possible to be quantified. Consequently, only the uptake on ZnO thin films without GO was further considered, allowing to obtain better results.

6. Release of gentamicin sulfate

After uptake experiments, the release of loaded gentamicin in SBF was performed. These experiments were carried out into an orbital shaker, at 160 rpm, and at steady temperature of 37 °C to simulate that of human body. Depending of the results obtained by uptake experiments on porous ZnO thin films, the optimal uptake time chosen was 2 hour. In particular, the release experiments were carried out on drug-loaded porous ZnO thin films with and without a layer of GO (which was added after the drug uptake process). In this way, it was possible to study and compare the release kinetics. Actually, it is expected that the presence of GO would slow down the release of the drug and would thus represent an effective way to control the delivery process.

6.1 Release of GS from porous ZnO thin films

In the first part, the release of gentamicin sulfate, previously loaded by the uptake process, was evaluated. As already mentioned, the drug uptake process was carried for 2h, since it ensures the optimal uptake condition. In particular, two identical uptake solutions and samples, named sample 1 and sample 2, were put into the orbital shaker in order to have a duplicate and to compare the results. A volume of 350 ul of solution was extracted at fixed times in order to analyse the release of GS by UV-Vis spectroscopy. If the gentamicin would have been released from the ZnO thin film samples to the SBF, an absorbance peak located at 251 nm would be expected and should increase over time. Release spectra of sample 1 and sample 2 are shown in Figures 6.1 and 6.2.

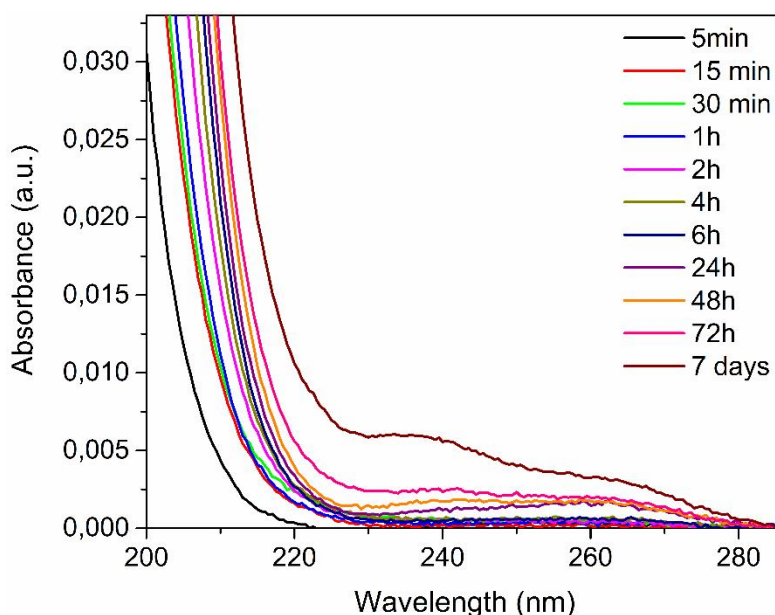


Figure 6.1: Release spectra of GS/SBF solutions from porous ZnO thin film at different times, sample 1.

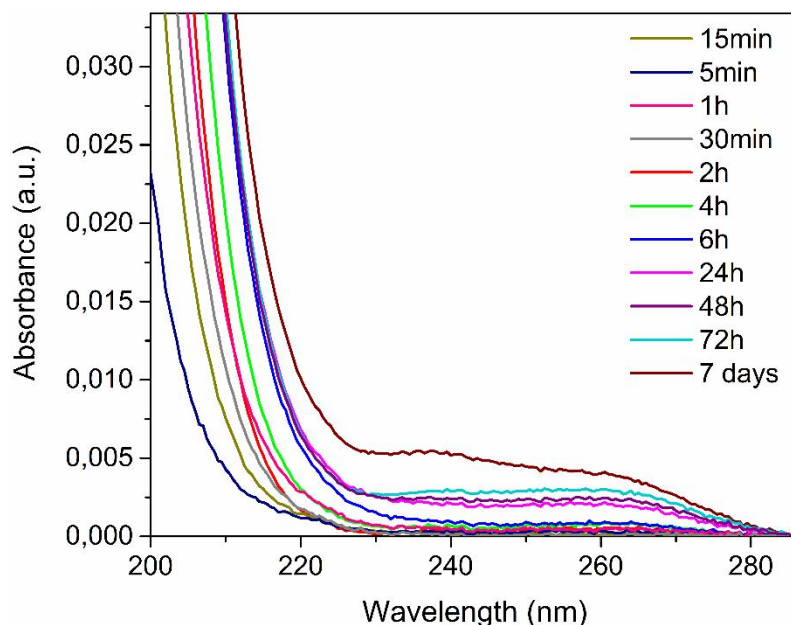


Figure 6.2: Release spectra of GS/SBF solutions from porous ZnO thin film at different times, sample 2.

Considering the characteristic peak at 251 nm, the calibration curve, and the residual volume of solution remained after each 350 ul-volume removal, the value of concentration was calculated for both samples at each release time step. Table 6.1 shows the values of concentration and the weight of drug released obtained for each time step and their average. In particular, the data show that the release of drug increases gradually with time. Comparing with quantity of about 800 ug loaded on ZnO during the uptake experiments, it can be assumed that the release ended before 24h. Actually at this time point the calculated mass of drug is greater than the initial one. This effect is due to the contribution of Zn^{2+} ions dissolved into the SBF solution during the GS release. However, it was not possible to evaluate the exact quantification of this contribution.

Table 6.1: Concentration and average drug released in solution

| Release time [h] | Volume of solution [ml] | Concentration [ug/ml] | Concentration [ug/ml] | Released drug [ug] | Released drug [ug] | Average drug released [ug] |
|------------------|-------------------------|-----------------------|-----------------------|--------------------|--------------------|----------------------------|
| | | Sample 1 | Sample 2 | Sample 1 | Sample 2 | |
| 5 min | 10 | 0 | 1 | 0 | 10 | 5 |
| 15 min | 9,65 | 0 | 0 | 0 | 0 | 0 |
| 30 min | 9,3 | 21,5 | 0 | 199,95 | 0 | 99,975 |

| | | | | | | |
|-----|------|------|------|--------|--------|----------|
| 1h | 8,95 | 6,5 | 3 | 58,175 | 26,85 | 42,5125 |
| 2h | 8,6 | 39,5 | 15 | 339,7 | 129 | 234,35 |
| 4h | 8,25 | 47,5 | 54,5 | 391,87 | 449,62 | 420,75 |
| 6 | 7,9 | 49,5 | 69,5 | 391,05 | 549,05 | 470,05 |
| 24 | 7,55 | 181 | 281 | 1366,5 | 2121,5 | 1744,05 |
| 48 | 7,2 | 237 | 322 | 1706,4 | 2318,4 | 2012,4 |
| 72 | 6,85 | 301 | 444 | 2061,8 | 3041,4 | 2551,625 |
| 168 | 6,5 | 576 | 676 | 3744 | 4394 | 4069 |

To overcome the limitation due to ZnO dissolution, a centrifugation process (20'000 rpm for 5 min) was applied to all the solution extracted from the release batch before the UV-VIS analysis. The release curves of the centrifuged solutions are reported in Figure 6.3 and Figure 6.4.

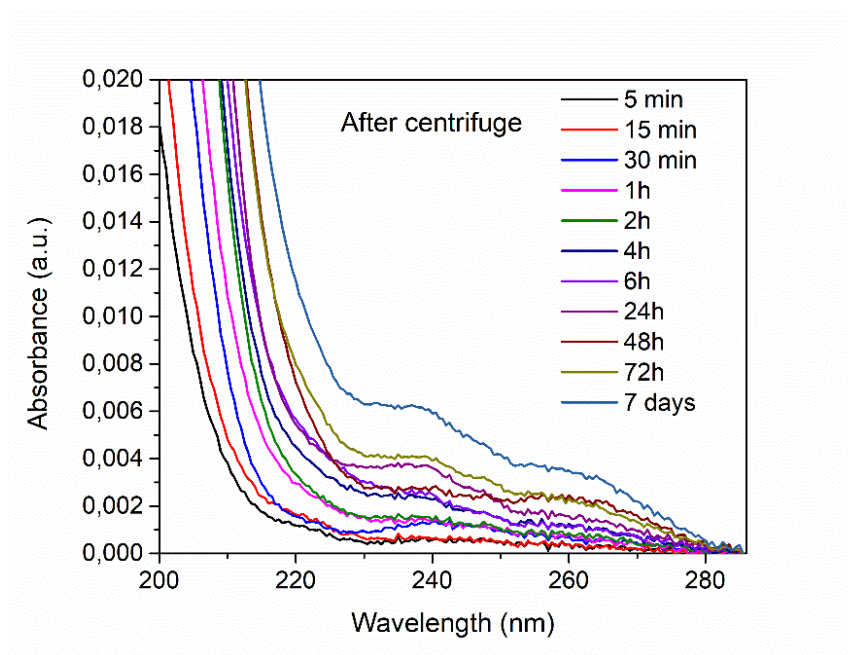


Figure 6.3: Release spectra of GS/SBF centrifuged solutions from porous ZnO thin film at different times, sample 1.

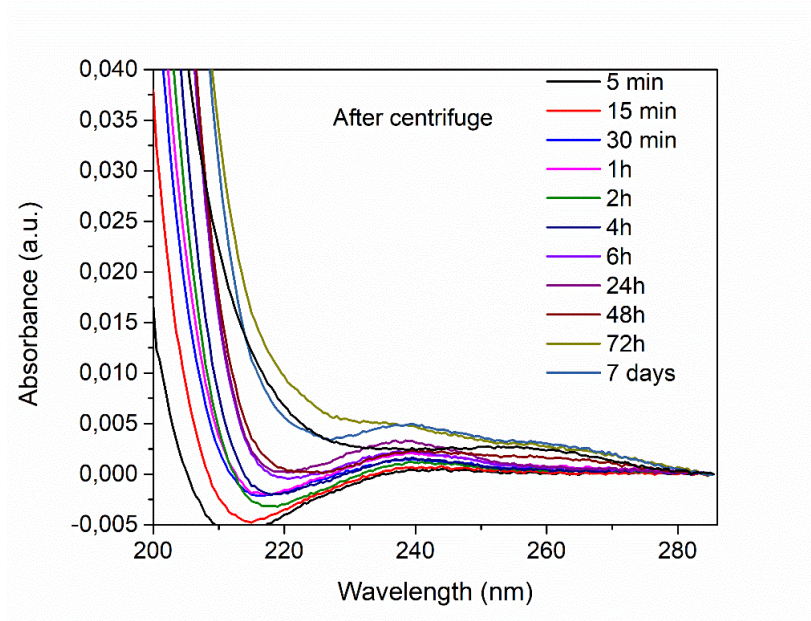


Figure 6.4: Release spectra of GS/SBF centrifuged solutions from porous ZnO thin film at different times, sample 2.

As for the starting samples, Table 6.2 shows the values of concentration and the amount of released drug obtained for each centrifuged solution and their average.

Table 6.2: Concentration and average drug released in solution after the centrifugation process.

| Release time [h] | Volume of solution [ml] | Concentration [ug/ml] | | Released drug [ug] | | Average drug released [ug] |
|------------------|-------------------------|-----------------------|----------|--------------------|----------|----------------------------|
| | | Sample 1 | Sample 2 | Sample 1 | Sample 2 | |
| 5 min | 10 | 22 | 0 | 220 | 0 | 110 |
| 15 min | 9,65 | 10 | 2 | 96,5 | 19,3 | 57,9 |
| 30 min | 9,3 | 84,5 | 61 | 785,85 | 567,3 | 676,575 |
| 1h | 8,95 | 96 | 142 | 859,2 | 1270,9 | 1065,05 |
| 2h | 8,6 | 106 | 49,5 | 911,6 | 425,7 | 668,65 |
| 4h | 8,25 | 156 | 65 | 1287 | 536,25 | 911,625 |

| | | | | | | |
|-----|------|-----|-----|---------|---------|----------|
| 6 | 7,9 | 147 | 114 | 1161,3 | 900,6 | 1030,95 |
| 24 | 7,55 | 239 | 147 | 1804,45 | 1109,85 | 1457,15 |
| 48 | 7,2 | 307 | 251 | 2210,4 | 1807,2 | 2008,8 |
| 72 | 6,85 | 377 | 480 | 2582,45 | 3288 | 2935,225 |
| 168 | 6,5 | 577 | 522 | 3750,5 | 3393 | 3571,75 |

Unfortunately, the results obtained by UV-Vis spectrometry after centrifugation are not better than the experiments without centrifugation, in contrast the dissolution behaviour seems to be more pronounced. In this case, the value of 800 ug related to drug loaded previously is reached before, at the time of about 2h. Then, the concentration continue to increase.

For the construction of release profile, the percentage of drug released with respect to the starting amount was considered. In particular, the trend regards the mean value between non-centrifuged and centrifuged samples. Table 6.3 reports the percentages of gentamicin released at different intervals of time for both samples and their average. These values were calculated from the average mass value of drug present in the solution at a specific time and the initial value of loaded drug (about 800 ug), and finally multiplied for 100. The profile of Figure 6.5 shows that the percentage of drug released increases with time gradually until 6 h and reach the value of 100% after 24h. As already mentioned, the values of drug released after 24 h are greater than the value of drug loaded in the porous ZnO film and the phenomena is probably due to the dissolution of the film. For this reason, these values were considered independent by release of drug, which it assumed to end after 6h. Consequently, after 6h the release percentage is considered to be 100. The amount of gentamicin in solution reaches the asymptote and remain constant.

Table 6.3: Percentage of gentamicin released respect to starting amount

| Release time [h] | GS released | GS released | GS released |
|---------------------|--------------------------|------------------------------|---------------|
| | %, w/w | %, w/w | %, w/w |
| | From ZnO - no centrifuge | From ZnO - con centrifuge | Average value |
| 0 | 0 | 0 | 0 |
| 0,08 | 0,625 | 13,75 | 7,1875 |
| 0,25 | 0 | 7,2375 | 3,61875 |
| 0,5 | 12,49688 | 84,57188 | 48,53438 |

| | | | |
|-----|----------|----------|----------|
| 1 | 5,31406 | 100 | 52,65703 |
| 2 | 29,29375 | 83,58125 | 56,4375 |
| 4 | 52,59375 | 100 | 76,29688 |
| 6 | 58,75625 | 100 | 79,37813 |
| 24 | 100 | 100 | 100 |
| 48 | 100 | 100 | 100 |
| 72 | 100 | 100 | 100 |
| 168 | 100 | 100 | 100 |

Therefore, the release profile follows a first-order exponential decay model (see the fitting curve in red), with a release rate constant of 0,52 s⁻¹. The equation (6.1) mathematically describes the first-order model:

$$\frac{\%Q_t}{\%Q_\infty} = 1 - e^{-bt} \quad (6.1)$$

In the equation (6.1) %Q_t represent the percentage of drug released at time t, %Q_∞ is the total percentage of drug released and consequently their rapport is the fraction of drug release at time t. b is the release rate constant while t is the generic time. This model allows asserting that the release mechanism of gentamicin is regulated only by diffusion. In fact the model derives by integration of equation (6.2), that is the Noyes–Whitney equation:

$$\frac{dC_t}{dt} = kS(C_s - C_t) \quad (6.2)$$

In the equation 6.2, C_t is the concentration of the drug at time t, S is the solvent accessible area, C_s is the drug solubility in equilibrium at the test temperature and k is a first order

proportionality constant. This constant is related to diffusion coefficient D and the geometry of the pores by means of Fick's first law.

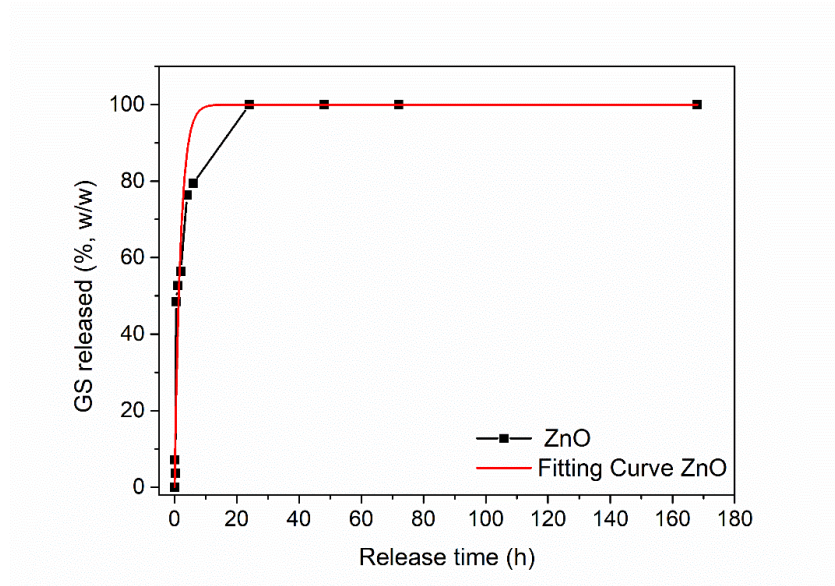


Figure 6.5: Release profile of gentamicin in SBF from porous ZnO thin film

X-ray diffraction post-release

X-ray diffraction technique was performed on ZnO-GO sample after the release process to evaluate any change in the crystal structure. Figure 6.6 and Figure 6.7 shows the XRD pattern for sample 1 and sample 2 comparing with the XRD spectra of ZnO after uptake of 2h. The characteristic peaks of hexagonal wurtzite structure are always present. This aspect suggests that crystal structure of ZnO material has been maintained after the release.

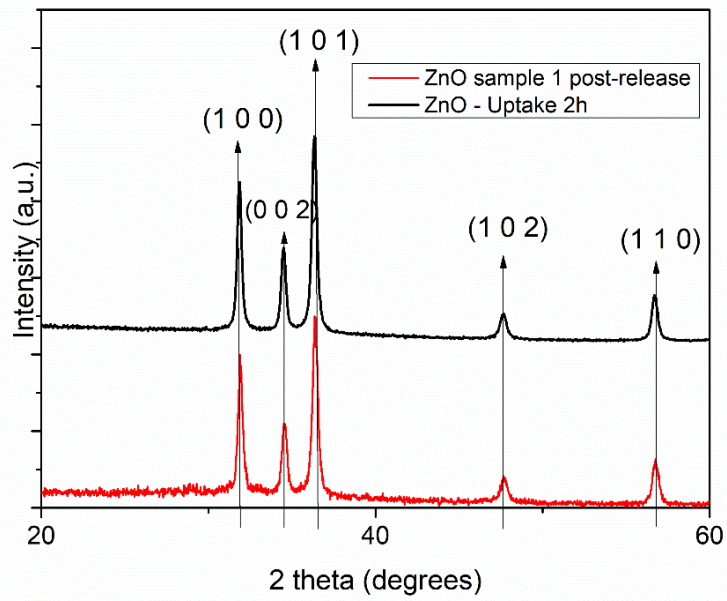


Figure 6.6: XRD spectra of sample 1 after and before release

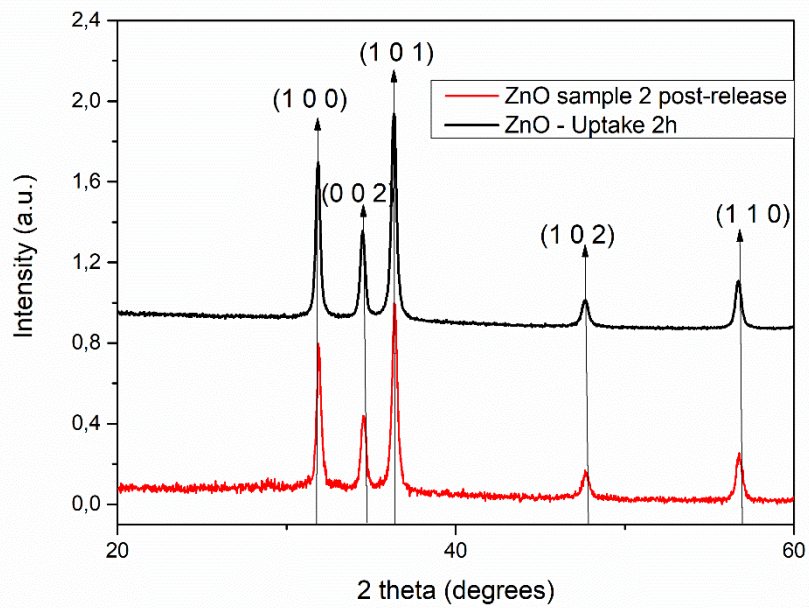


Figure 6.7: XRD spectra of sample 2 after and before release

FESEM ZnO post-release

Porous ZnO thin films were analyzed after the release time of 7 days through FESEM analyse. The scope was the investigation of morphology of the samples to evaluate the degradation of material in time. Figure 6.8 compares FESEM images before the release process ((a) and (c)) and after the release ((b) and (d)) for different magnifications (25.00 KX and 50.00 KX). It can be see that the porous ZnO film acquired a more compact structure after 7 days than the initial morphology. It is probably due to loss of material which affects negatively the porosity. This aspect confirm the data obtained with UV-Vis analyses.

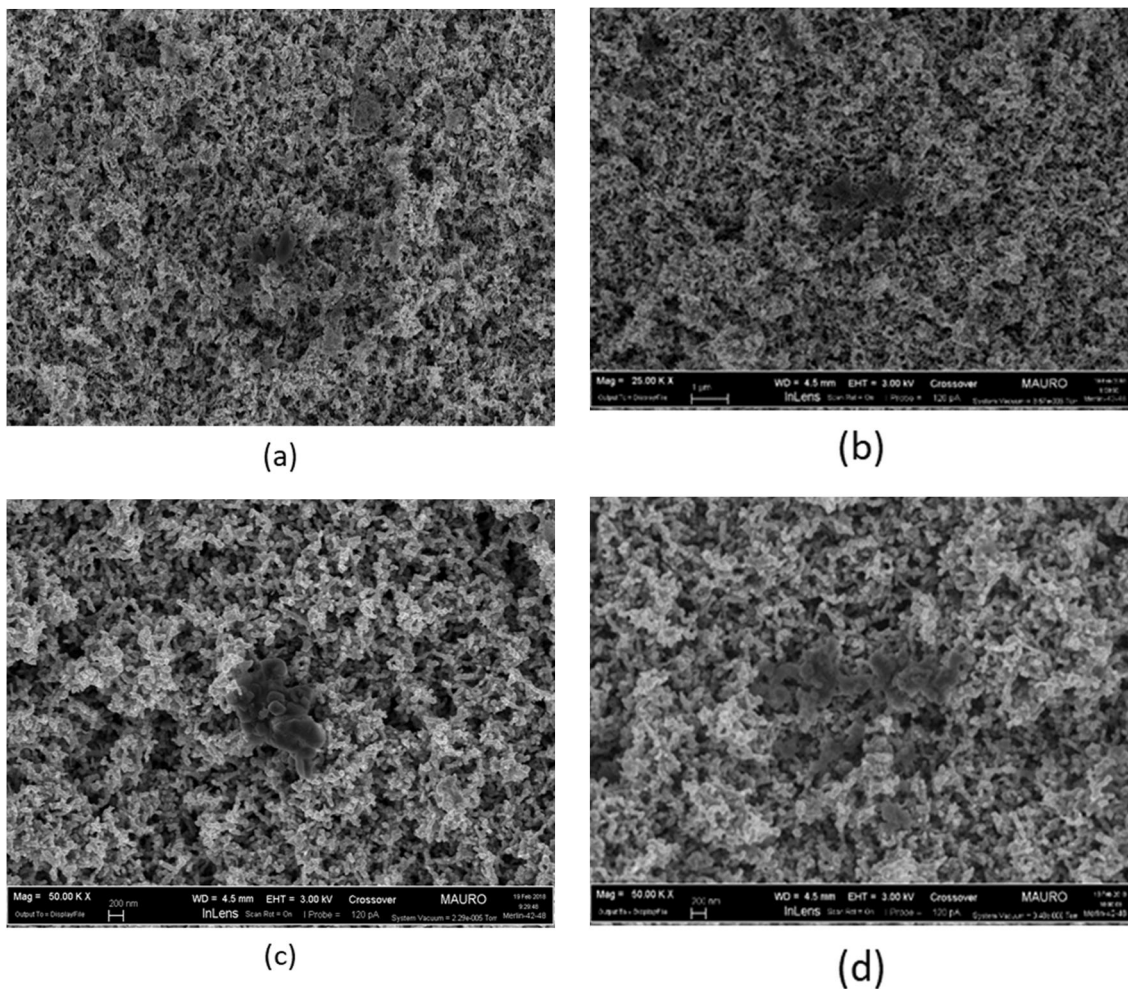


Figure 6.8: Comparison of FESEM images acquired before the release process ((a) and (c)) and at the end of the release experiment ((b) and (d)) for different magnifications of 25.00 KX and 50.00 KX.

FTIR-analysis post release

Infrared analyses were performed after the release time of 7 days to evaluate the eventual absence of characteristic group of gentamicin sulfate that was released in the first 24h. Figure 6.9 compares the IR spectra of pristine ZnO, GS, ZnO sample after uptake of GS for 2h and ZnO sample after release of GS for 7 days. It can be seen that the characteristic peak of sulphate at about 620 cm^{-1} is present only after the uptake of the drug. The two peaks at similar position after the release of the drug are due to the precipitation of phosphates.

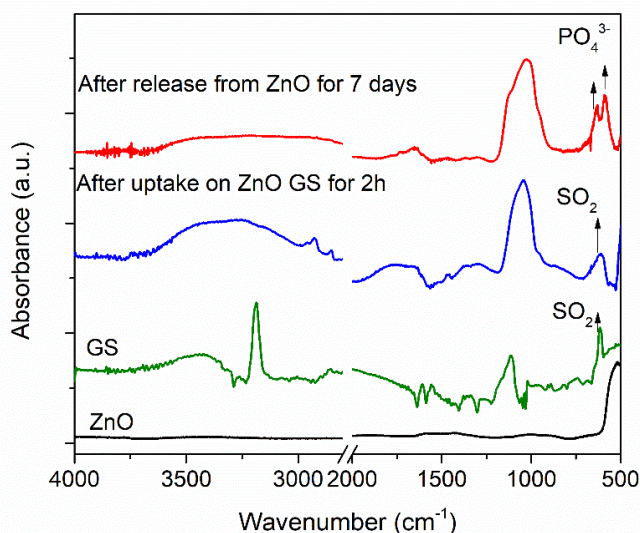


Figure 6.9: IR spectra of pristine ZnO, GS, ZnO after uptake for 2h and ZnO after release of 7 days.

6.2 Release of GS from GO-coated porous ZnO thin films

As already mentioned at the beginning of chapter, the use of graphene oxide as layer on the porous ZnO film was carried out to evaluate the release capacity of the system and compare it with the previous results. The aim of this experiment is the achievement of a controlled drug delivery system, able to release the drug slower than the pristine ZnO thin film. In fact, a controlled release kinetic is an aspect extremely important in several drug delivery applications. Again, the starting point of the release process is the amount of drug loaded during the uptake. The presence of GO does not affect this amount because its deposition occurred after the drug uptake. In this case, only one sample was evaluated and the operating modes were the same of previous release process. Figure 6.10 shows the release spectra of GS/SBF solutions during the soaking a ZnO-GO sample.

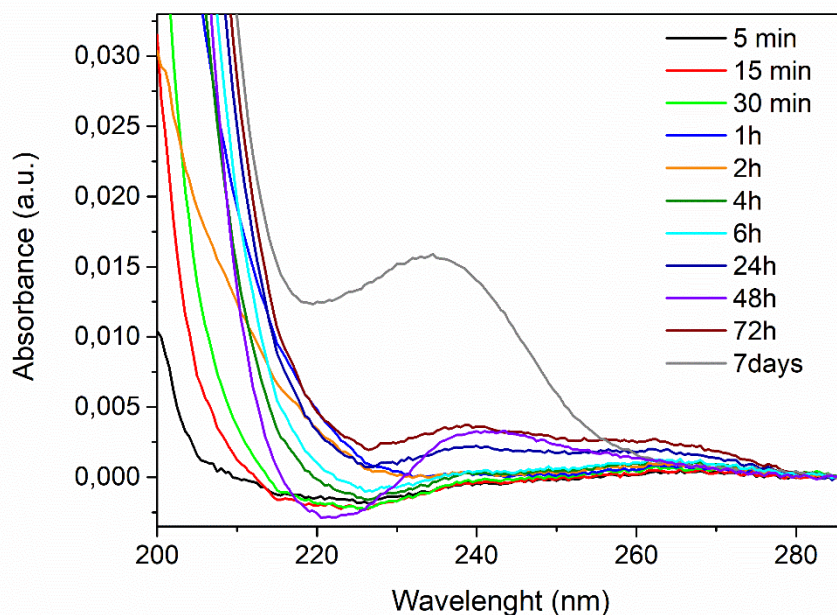


Figure 6.10: Release spectra of GS/SBF solutions from porous ZnO-GO at different times.

Table 6.4 shows the values of concentration and the amount of drug released obtained analysing 350 μ l volume at each time step. As before, the amount of drug released in time increases gradually. However, in this case until 1h, the release was zero. This is probably due to the barrier effect of GO, which is able to slow down the delivery process. Therefore, the release is complete as the previous case before the time of 24h.

Table 6.4: Concentration and amount of drug released at different times from the ZnO-GO system

| Release time [h] | Volume of solution [ml] | Concentration [μ g/ml] | Released drug [μ g] |
|---------------------|----------------------------|--------------------------------|-----------------------------|
| 5 min | 10 | 0 | 0 |
| 15 min | 9,65 | 0 | 0 |
| 30 min | 9,3 | 0 | 0 |
| 1h | 8,95 | 0 | 0 |
| 2h | 8,6 | 1 | 8,6 |
| 4h | 8,25 | 13 | 107,25 |
| 6 | 7,9 | 28 | 221,2 |

| | | | |
|-----|------|-----|--------|
| 24 | 7,55 | 224 | 1691,2 |
| 48 | 7,2 | 306 | 2203,2 |
| 72 | 6,85 | 376 | 2575,6 |
| 168 | 6,5 | 756 | 4914 |

The construction of the release profile follows the same procedure described previously. Table 6.5 shows the percentage of gentamicin released with respect to its initial quantity. As before, over the values of 800 ug, the release of drug is considered to be the maximum and the continue increase of the values is attribute to Zn^{2+} ions.

Figure 6.5: Percentage of gentamicin released with respect to the starting amount.

| Release time [h] | GS released %, w/w |
|---------------------|-----------------------|
| 0 | 0 |
| 0,08 | 0 |
| 0,25 | 0 |
| 0,5 | 0 |
| 1 | 0 |
| 2 | 1,1 |
| 4 | 13,4 |
| 6 | 27,7 |
| 24 | 100 |
| 48 | 100 |
| 72 | 100 |
| 168 | 100 |

Figure 6.11 shows the release profile of gentamicin for the ZnO-GO system. The amount of released drug is zero at first hours of the process, then it increase slowly reaching the value of 100% at about the time of 24h and remain the same until 7 days. As before, the release profile follows a first-order exponential decay model (see the fitting curve in red), with a release rate constant of $0,07 \text{ s}^{-1}$, a value lower than the b obtained in the previous case. This aspect confirms a slowdown of release process due to presence of GO. The equation 6.3, mathematically describes the first-order model:

$$\frac{\%Q_t}{\%Q_\infty} = 1 - e^{-bt} \quad (6.3)$$

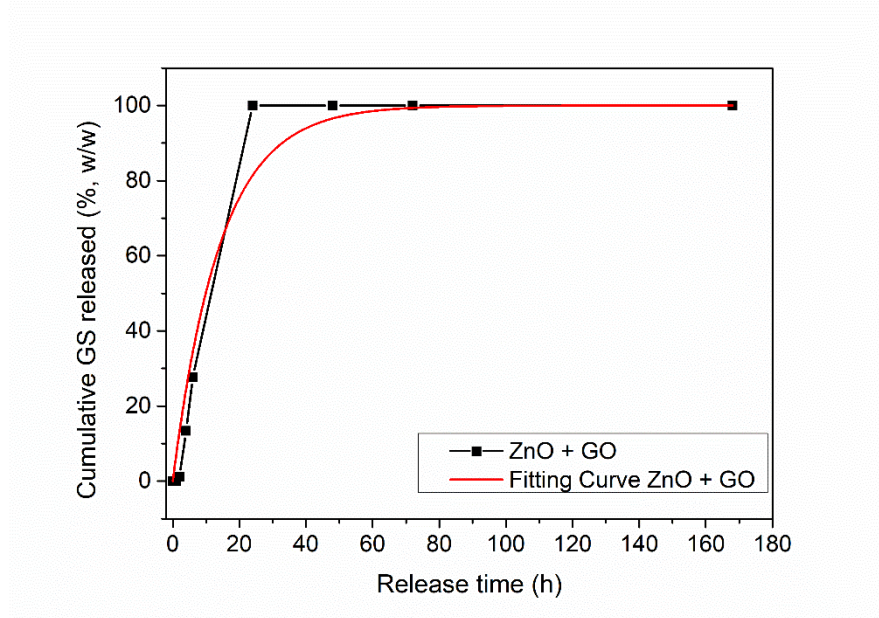


Figure 6.11: Release profile of gentamicin in SBF from the porous ZnO-GO film.

Figure 6.12 shows the comparison between the release profiles for both pristine ZnO and GO-coated ZnO porous thin films at different time scales. It is clear that the presence of GO allows to obtain a controlled release of the drug until 24 hours. Actually, the process is slower than in the case from pristine ZnO, although the release end occurs in both cases at 24 hours. Thus, it can be concluded that GO, thanks to its particular structure, offers a barrier effect against the release of drug, when it is deposited on the drug-loaded porous ZnO films. The reaching of 100% release in 24h is probably due to partial separation of GO flakes after the first hours caused both by its hydrophilicity in SBF and a weak bond formed with ZnO structures.

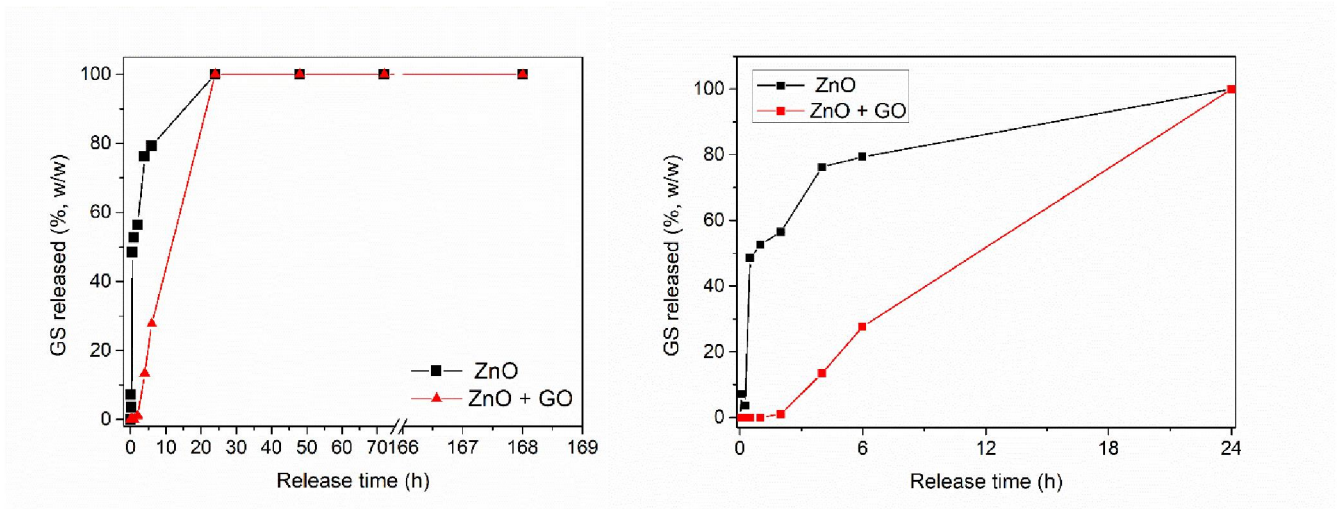


Figure 6.12: Comparison between the release profiles of GS from ZnO and ZnO-GO.

X-ray diffraction post-release

X-ray diffraction technique was performed on ZnO-GO sample after the release process to evaluate any change in the crystal structure. Figure 6.13 shows the XRD pattern, where the characteristic peaks of hexagonal wurtzite structure are always present. This aspect suggests that crystal structure of ZnO material has been maintained after the release.

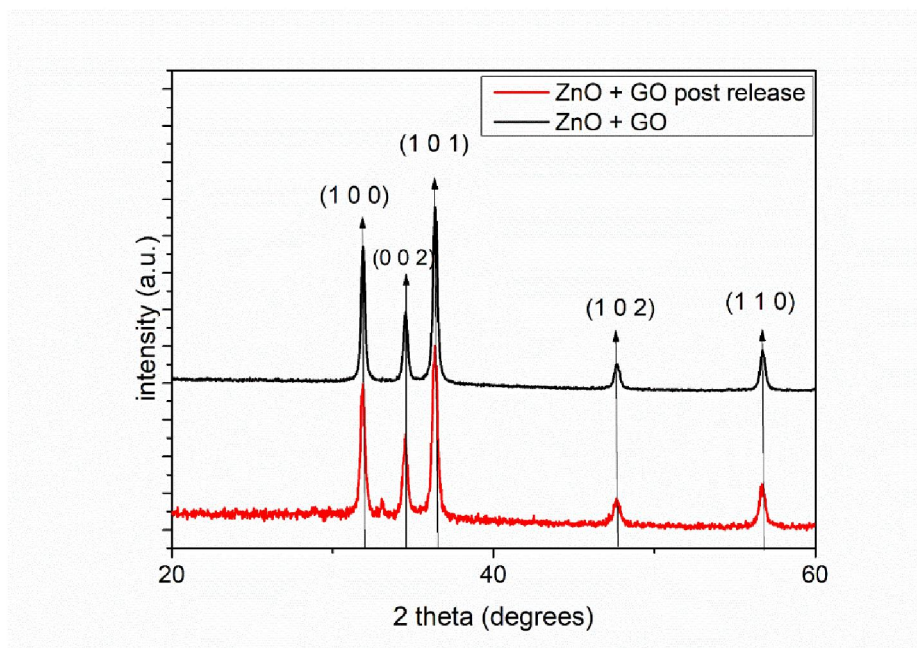


Figure 6.13: XRD pattern for the GO-coated porous ZnO film after and before drug release.

FESEM of ZnO-GO post-release

The FESEM analysis was carried out after the release of gentamicin sulfate in order to highlighting the possible changes in morphology occurred on the sample. In particular, the aim was to evaluate if the GO is still present on the surface of ZnO and if possible degradation of ZnO over time occurred. Figure 6.14 shows different magnifications of ZnO-GO sample after the release for 7 days. In particular, it is possible notes the presence of discontinuities for high magnifications as 100.00 KX and 150.00 KX due to separation of GO flakes. This is mainly due to hydrophilicity of GO in SBF and a weak bond formed with ZnO structures.

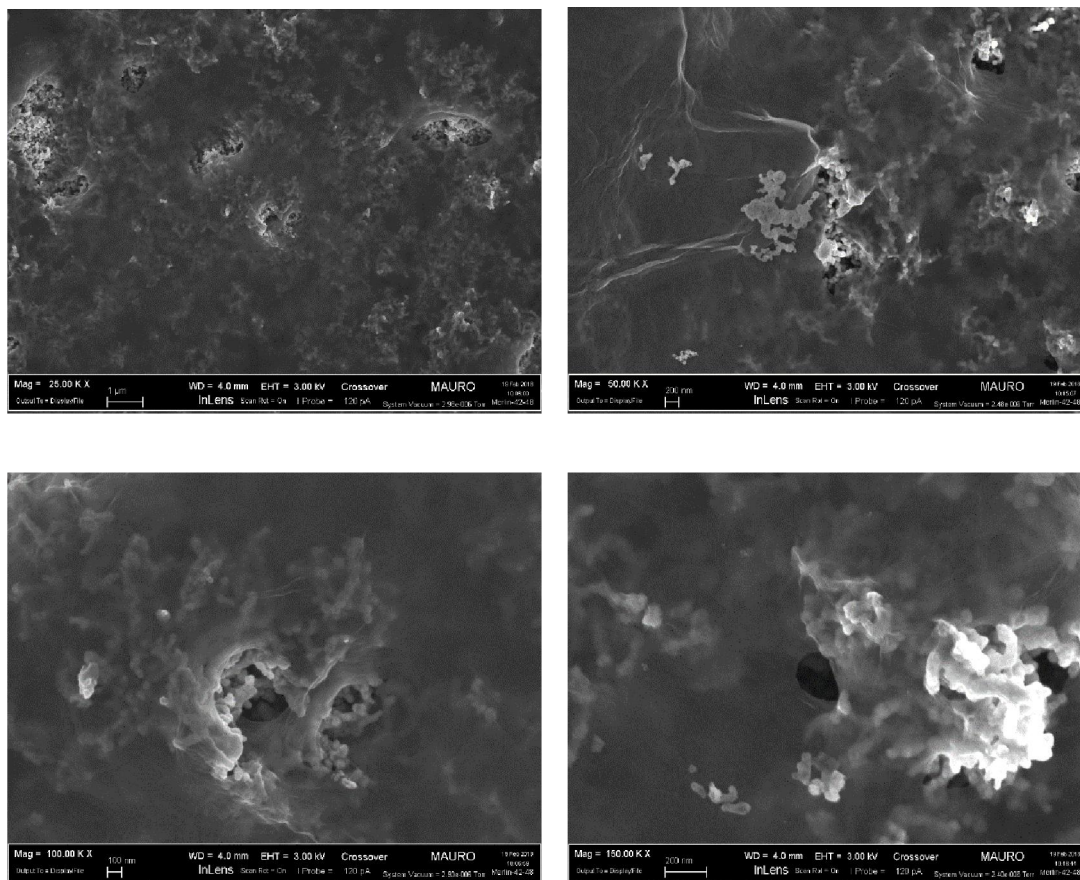


Figure 6.14: Different magnification images of porous ZnO-GO sample after release

IR post release

Infrared analyse has been performed after the release time of 7 days to evaluate the eventual absence of characteristic group of gentamicin sulfate that was released in 24h. Figure 6.15 compare the IR spectra of pristine ZnO-GO, GS, ZnO-GO sample after uptake GS for 2h and ZnO-GO sample after release of GS for 7 days. It can be see that the characteristic peak of sulphate at about 620 cm^{-1} is present only after the uptake of the drug. The two peaks at similar position after the release of the drug are due to the precipitation of phosphates.

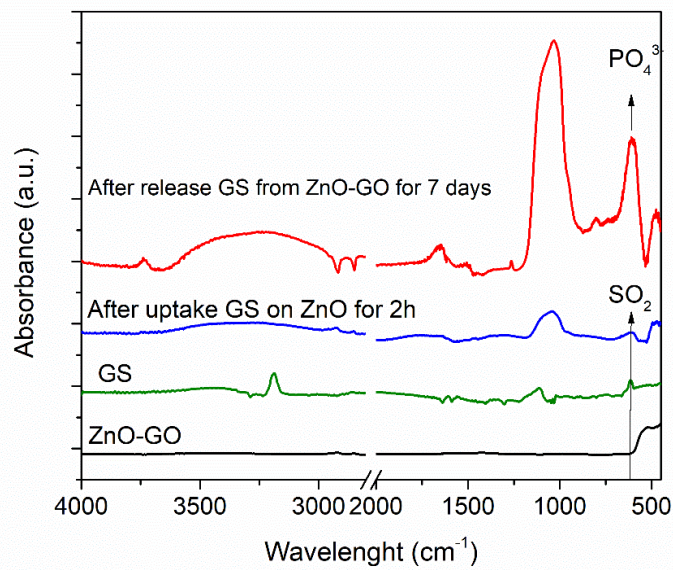


Figure 6.15 : IR spectra of ZnO-GO, GS, ZnO after uptake for 2h and ZnO after release of 7 days.

7. Conclusion

In this experimental thesis the uptake and release properties of porous ZnO thin films and graphene oxide-coated porous ZnO thin films were evaluated and described. Porous ZnO thin films were obtained by sputtering metallic Zn layers on silicon substrates and their conversion into ZnO by thermal oxidation. The drug used for all uptake and release experiments was gentamicin sulfate.

It was shown that the degradation behaviour of ZnO film in deionized water is due to the acidic characters of the uptake solution, and is more pronounced by increasing the GS uptake time. Both pH of GS solution and uptake time induce the dissolution of material, the loss of porosity and a process efficiency reduction. The use of SBF, a buffered solution simulating the inorganic composition of human plasma, limits the dissolution phenomena for short times. It is thus possible to load a discrete quantity of drug without compromising the nanomaterial. Moreover, the use of only porous ZnO thin films for uptake is better than GO-coated ZnO films because in this last case there is a ZnO dissolution effect and a greater co-precipitation of CaP due to interaction between ZnO and SBF and ZnO dissolution.

Starting from the amount of gentamicin loaded in the uptake phase, the release of the drug was possible both using the pristine ZnO sample and ZnO-GO samples. The presence of GO layer on ZnO sample allows to obtain a controlled release system. Comparing the release kinetics in both cases, the ZnO-GO system is able to produce a “barrier effect”, slowing down the delivery kinetics in the short-time range.

The results showed that porous ZnO thin films, combined with the presence of GO flakes, could serve as an efficient system for drug-delivery applications. For the future, the pore chemical structure or pore entrances should be further engineered, using chemistry to modify the surface of ZnO, in order to achieve a smart and even remote control over the drug delivery kinetics. Furthermore, tests on the final biodegradation of the ZnO coating and its antibacterial properties would corroborate to obtain a smart and programmable nanostructured coating for the next-generation of biomedical implants.

References

- [1] Kumar V. B., Annamanedi M., Prashad M. D., Arunasree K. M., Mastai Y., Gedanken A., Paik P. 2013, Synthesis of mesoporous SiO₂-ZnO nanocapsules: encapsulation of small biomolecules for drugs and “SiOZO-plex” for gene delivery. *J Nanopart Res* (2013) 15:1904
- [2] Nel A, Xia T, Madler L, Li N., 2006, Toxic potential of materials at the nanolevel. *Science* Vol. 311, Issue 5761
- [3] Lanone S, Boczkowski J. Biomedical applications and potential health risks of nanomaterials: molecular mechanisms. *Curr Mol Med* 2006; 6:651–63.
- [4] Gultepe E., Nagesha D., Sridhar S., Amiji M., 2009, Nanoporous inorganic membranes or coatings for sustained drug delivery in implantable devices. *Advanced Drug Delivery Reviews* 62 (2010) 305–315
- [5] Sinha V. R., Kumria R., 2003, Coating polymers for colon specific drug delivery: A comparative in vitro evaluation. *Acta Pharm.* 53 (2003) 41–47
- [6] La W. G., Park S., Yoon H. H., Jeong G. J., Lee T. J., Bhang S. H., Han J. Y., Char K., Kim B. S., 2013, Delivery of a therapeutic protein for bone regeneration from a substrate coated with graphene oxide. *Small*, 9(23), 4051-4060
- [7] G.C. Wood, J.P.O. Sullivan, B. Vaszko, The direct observation of barrier layers in porous anodic oxide films, *Journal of The Electrochemical Society* 115 (6) (1968) 618–620.
- [8] C.A. Grimes, Synthesis and application of highly ordered arrays of TiO₂ nanotubes, *Journal of Materials Chemistry* 17 (15) (2007) 1451–1457.
- [9] J. Salonen, A.M. Kaukonen, J. Hirvonen, V.-P. Lehto, Mesoporous silicon in drug delivery applications, *Journal of Pharmaceutical Sciences* 97 (2) (2008) 632–653.
- [10] Morkoç Ü. Ö. H., 2009, «Zinc Oxide: Fundamentals, Materials and Device Technology,». WILEY-VCH Verlag GmbH & Co. KGaA, Weinheim
- [11] M. Laurenti, 2015, «Synthesis and characterization of piezoelectric thin films functional materials for sensing. PhD thesis,»
- [12] Wang Z. L., 2004, Nanostructures of zinc oxide. *Mater. Today*, 7, 26 .
- [13] Degen A, Kosec M. Effect of pH and impurities on the surface charge of zinc oxide in aqueous solution. *J European Ceramic Society* 2000;20:667–73.
- [14] Nagao M. Physiosorption of water on zinc oxide surface. *J Phys Chem* 1971;75:3822–8.
- [15] Y. H. Chen , Y. M. Shen , S. C. Wang , J. L. Huang , *Thin Solid Film* **2014** , 570 , 303
- [16] Q. P. Luo , B. X. Lei , X. Y. Yu , D. B. Kuang , C. Y. Su , *J. Mater. Chem.* **2011** , 21 , 8709
- [17] M. H. Huang , Y. Wu , H. Feick , N. Tran , E. Weber , P. Yang , *Adv. Mater.* **2001** , 13 , 113.
- [18] T.-J. Kuo , C. N. Lin , C. L. Kuo , M. H. Huang , *Chem. Mater.* **2007** , 19 , 5143.

- [19] A.M. Gas'kov, M.N. Rumyantseva, *Russ. J. Appl. Chem.* 74 (2001) 440.
- [20] Wang, Nanostructures of Zinc Oxide, *Materials Today*, Volume 7, Issue 6, June 2004, Pages 26-33
- [21] X. Gao , Y. Cui , R. M. Levenson , L. W. K. Chung , S. Nie , *Nat. Biotechnol.* 2004 , 22 , 969.
- [22] R. A. Petros , J. M. DeSimone , *Nat. Rev. Drug Discovery* 2010, 9, 615.
- [23] X. J. Kang , Y. L. Dai , P. A. Ma , D. M. Yang , C. X. Li , Z. Y. Hou , Z. Y. Cheng , J. Lin , *Chem. Eur. J.* 2012 , 18 , 15676
- [24] W. Fang , J. Yang , J. Gong , N. Zheng , *Adv. Funct. Mater.* 2012 , 22 , 842
- [25] J. Z. Du , X. J. Du , C. Q. Mao , J. Wang , *J. Am. Chem. Soc.* 2011 , 133 , 17560.
- [26] J. Croissant , J. I. Zink , *J. Am. Chem. Soc.* 2012 , 134 , 7628.
- [27] V. Voliani , F. Ricci , G. Signore , R. Nifosi , S. Luin , F. Beltram , *Small* 2011 , 7 , 3271
- [28] N. Singh , B. Manshian , G. J. S. Jenkins , S. M. Griffiths , P. M. Williams , T. G. G. Maffei , C. J. Wright , S. H. Doak , *Biomaterials* 2009 , 30 , 3891.
- [29] Yuan Q, Hein S, Misra RD. New generation of chitosan-encapsulated ZnO quantum dots loaded with drug: Synthesis, characterization and in vitro drug delivery response. *Acta Biomater* 2010; 6:2732–9. [PubMed: 20100604]
- [30] Nie L, Gao L, Yan X, Wang T. Functionalized tetrapod-like ZnO nanostructures for plasmid DNA purification, polymerase chain reaction and delivery. *Nanotechnology* 2007;18:015101–7.
- [31] Zhang P, Liu W. ZnO QD@PMAA-co-PDMAEMA nonviral vector for plasmid DNA delivery and bioimaging. *Biomater* 2010;31:3087–94.
- [32] F. Muhammad , M. Y. Guo , W. X. Qi , F. X. Sun , A. F. Wang , Y. J. Guo , G. S. Zhu , *J. Am. Chem. Soc.* 2011 , 133 , 8778.
- [33] Z. Y. Zhang , Y. D. Xu , Y. Y. Ma , L. L. Qiu , Y. Wang , J. L. Kong , H. M. Xiong , *Angew. Chem. Int. Ed.* 2013 , 52 , 4127.
- [34] K. J. M. M. e. a. Muller KH, «pH-dependent toxicity of high aspect ratio ZnO nanowires in macrophages due to intracellular dissolution.» *ACS Nano.*, 2010.
- [35] Hafeli UO, Riffle JS, Harris-Shekhawat L, et al. Cell uptake and in vitro toxicity of magnetic nanoparticles suitable for drug delivery. *Mol Pharm* 2009;6:1417–28. [PubMed: 19445482]
- [36] Liu J., Cui L., Losic D., 2013, Graphene and graphene oxide as new nanocarriers for drug delivery Applications. *Acta Biomaterialia* 9 (2013) 9243–9257
- [37] Langer R. Drugs on target. *Science* 2001;293:58–9.
- [38] Zhang LM, Xia JG, Zhao QH, Liu LW, Zhang ZJ. Functional graphene oxide as a nanocarrier for controlled loading and targeted delivery of mixed anticancer drugs. *Small* 2010;6:537–44.

- [39] Triggs E, Charles B. Pharmacokinetics and therapeutic drug monitoring of gentamicin in the elderly. *Clin Pharmacokinet.* 1999;37:331–41. [PubMed]
- [40] Šoltés, L. Aminoglycoside antibiotics—two decades of their HPLC bioanalysis. *Biomedical Chromatography*, 1999; 13(1), 3-10.
- [41] Pichavant L., Amador G., Jacqueline C., Brouillaud B., Hèroquez V., Durrieu M. C., 2012, pH-controlled delivery of gentamicin sulfate from orthopedic devices preventing nosocomial infections. *Journal of Controlled Release* 162, 373-381.
- [42] JCPDS-ICDD database (Joint Committee on Powder Diffraction Standards- International Centre for Diffraction Data) card no. 89–1397
- [43] Fatehah M. O., Aziz H. A., Stoll S., 2014, Stability of ZnO nanoparticles in solution. Influence of pH, dissolution, aggregation and disaggregation effects. *Journal of Colloid Science and Biotechnology*, Vol 3. 1-10.
- [44] Atienza S. A., 2017, “In-vitro Evaluation of Bioactivity, Biodegradation and Molecule Uptake/Release Properties of Porous ZnO Structures for Tissue Engineering”, Master Degree in Biomedical Engineering

Websites

Figure 2.1: What is zinc oxide?

<https://whatiszincoxide.weebly.com/reference-page.html>

Figure 2.2: Nanostructures of zinc oxide.

<https://www.sciencedirect.com/science/article/pii/S136970210400286X>

Figure 2.3: Graphene Oxide.

<http://www.tcichemicals.com/g-cmn/contents/en/st75200000026u8c-img/G0443,4-1g.gif>

Figure 2.4: Graphene and graphene oxide as new nanocarriers for drug delivery applications

<https://ars.els-cdn.com/content/image/1-s2.0-S174270611300408X-gr2.jpg>

Figure 2.5: Gentamicin C1 sulfate

<https://pubchem.ncbi.nlm.nih.gov/image/imgsrv.fcgi?cid=44563965&t=1>